High Pressure Scanning Tunneling Microscopy and High Pressure X-ray Photoemission Spectroscopy Studies of Adsorbate Structure, Composition and Mobility During Catalytic Reactions on a Model Single Crystal.

by

Max O. Montano

B.S. (Pacific University) 2000

A dissertation submitted in partial satisfaction of the

requirements for the degree of

Doctor of Philosophy

in

Chemistry

in the

Graduate Division

of the

University of California, Berkeley

Committee in charge:

Professor Gabor A. Somorjai, Chair
Professor Heino Nitsche
Professor Kyriakos Komvopoulos

Spring 2006

High Pressure Scanning Tunneling Microscopy and High Pressure X-ray Photoemission Spectroscopy Studies of Adsorbate Structure, Composition and Mobility During Catalytic Reactions on a Model Single Crystal.

by Max O. Montano

Abstract

High Pressure Scanning Tunneling Microscopy and High Pressure X-ray Photoemission Spectroscopy Studies of Adsorbate Structure, Composition and Mobility During Catalytic Reactions on a Model Single Crystal.

by

Max O. Montano

Doctor of Philosophy in Chemistry

University of California, Berkeley

Professor Gabor A. Somorjai, Chair

Our research focuses on taking advantage of the ability of scanning tunneling microscopy (STM) to operate at high-temperatures and high-pressures while still providing real-time atomic resolution images. We also utilize high-pressure x-ray photoelectron spectroscopy (HPXPS) to monitor systems under identical conditions thus giving us chemical information to compare and contrast with the structural and dynamic data provided by STM.

STM was employed to study the structures formed by cyclic C_6 hydrocarbon monolayers adsorbed on a platinum (111) crystal surface. Cyclohexane. cyclohexene, 1,3-cyclohexadiene, 1,4-cyclohexadiene and benzene were exposed to the platinum surface in the 10^{-6} Torr pressure regime. Upon adsorption on Pt (111) both cyclohexane and cyclohexene produced the same ($\sqrt{7}$ x $\sqrt{7}$) R19.1° hexagonal structure, which corresponds to the partially dehydrogenated π-allyl (C_6H_9). 1,3-cyclohexadiene and

benzene produced a (2√3 x 2√3) R30.0° structure composed of pure benzene. 1,4-cyclohexadiene forms a structure very different from the others, which we attributed to a (√43 x √43) R7.6° structure composed of molecular 1,4-cyclohexadiene.

STM studies on catalytic reactions of cyclohexene and its poisoning with carbon monoxide on Pt (111) were also performed in the presence of hydrogen at pressures slightly below 1Torr in the 300K - 350K temperature range. At room temperature in the presence of 20 mTorr hydrogen and 20 mTorr cyclohexene, the surface formed the (√7 x √7) R19.1° π-allyl structure and no products were detected. Increasing the hydrogen pressure to 200 mTorr caused the catalyst to begin producing cyclohexane and some benzene, while also causing the STM images to disorder. The addition of 5 mTorr of CO to the system stopped all catalysis and formed an ordered CO overlayer. At 353K with 200 mTorr H_2 and 20 mTorr C_6H_{10}, the surface was more catalytically active that at lower temperatures, and again the addition of CO stopped all catalysis. STM revealed a mobile disordered surface suggesting that, although mobile, the surface was dominated by CO, which blocked adsorption of reactants.

Catalytic hydrogen/deuterium exchange on a platinum(111) single crystal and its poisoning with carbon monoxide was studied using STM, and high-pressure X-ray photoelectron spectroscopy (HPXPS). At 298K, and in the presence of 200 mTorr of hydrogen and 20 mTorr of deuterium, the surface is catalytically active and STM images appear disordered. The addition of 5 mTorr of CO stops all reaction and produces an ordered surface structure. At 353K in the presence of 200 mTorr of hydrogen and 20 mTorr of deuterium, again the surface is catalytically active and STM images are disordered. The addition of 5 mTorr of CO slows the reaction considerably, but turnover

continues as the H_2/D_2 activation energy increases from ~5.3 kcal/mol to 17.4 kcal/mol. XPS shows us however, that the amount of the CO on the surface is only ~10% less than at room temperature, and the surface structure is largely unchanged. As the temperature is increased the surface CO decreases while the activity increases. At around 370K XPS displays an abrupt change in the ratio of atop to bridge bound CO corresponding to a surface phase change. Cooling the sample back to room temperature restores the original structure as shown by both STM and XPS. From these data, a CO dominated, mobile and catalytically active surface model has been proposed.

STM studies of Pt (111) catalyzed benzene hydrogenation were performed at near ambient conditions from 300K –350K. Exposing the platinum surface to 10 Torr of benzene resulted in the formation of a mostly disordered overlayer of molecular benzene with small patches of order corresponding a c ($2\sqrt{3}$ x 3) structure. No catalysis was observed. Addition of 100 Torr of H_2 and 600 Torr of Argon induced a largely disordered surface and low catalytic activity. Heating the sample to 350K induced complete mobility and the steady production of cyclohexane was observed. The addition of 5 Torr of CO at 350K resulted in a mobile but catalytically poisoned surface. Cooling to room temperature recovered an ordered CO overlayer.

Dedicated to anyone and everyone who has ever helped me in any way.

Table of Contents

List of Figures

Acknowledgments

There have been many people who have played a major role in helping me accomplish my goal of receiving a Ph.D. First and foremost, I would like to thank my research advisor Professor Gabor Somorjai. I appreciate the opportunity he gave me to work in his research group. He provided me with financial support and guidance all the while giving me the freedom to design my own experiments and learn from my mistakes. Professor Somorjai provided me with comfortable and understanding leadership and created the perfect balance between pushing me for results and letting me work at my own pace. Coming to graduate school, I never imagined working in a group that suited me so well and to this day I don't think I could have made a better choice. Thank you Gabor, I am in your debt.

I would also like to thank Dr. Miquel Salmeron for all of his advice and guidance. His mastery of STM was crucial in helping me interpret my data and solve system problems. Although, I rarely appreciated it at the time, he always showed me the gaps in my logic and helped me decide how to fill them. To this day, I don't think I have ever seen Miquel in a bad mood.

I would like to thank the entire Somorjai group, for creating a friendly and comfortable atmosphere in which to conduct my research. Kevin Hwang introduced me to UHV and STM and was patient with me when I was making mistakes. Derek Butcher who has worked with me for the last six months and will carry on the work that we have been doing. Others who deserve thanks are Anthony Contreras, Sasha Kweskin, Kaori Kitano, Roger York, Katie Bratlie, Minchul Yang, Andy Marsh, Jeff Grunes, Telly Koffas, Aric Opdahl, Mike Grass, Xiaoming Yan, Ji Zhu, James Hoefelmeyer, Jeong

Park, Chris Kliewer, Russ Renzas, Rob Rioux, Jessica Parker, Yuri Borodko, Mario Farias, Lucio Flores, Inger Coble, Mike Fergusen, Diana Phillips, Ozzy Mermut, Simon Humphrey, Matthias Koebel, Kristian Nienz, Kevin Becraft, Guido Kettler, Paul Ashby, Evgeny Fermin, Frank Ogletree, Tomoko Shimizu, Aitor Mugarza, Yabing Qi, Mous Tatarkhanov, Christoph Weis, Hendrik Bluhm, Simon Mun.

I would also like to thank my friends outside of my research group for making my graduate school experience enjoyable. In particular Christina Stuart, I wish you the best and hope everything works out. Also I want to thank Bryan, Lynn, and Nick.

I would also like to thank the federal government (yes the federal government). There have been several times during my academic career that they have been my only source of financial support. Without all of the grants and loans I received over the years, I could never have afforded to continue my education. Of all of the people and things I am thankful for, the US government is the only one that I could absolutely not have accomplished my goals without.

Finally I would like to thank my family for all of their support through the last four years. My parents JoJo O'Connor and Louie Montano both ex-Berkeley students themselves. My girlfriend Amanda who has helped me balance life and work. My sister Carmen. My grandmother Nellie who has always been there when I wanted to talk, no mater what the time. My grandpa Louis, I wish he could have been here to see it. My Grandparents Bob and Rita, who live nearby in Palo Alto. It has been so wonderful to have a place that feels like home so close by. Thank you all for you help and support.

On a personal note, this graduate school experience has been one of the greatest adventures of my life. I have accomplished things that I never thought possible and have

learned as much about myself as I have about science. I've made friends whom with I will no doubt stay in touch for the rest of my life and have created memories that are too numerous to count. Along the way I have learned how to play foosball, and have discovered the sport of surfing, something that will no doubt remain with me from here on out. I've had the opportunity to travel all over the world and meet some of the world's most brilliant minds. It has been an amazing time. Thank you everyone who has helped make this experience what it was.

Chapter 1 :Introduction

The study of the surfaces of materials has proven especially intriguing due in large part to the fact that surface properties often change dramatically from those of the bulk. Many metals for example will reconstruct or rearrange their surface structure in order to lower their energy thus producing surfaces that are very far removed from a bulk terminated model [1]. Organic molecules will often show preferential direction for specific functional groups at the surface that is not observed in the bulk [2]. The driving factor for these rearrangements is a reduction in the surface energy of the material, which can change dramatically depending on the presence and type of the outside gas/liquid/or solid.

It is the outermost few layers of atoms of a material that are in contact with a substance's outside environment and subsequently determine many factors including solubility, reactivity and catalytic activity. Immediately upon exposure to gases or liquids a clean surface is covered by an adsorbed monolayer of molecular or ionic species. To obtain the surface structures of atoms and adsorbed molecules in equilibrium with the gas or liquid at the interface has been the dream of many surface scientists.

Traditionally surface science studies have been performed at very low pressures and temperatures, both of which are far removed real-life catalytic conditions. This makes applying insight gained from these studies to practical systems difficult. Low

energy electron diffraction (LEED) [3,4] or ion scattering [5] experiments carried out to obtain surface structures can only be performed at low pressures because of the high scattering cross sections of both electrons and ions. Auger electron spectroscopy (AES) and most x-ray photoemission spectroscopy (XPS) experiments performed to investigate the chemical nature of surfaces again fail at high pressures due to the scattering of electrons. In fact, the major obstacle that has prevented a more complete understanding of surfaces in equilibrium with gases or liquids is the scarcity of high-pressure techniques available. Our research has focused on using high-pressure/high-temperature scanning tunneling microscopy to investigate the surface structure of the adsorbed monolayer and high pressure X-ray photoemission spectroscopy to investigate the chemical makeup of the surface.

One area of surface chemistry at high pressures that is hugely important to the world economy is the study of heterogeneous catalysis. Briefly, heterogeneous catalysts are materials, usually solids, that increase the rate of formation of product molecules in a reaction and are made up of a different phase than that of the reactants. Another major purpose of catalysts is to increase the rate of formation of one particular product. That is change the ratio of potential products. Most industrial catalysts are solids in small particle form, and transition metal catalysts in particular are used today in the synthesis of ammonia and the refining of hydrocarbons.

The application of platinum metal as a catalyst started in the early 1800s with the first discovery of a surface catalyzed reaction. The reaction was hydrogen and oxygen reacting to form water, and platinum has been an important, if not the most important catalyst material, ever since. Its ability to effectively catalyze reactions stems largely

from the fact that platinum has very strongly bound valence electrons which "feel" a relatively large effective nuclear charge due to the poor shielding of the d and f shell electrons. These strongly bound electrons prevent the formation of stable surface compounds such as oxides, which can severely reduce the activity of the catalyst. Despite this, these electrons are still available to interact with adsorbed molecules by donating electron density to the anti-bonding orbitals of adsorbates. In addition, platinum also has a partially filled valence shell that can accept electron density from the bonding orbitals of adsorbed molecules, further weakening intramolecular bonds. The breaking of these intramolecular bonds is often what is responsible for the energy barrier for reaction.

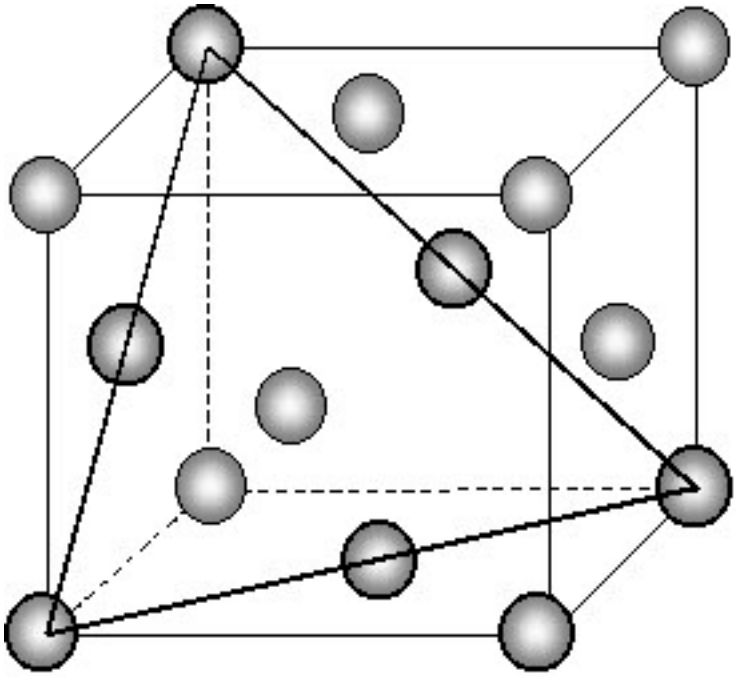

Figure 1.1 – Schematic of a unit cell of an fcc crystal.

In this work a Pt(111) single crystal is used for all of our experiments. Platinum has a face centered cubic unit cell that consists of a cube with an atom in the center of each face as well as at each corner. A diagram of the unit cell is shown in figure 1.1.

Depending on the angle at which the single crystal is cut, the surface structure can be very different. The Miller indices (hkl) determine how a plane is cut. The crystal surfaces (111), (110), and (100) are the three most common crystal planes and are shown in figure 1.2. As can be seen from figure 1.2, surface atoms lying in the plane of each type of surface differ in number of surface nearest neighbors as well as in total coordination number. Each of these surfaces presents different binding sites for adsorbates. Four common sites (atop, bridge, three-fold and four-fold) are highlighted in figure 1.3. The presence of a higher ratio, or lack thereof, of a particular site can cause the surfaces to have very differing activities for the same reaction. Of the three crystal planes discussed, the (111) is the most energetically stable, and is considered to be the most abundant in real catalytic systems.

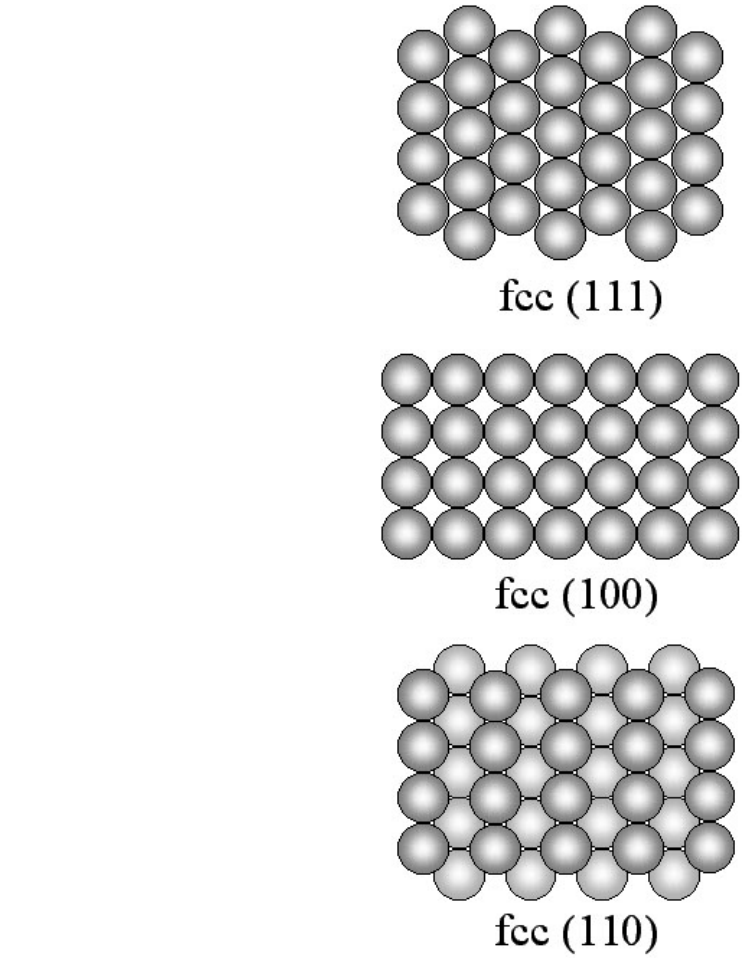

Figure 1.2 – Representations of the three most common fcc crystal faces, (111) (top), (100) center, and (110) (bottom).

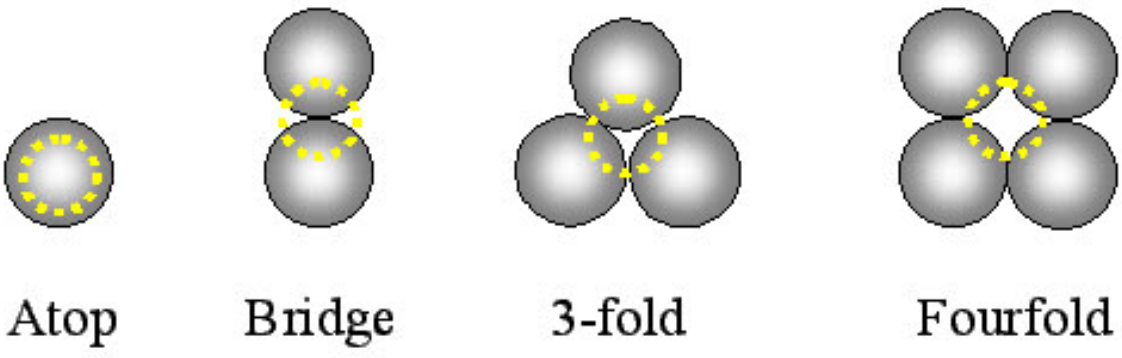

Figure 1.3 – The four most common types of adsorption sites on single crystal terraces.

Many of the studies in this dissertation involve investigating the surface structures that organic molecules form when adsorbed on a metal single crystal. On a single crystal of (111) orientation, the unit cell is hexagonal and can be designated as (1x1). The unit cell is highlighted in figure 1.4a. The numbers in the (1x1) nomenclature refer to the each side of the unit cell, and are essentially multiples of the basis vectors, or interatomic distances of the substrate. For example, structure that can be considered (2x2) is displayed in figure 1.4b. If the axis of symmetry of the adsorbed overlayer aligns with the substrate, then no denotation is given and the overlayer and substrate are aligned. If however, it is rotated with respect to the underlying substrate, then it denoted after the cell distances by an R followed by the rotation angle. For example R 23.4˚. It is also important to remember that unless otherwise noted, the unit cell of the adsorbate has the same rotation as that of the substrate.

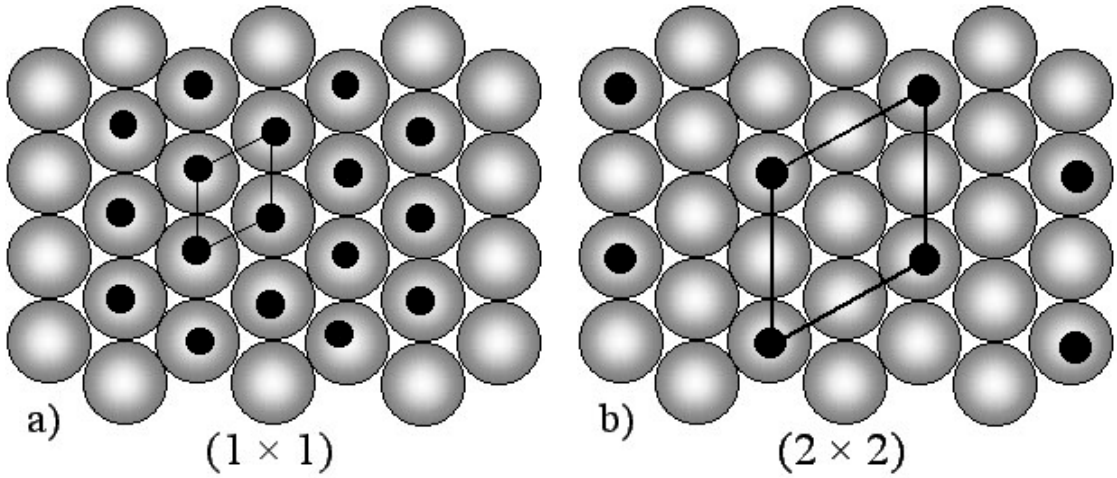

Figure 1.4 – Two different types of adsorption structures on the (111) crystal surface, a) (1x1) and b) (2x2)

Recently there has been an increase in the number of techniques that have the ability to study surfaces under high-pressure conditions. Sum frequency generation vibrational spectroscopy (SFG), is an inherently surface sensitive technique that can be used to study virtually any interface including heterogeneous catalyst surfaces and biological surfaces. Grazing angle x-ray diffraction [6] using high intensity tunable x-rays from a synchrotron shows promise for surface structure determination of atoms and molecules in the adsorbed monolayer, monitoring substrate restructuring at high pressures. Thus far, however, it has rarely been employed for these types of studies. Included in this new class of surface sensitive high-pressure techniques are STM and XPS using a differentially pumped electrostatic lens system. Of all of these techniques however, only STM can give surface structural information

Due to the development of these different techniques, there has also been an increase in the number of studies involving surfaces under high-pressures and especially catalysts. Among these are the investigation of transition metal single crystal catalysts under working conditions [7-9], as well as the effects of poison molecules such as CO or sulphur on catalytic activity [10-13] Other surface studies have independently investigated the interaction of Pt(111) with CO [14-17], and Pt(111) catalyzed H_2/D_2 exchange [18,19]. It has been suggested that in the case of catalytic ethylene hydrogenation over Pt(111) and its poisoning with CO, the role of surface mobility is crucial in allowing catalysis to proceed. The unreactive spectator species ethylidyne allows continuous catalysis because of its ability to quickly diffuse on the surface, which opens reactive sites. The introduction of CO into the system does not displace ethylidyne

but immobilizes it, which poisons the catalyst. Our studies hope to shed some light on the role of the adsorbed monolayer and surface mobility during the catalytic process.

This dissertation describes in detail the experiments performed from 2002 to 2006 using high pressure, high-temperature STM and high-pressure XPS. Chapter 2 is an introduction to the techniques of STM and XPS. Chapter 3 describes our experimental apparatus as well as the complimentary techniques used. Chapter 4 discusses the results obtained from the study of low-pressure C_6 hydrocarbons adsorbed to Pt(111) studied by STM. Chapter 5 describes the catalytic hydrogenation/dehydrogenation of cyclohexene and its poisoning with CO studied by STM. Chapter 6 discusses catalytic H_2/D_2 exchange on Pt(111) and its poisoning with CO studied by STM and XPS. Chapter 7 discusses the catalytic hydrogenation of benzene and its poisoning with CO studied by STM. Finally, conclusions and the future directions of research for my system are discussed in chapter 8.

References

[1] Chan, C. M.; Van Hove, M. A.; Weinberg, W. H.; Williams, E. D. *Surface Science* **1980**, *91*, 440.

[2] Chen, Z.; Ward, R.; Tian, Y.; Baldelli, S.; Opdahl, A.;Shen, Y. R.; Somorjai, G. A. *Journal of the American Chemical Society* **2000**, *122*, 10615.

[3] Koestner, R. J.; Van Hove, M. A.; Somorjai, G. A. *Surface Science* **1981**, *107*, 439.

[4] Van Hove, M. A.; Koestner, R. J.; Somorjai, G. A. *Journal of Vacuum Science and Technology* **1982**, *20*, 886.

[5] Dekoven, B. M.; Overbury, S. H.; Stair, P. C. *Physics Review Letters* **1984**, *53*, 481.

[6] Wang, J. X.; Robinson, I. K.; Ocko, B. M.; Adzic, R. R. *Journal of Physical Chemistry B* **2005**, *109*, 24.

[7] Tang, D. C.; Hwang, K. S.; Salmeron, M.; Somorjai, G. A. *Journal of Physical Chemistry B*. **2004**, *108*, 13300.

[8] Hwang, K. S.; Yang, M.; Zhu, J.; Grunes, J.; Somorjai, G. A. *Journal of Molecular Catalysis A.* **2003**, *204-205*, 499.

[9] Montano, M; Salmeron, M; Somorjai, G.A; *Surface Science* **2006** (To Be Published)

[10] Tilquin, J. Y.; Cote, R.; Guay, D.; Dodelet, J. P.; Denes, G. *Journal of Power Sources* **1996**, *61*, 193.

[11] Grunes, J.; Zhu, J.; Yang, M.; Somorjai, G. A. Catalysis Letters, 2003, 86, 157.

[12] Jones, J. M.; Dupont, V. A.; Brydson, R.; Fullerton, D. J.; Nasri, N. S.; Ross, A. B.; Westwood, A. V. K. *Catalysis Today* **2003**, *81*, 589.

[13] Kimura, H.; Ishikawa, K.; Nishino, K.; Nomura, S. *Applied Catalysis A* **2005**, *286*, 120.

[14] Longwitz, S.R; Schnadt, J; Kruse Vestergaard, E; Vang, R.T; Laesgsaard, E; Stensgaard, I; Brune, H; Besenbacher, F *Journal of Physical Chemistry B* **2004,** *108*, 14497.

[15] Ertl, G.; Neumann, M.; Streit, K. M. *Surface Science* **1977**, *64*, 393.

[16] Kinne, M.; Fuhrmann, T.; Whelan, C.M.; Zhu, J.F.; Pantforder, J.; Probst, M.; Held, G.; Denecke, R.; Steinruck, H.-P *Journal of Chemical Physics* **2002**, *117*, 10852.

[17] Ma, J.; Xiao, X.; Dinardo, N. J.; Loy, M. M. T. *Physical Review B* **1998**, *58*, 4977.

[18] Lu, K. E.; Rye, R. R. *Journal of Vacuum Science and Technology*, **1975**, *12*, 334.

[19] Bernasek, S. L.;Siekhaus, W. J.; Somorjai, G. A. *Surface Science* **1974**, *30*, 1202.

Chapter 2: Scanning Tunneling Microscopy / X-ray Photoelectron Spectroscopy

The two major techniques employed for our studies were high-pressure scanning tunneling microscopy (HPSTM) and high-pressure x-ray photoelectron spectroscopy (HPXPS). Each of these techniques provides very different information about gas/metal interface at high pressures. When used together, these techniques complement each other and can give one an in depth understanding of surface dynamics, structure, and chemical bonding.

2.1 Scanning Tunneling Microscopy

STM is a type of scanning probe microscopy that was developed in the early 1980's by two scientists named Gerd Binnig and Hendrich Rohrer [1,2]. Their early experiments yielded atomically resolved images of silicon single crystal surfaces and proved that STM was a unique technique that allowed *in situ* monitoring of surfaces on the atomic level. Much of the theory behind STM was developed by two American scientists Tersoff and Hamann at Bell Laboratories [3]. STM also spurred the development of a variety of other types of probe microscopes including, atomic force microscopy (AFM), lateral force microscopy (LFM), magnetic force microscopy (MFM),

scanning thermal microscopy (SThM), and near-field scanning optical microscopy (NSOM) among others. For their discovery, Binnig and Rohrer were deservedly awarded the Nobel Prize in physics in 1986.

STM has significant advantages over conventional optical microscopies in that it is not limited by the wavelength of light. This fact causes optical microscopy to fail to resolve features less than ~250 nm. The major fact that limits the spatial resolution of an STM is the quality of the tip and the ability of the instrument to accurately control tip position. To date, lateral resolution of 0.1 Å and vertical resolution of 0.01 Å are commonly achieved. STM is also able to provide images of molecular resolution under a variety of conditions including, ultra-high vacuum [4-6], high-pressures [7-9] and temperatures and in liquids [10] making it one of the most versatile techniques ever developed. Representative images of Pt(111) in vacuum, and under 5 Torr of CO are displayed in figure 2.1 [11]. The major limiting factor of STM, however, is the fact that it requires a conducting surface to yield images. Polymers, oxides and organic systems cannot be directly imaged. Organic molecules adsorbed onto conducting surfaces can be easily imaged however [12]. Some efforts have been made to coat insulating systems with thin layers of conducting materials in order to achieve a conducting surface but the practical value of this technique has yet to be proven. This section discusses in detail the theory behind the development of STM and some of the experimental aspects that must be considered when employing this powerful technique.

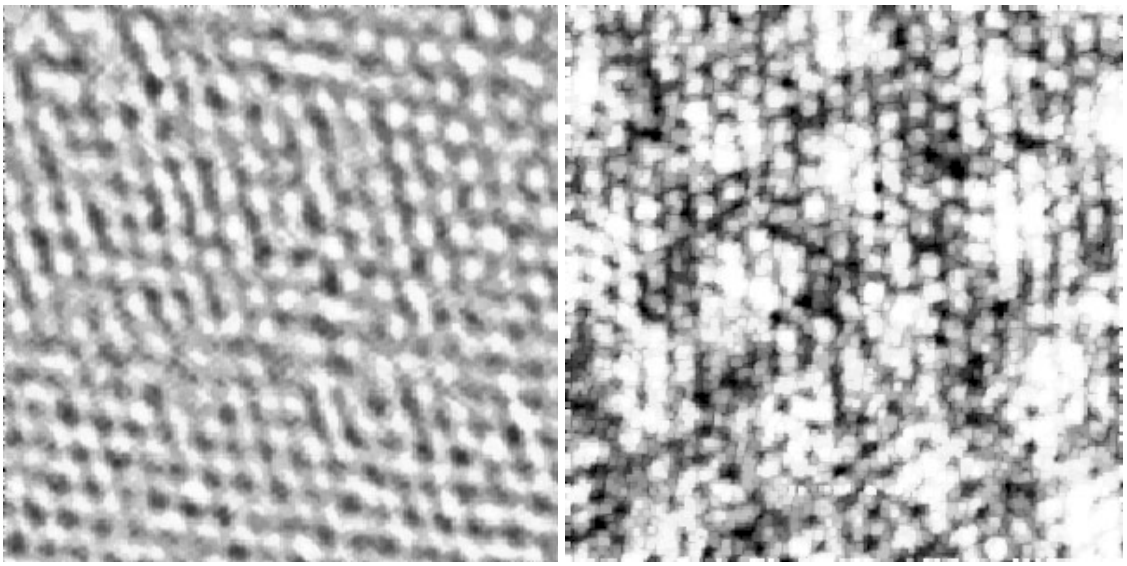

a) **b)**

Figure 2.1 – Pt(111) a) in vacuum, atomic periodicity is observed. b) in the presence of 5 Torr of CO, (√19 x √19) R23.4º CO structure is observed.

2.1.1 STM Theory

STM achieves its amazing resolution by exploiting a quantum mechanical phenomenon called tunneling. In the process of tunneling a fraction of particles (in this case electrons) with energy lower than a potential barrier are able to penetrate into the barrier to a depth of the order of 1-10Å. The probability of finding a particle a given distance within the barrier (d) decays away exponentially as distance is increased, and can be expressed by equation 2.1.

Equation 2.1 - $P \propto e^{\frac{-2d\sqrt{2m\phi}}{\hbar}}$

d = distance

m = mass of the particle

ϕ = height of the potential barrier

$\hbar$ = Plank's constant

The rate of decay is determined by the height of the potential barrier (Φ) and the mass of the particle (m). If the barrier is thin enough, some fraction of the particles can make it through and have a probability of exiting on the other side of the barrier (Figure 2.2). In the case of STM, electrons which classically would be confined within an atomically sharp metallic tip penetrate out into the barrier of the gas or vacuum surrounding the tip. A scanning electron microscopy image of a sample tip is shown in figure 2.3. If the tip is then brought sufficiently close (5-10 Å) to a conducting substrate, some of the electrons within the tip can travel to the substrate, and likewise electrons from the substrate can travel to the tip. In the absence of an external voltage electrons will migrate to create an interface potential sufficient to shift the Fermi levels of each material until they are equal energies.

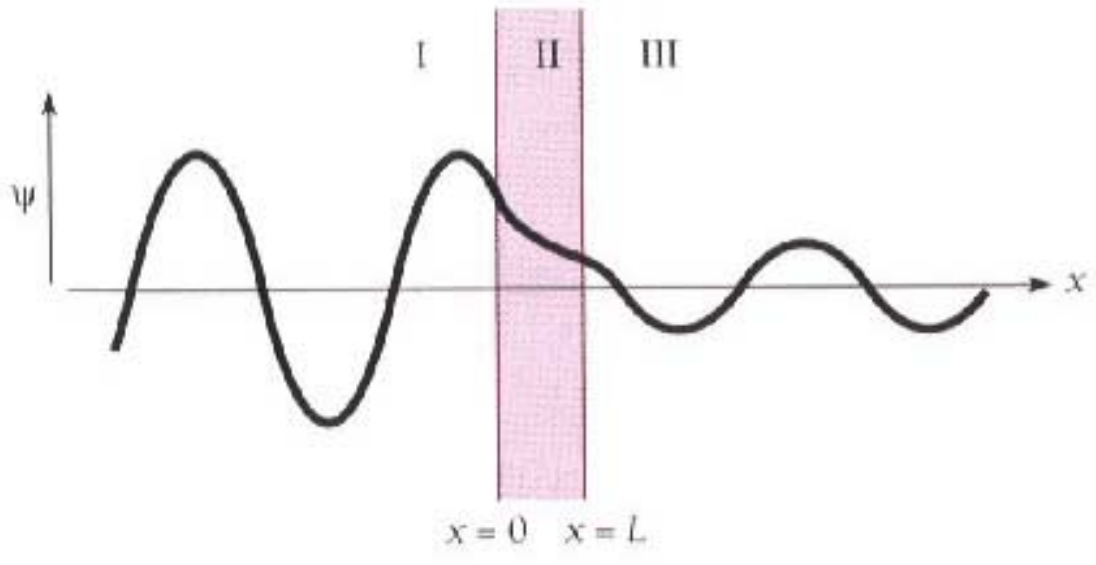

Figure 2.2 – Illustration of a particle tunneling through a potential barrier.

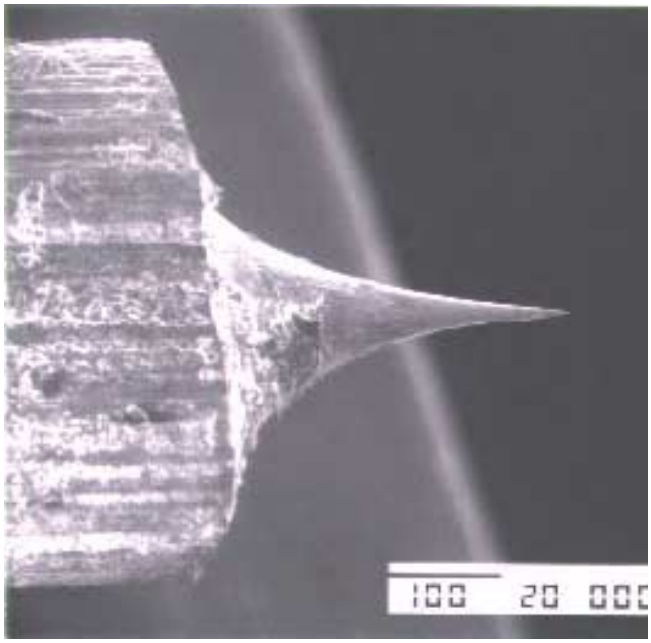

Figure 2.3 – SEM image of an etched tungsten STM tip.

During STM a potential is applied across the tip and substrate which causes a shift of the Fermi level of the tip above or below that of the substrate depending on polarity. Figure 2.4 shows a schematic of the Fermi level shift, as well as, the resulting probability of electron tunneling. The shift of one Fermi level with respect to the other causes preferential current flow from the higher Fermi level to the lower. The magnitude of the current (I), as displayed by equation 2.2, is linearly dependent on the applied voltage (V), but more importantly it is exponentially dependent on the tip/sample distance.

Equation 2.2 - $I \propto Ve^{\frac{-2d\sqrt{2m\phi}}{\hbar}}$

V = applied voltage between tip and sample

d = tip/sample distance

m = mass of the particle

ϕ = height of the potential barrier

$\hbar$ = Plank's constant

This means, that an increase in tip sample distance of just 1 Å, results in a decrease in tunneling current of more than one order of magnitude. Thus, by maintaining a constant current and rastering the tip across the surface, an electronic map of the surface can be generated. This electronic map often looks very similar to a topographical map of the surface.

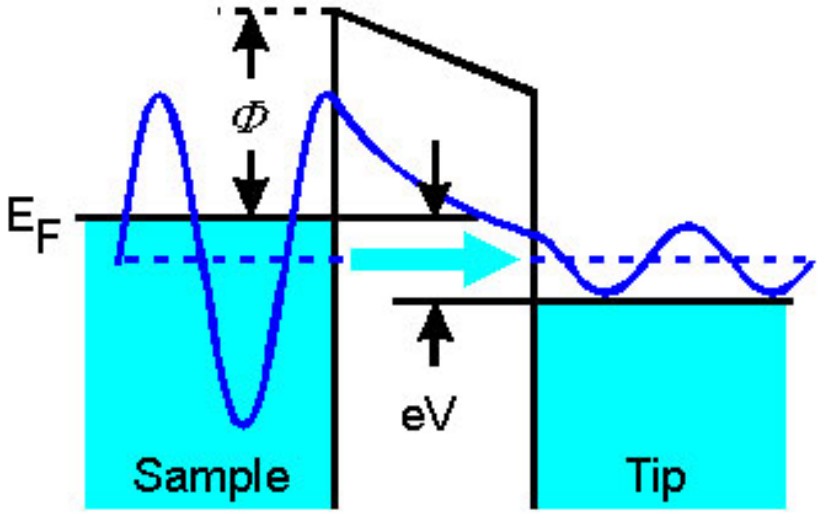

Figure 2.4 – Schematic showing how the application of an external voltage across the tip and sample results in a shift in the Fermi level, and thus the flow of current. Dashed lines represent initial Fermi level energies, and solid lines represent Fermi levels after the application of the potential.

The polarity of the voltage applied dictates weather the tip is probing empty or filled orbitals of the surface. A negative bias causes current to flow into the sample and

into the empty orbitals of the surface atoms or molecules. Thus a major factor in the appearance of the resulting image is the density of states of these empty orbitals. Similarly, sample to tip current probes the filled states of the surface atoms and molecules. For this reason, conducting materials such as metals whose HOMO and LUMO orbitals are degenerate generally yield identical images for either polarity, while semiconducting materials or insulating molecules adsorbed on a conducting substrate may yield drastically different images.

2.1.2 STM Experimental Considerations

The extreme accuracy with which an STM must be moved discards the possibility that these movements could be achieved using conventional motors and gears. For this reason STM uses piezoelectric materials (piezos) to control the tip movement with adequate accuracy. Piezos are materials that can be permanently electrically polarized when heated in the presence of a large electric field. The unique property of peizos is that they then will change their shape when a voltage is applied to them. As long as the piezos are not heated above a certain temperature referred to as their Curie temperature, they can reproducibly be manipulated with subangstom precision simply by applying voltages. In practice in most piezos some hysteresis is observed, but it can be largely limited by staying well within the linear portion of the hysteresis curve. Accomplishing bending of a piezo is done by forming piezoelectric materials into tubes that are separated lengthwise into four quadrants by an insulating gap. The insides and the outsides of the tubes are then coated with conducting materials. By applying opposite voltages across opposite quadrants, an overall bending of the tube is accomplished. Applying the same

voltages to all quadrants results in contraction or expansion of the entire tube. Figure 2.5 illustrates the process of bending a piezo by application of voltages.

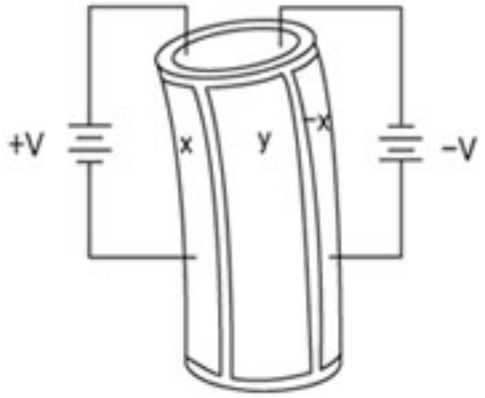

Figure 2.5 – Image illustrating how applying voltages of opposite signs to opposite side of a piezoelectric tube can result in it bending.

Most STMs may be operated in one of two types of scanning modes, each of which has its benefits and drawbacks. The first type is constant current mode. In this mode, the current between the tip and sample, which is in practice dictated by tip-sample separation and the local density of states of the substrate near the Fermi level [13], is held constant. The tip is then rastered across the surface using the piezoelectric tube (Figure 2.6). As the tip encounters a feature which is raised or lowered from the surface, or has a higher or lower DOS near the Fermi level its height must be adjusted by the piezos to maintain a constant tunneling current. The adjustments in the height of the tip are monitored and displayed on a computer screen giving the user an electronic map of the surface. The main advantages of the constant current mode are that it can be performed

on relatively rough surfaces and the movements of the tip height are a fairly direct method of surface measurement.

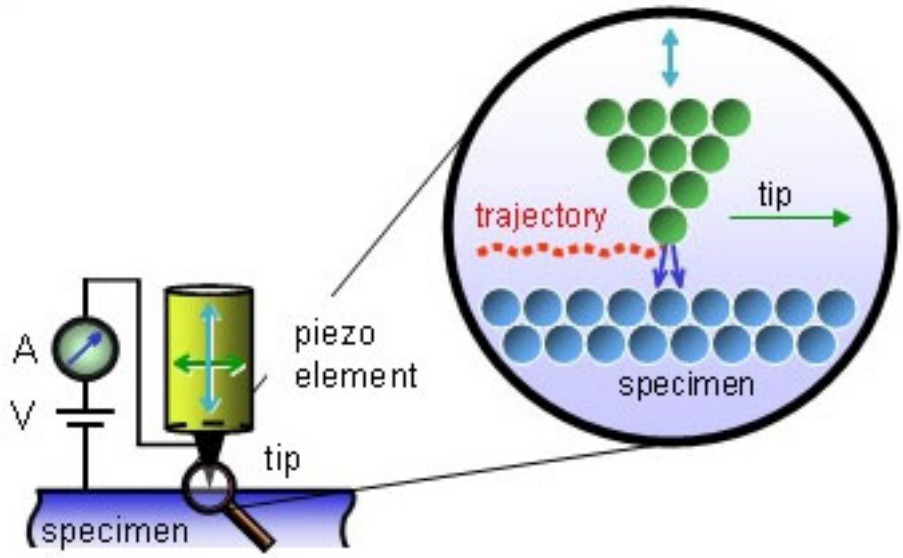

Figure 2.6 – Schematic of an STM tip as it is rastered across the surface of a single crystal.

The other major type of scanning is constant height mode. In this case, the tip height is held constant as the tip is rastered across the surface and the changes in tunneling current are monitored. For example, as the tip passes over an adsorbate which extends away from the surface, the tunneling current will increase as the tip sample separation is smaller. The changes in current are monitored and converted to a surface topography map which can be displayed on a computer. The main advantage of constant current mode is that it can be performed much faster than constant current mode, as there is no physical adjustment of the tip height by a feedback loop. However, constant height mode does necessitate extremely flat surfaces to operate. One must therefore consider the benefits and drawbacks of each mode before deciding whether a system should be

investigated using constant height or constant current mode. Illustrations of each mode are shown in figure 2.7.

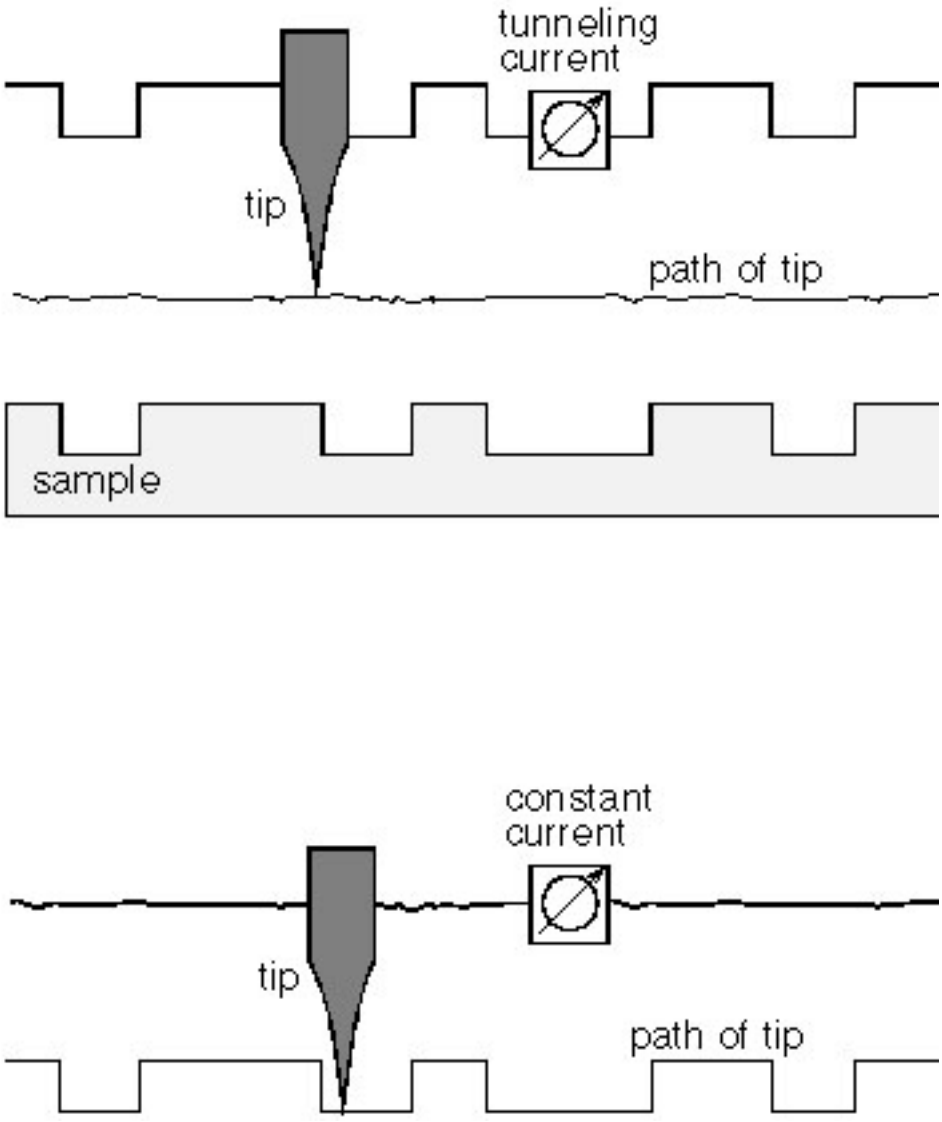

Figure 2.7 – Schematic of the movement of the STM tip and the resulting tunneling current during scanning in constant height mode (top) and in constant current mode (bottom)

The exponential dependence of current on tip-sample separation that is responsible for the excellent vertical resolution of STM, and the small scale of the

currents measured make STM extremely sensitive to external noise. It is this noise in fact that is commonly the limiting factor in the resolution of images obtained. Much care must thus be taken to limit any noise in the system. Mechanical vibrations which are generated from building noise, system vibrations and acoustic noise, are limited by various vibration dampening systems. Also, a STM scan head and tip with high resonance frequencies can limit the ability of external noise to excite the scan head. In addition the small scale of the currents being measured means that the utmost care must be taken in electrically insulating the system from external currents which may seriously compromise the capabilities of the system.

2.2 X-ray Photoelectron Spectroscopy

X-ray photoelectron spectroscopy (XPS), also referred to as electron spectroscopy for chemical analysis is a semi quantitative technique for determining chemical composition and is based on the photoelectric effect. This process, first discovered by Einstein in the 1920's, involves the photon-induced ejection of an electron from an atom, molecule or solid. For his efforts, Einstein received the 1921 Nobel Prize in physics [14]. In the mid 1960's, a Swedish scientist named Kai Seigbahn used this process to develop the technique of XPS [15]. One of the major benefits of XPS, and one that makes it especially applicable to our research, is its inherent surface sensitivity due to the low mean free path of the ejected electron within a solid. Thus, XPS provides us with a technique that can give chemical information about the surface of a system also studied with STM under identical conditions.

2.2.1 XPS Theory

XPS is traditionally a high vacuum technique that utilizes the photoelectric effect to monitor the chemical composition of the top few layers of the surface of a material. During his experiments during the early part of the 20th century, Einstein noticed that irradiating the surface of a metal with high energy electromagnetic radiation can cause the ejection of electrons from the surface. Whether or not electrons were ejected did not depend on the intensity of the light, only the energy, or wave length of the light. For each material studied, there was a specific energy of light, above which electrons could be ejected, and below which had no effect. These experiments showed clear evidence of the particulate nature of light and these "particles" were subsequently called photons. In the process observed by Einstein, called the photoelectric effect, the high-energy photons, in our case soft x-rays cause electronic transitions in the surface atoms. Photons with sufficient energy are able to overcome the binding energy of the electrons and eject them out of the surface. This process is illustrated in figure 2.8, and the resulting current measurements are displayed in figure 2.9. Photons with an energy below the work function of the material do not result in ionization of the atom. The energy of the absorbed photon goes into the removal of the electron from the atom (binding energy), and kinetic energy of the ejected electron. Once ionized, the atom is left in an unstable state, with a core electron vacancy. The atom can then relax by undergoing the Auger process discussed in the subsequent chapter, or by ejecting a photon

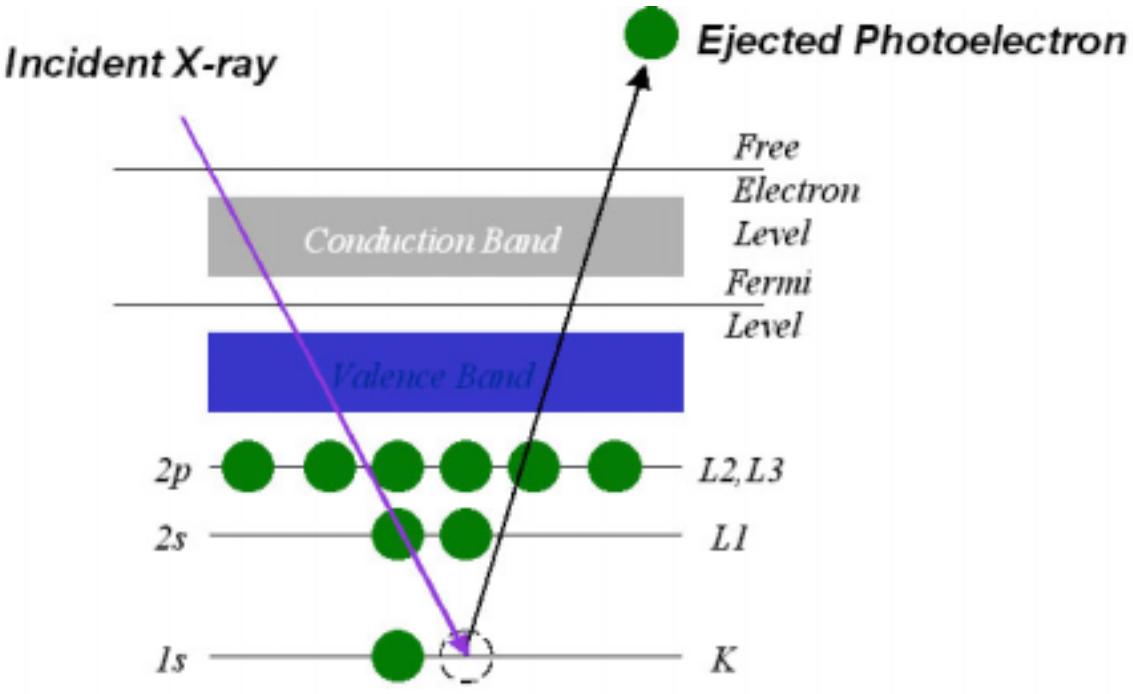

Figure 2.8 – Image displaying the ejection of a core level electron by an incident x-ray (The photoelectric effect)

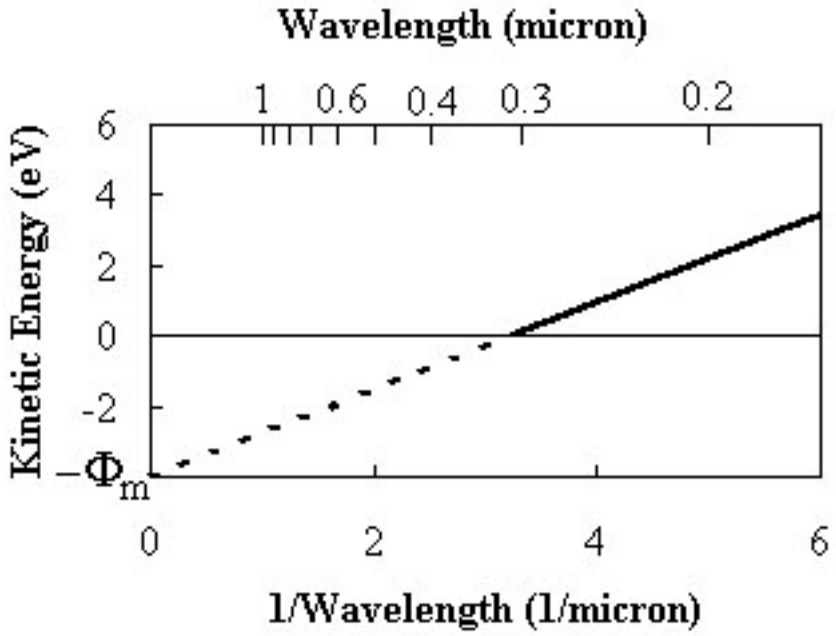

Figure 2.9 – Schematic of the kinetic energy of an ejected electron. Below a specific wavelength (in this case 300nm) corresponding to the work function of the material, no current is observed.

Although the penetration depth of the incident photons can be relatively large, on the order of a micrometer, the escape depth of the photoelectron is generally subnanometer. It does however, vary with electron energy as well. By using a known incident photon energy and monitoring the kinetic energy(KE) of the ejected electrons, one can determine the binding energy of the electrons within the atom by using equation 2.3.

Equation 2.3 - $KE = h\nu - BE - \phi$

$h\nu$ = energy of incident photon

BE = binding energy of the electron

ϕ = work function of the detector

Equation 2.3 displays the relationship between the kinetic energy of the photoelectron, the incident photon energy and the binding energy. In practice, the equation must also include the quantity ϕ, the work function of the detector, generally a few electron volts. The binding energy of the a particular electron within an orbital is specific to each element, so monitoring the kinetic energy, and thus the binding energy, can give the chemical composition of the surface. In addition since most atoms have several electrons in several orbitals, many peaks can be cross referenced for further accuracy. One added benefit of XPS is the fact that small changes in the chemical environment of an atom can

cause binding energy shifts that are easily detected. For example a carbon atom in a hydrocarbon versus a carbon monoxide molecule is shifted by more than 2 eV, making resolving these separate peaks easy. This can be observed in Figure 2.10. Also, peak shifting due to adsorption site is also possible. The peak located at ~286 eV in figure 2.10 is clearly split into two peaks representing the bridge bound and atop bound CO molecules. A third example of the sensitivity of XPS is shown in figure 2.11 in which the platinum 4f peak is composed of three individual peaks corresponding to the bulk platinum, the free surface platinum, and the CO bound surface platinum atoms. By monitoring the relative intensity of the free surface atom and CO bound surface atom, information about surface coverages can be obtained. In addition two sets of similar peaks are shown that are due to spin orbit coupling effects.

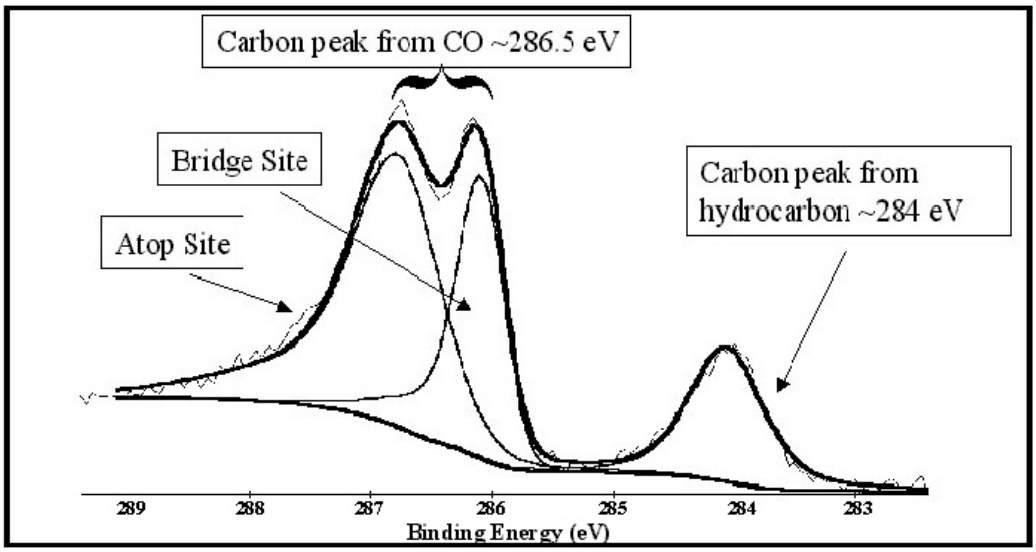

Figure 2.10 – Sample XPS spectrum showing splitting of carbon peaks from carbon atoms in a hydrocarbon (284 eV) and a carbon monoxide molecule (285.5 eV). The peak located at ~286.5 eV is split into two separate peaks corresponding to both the bridge bound and atop CO molecules.

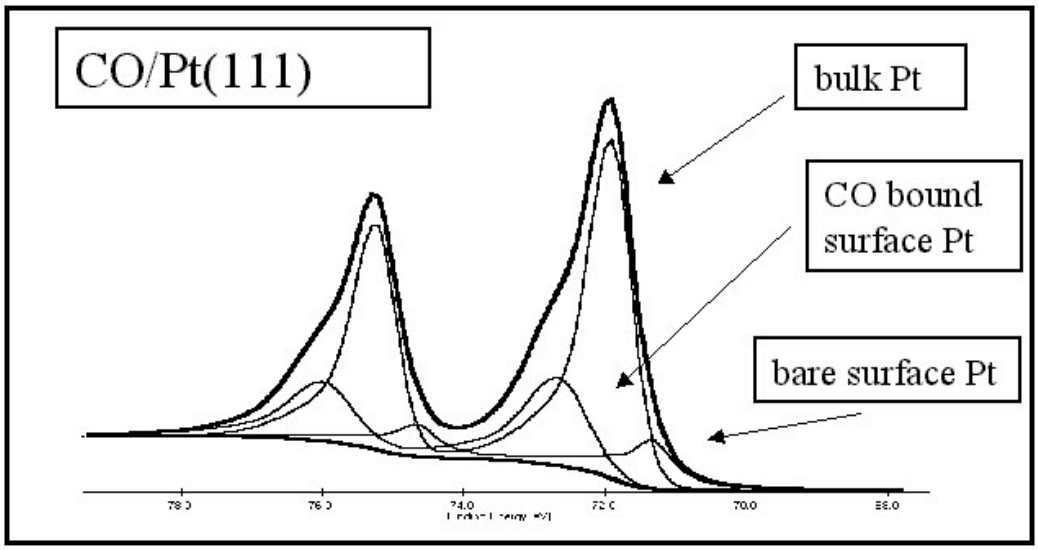

Figure 2.11 – Sample XPS spectrum in the platinum 4f region. The platinum peaks are split into bulk platinum, bare surface platinum and surface platinum the is bound to a CO molecule.

2.2.2 XPS Experimental Considerations

When performing XPS at high pressures, there are several experimental factors and complications that arise. The first of which is the quantitative nature of XPS. The intensity of an XPS peak is directly proportional to the number of species on the surface that give rise to that peak if all other parameters are held constant. A general formula for peak intensity is shown in equation 2.4.

Equation 2.4 – $I = N\sigma DJL\lambda AT$

N = atoms/cm^3 σ = photoelectric cross-section, cm^2

D = detector efficiency

J = X-ray flux, photon/cm^2-sec

L = orbital symmetry factor

λ = inelastic electron mean-free path, cm

A = analysis area, cm^2T = analyzer transmission efficiency

Of all of the parameters, the detector efficiency can cause many difficulties, as it may change due to diffraction effects resulting from surface structure changes. For example the transition from a c(4x2) structure of CO on Pt(111) to an incommensurate structure may cause changes in peak intensity that have nothing to do with surface populations. The nature of these effects is diffraction of the photoelectron, resulting in the area monitored by the detector not necessarily corresponding to a representative sample of surface composition. This effect has been studied fairly extensively over recent years[16,17]. One other concern when trying to extract relative quantities of different surface elements arises from the different sensitivities of different elements. These variations in sensitivities for different elements, are well understood, but much care must still be taken during data analysis to ensure accurate results.

Overall, however, the major experimental obstacles in high-pressure XPS stem from the presence of a significant backpressure of gas within the chamber during measurement. The initial processes included in the photoelectric effect remain largely unchanged, since photons can travel through high-pressures of gases fairly easily due to their low adsorption cross section. It is, however, important to begin with a large number of photoelectrons. To accomplish this, a high intensity source is necessary. In our experiments, we have used synchrotron radiation at the Advanced Light Source (ALS) in

Berkeley, California to ensure a large x-ray flux at the surface. Upon the ejection of the photoelectron, some problems arise. The first problem is the absorption or collision of the photoelectron with the gas molecules. The second is analyzing the energy of the electrons using a concentric hemispherical analyzer (CHA) that must operate in UHV conditions. To limit the gas phase absorption, an aperture with a diameter of ~1mm, is placed very close to the sample. This distance is variable but is generally about 0.5 mm. By providing a very small path length between the sample and the aperture, a significant fraction of the electrons can pass through the aperture before undergoing collision. On the other side of the aperture is a small chamber that is continuously pumped with a turbomolecular pump to reduce the pressure. Once they have passed through the aperture, the electrons are focused with an electrostatic lens system though another aperture at the rear of the chamber. The second chamber is also pumped by a turbomolecular pump. The process is repeated into a third chamber and finally analyzed using the CHA. Each stage of this differentially pumped electrostatic lens system can lower the pressure by three orders of magnitude, and experimental systems involving pressures up to 10 Torr correspond to pressures at the detector of ~1 x 10^{-8} Torr.

References

[1] Binnig, G; Rohrer, H; Gerber, C; Weibel, E. *Physical Review Letters* **1982**, *49*, 57.

[2] Binnig, G; Rohrer, H; Gerber, C; Weibel, E. *Applied Physics Letters* **1982**, *40*, 178.

[3] Tersoff, J; Hamann, D.R.; *Physical Review B* **1985**, *31*, 805.

[4] Guntherodt, H.J.; Wiesendanger, R., Eds. Scanning Tunneling Microscopy I; Springer-Verlag:Berlin, 1992.

[5] Borg, A; Hilmen, A.-M; Bergene, E; *Surface Science* **1994**, *306*, 10.

[6] Ritz, G; Schmid, M; Varga, P; *Physical Review B* **1997**, *56*, 10518.

[7] Montano, M; Salmeron, M; Somorjai, G.A; *Surface Science* **2006** (To Be Published)

[8] Longwitz, S.R; Schnadt, J; Kruse Vestergaard, E; Vang, R.T; Laesgsaard, E; Stensgaard, I; Brune, H; Besenbacher, F *Journal of Physical Chemistry B* **2004,** *108*, 14497.

[9] Hendriksen, B.L.M; Frenken, J.W.M; *Physical Review Letters* **2002,** *89***,** 046101.

[10] Yau, S.-L; Kim, Y.-G; Itaya, K *Journal of the American Chemical Society* **1996**, *118*, 7795.

[11] Montano, M; Tang, D.C; Somorjai, G.A. Catalysis Letters 2006, 107, 131.

[12] Land, T.A; Micheley, T; Behm, R.J; Hemminger, J.C; Comsa, G. *Journal of Chemical Physics*, **1992**, *91*, 6774.

[13] Wiesendanger, R.; Guntherodt, H.-J., Eds. *Scanning Tunneling Microscopy III*; Springer-Verlag: Berlin, 1993.

[14] Einstein, A.; *Annalen der Physik* **1905**, *17*, 132.

[15] Siegbahn, K.; Nordlin, C.; Fahlman, A.; Nordberg, R.; Hamerin, K; Hedman, J.; Johansson, G.; Bergmark, T,; Karlsson, S.-E.; Lindgren, I.; Lindberg, B. *Nova Acta Regiae Soc. Ups. Ser. IV* **1967**, *20*, 1.

[16] Kinne, M.; Fuhrmann, T.; Whelan, C.M.; Zhu, J.F.; Pantforder, J.; Probst, M.; Held, G.; Denecke, R.; Steinruck, H.-P *Journal of Chemical Physics* **2002**, *117*, 10852.

[17] Bondino, F.; Comelli, G.; Esch, F.; Locatelli, A.; Baraldi, A.; Lizzit, S.; Paolucci, G. Rosei, R. *Surface Science* **2000**, *49*, L467.

Chapter 3: Experimental System and Supporting Techniques

All scanning tunneling microscopy experiments were performed on the two-chamber system described below and shown in figure 3.1 [1,2]. Briefly, the system is composed of a UHV sample preparation chamber equipped with, sputtering, annealing, mass spectrometry, and Auger electron spectroscopy capabilities. There is also a high-pressure reaction cell in which STM experiments were performed. A load lock, which can be pumped independently, is attached to the STM chamber, which allows for transfer of the sample, and/or tip to the system without having to vent either chamber. The entire system is bolted to a wooden frame made of 4" x 4" Douglas fir. Four air legs (Newport Laminar Flow Isolators, I-2000 series) support the system and help to dampen vibrations from the building coming through the floor.

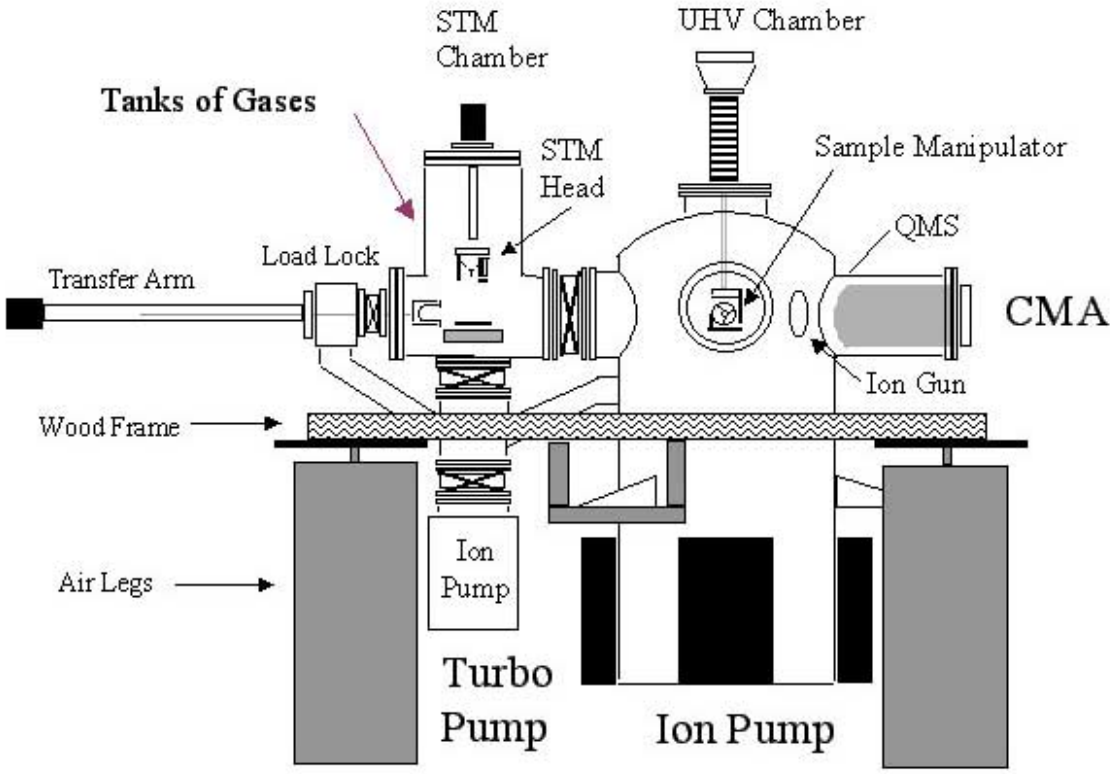

Figure 3.1 – Diagram of the two-chamber STM system. From [3]

All of the high-pressure x-ray photoelectron experiments were performed in a two-chamber system at beamline 11.0.2 at the Advanced Light Source in Berkeley. A prototype of the system has been discussed in detail [4]. The system is composed of a sample preparation chamber equipped with sputtering, annealing, mass spectrometry and LEED capabilities. The system also contains a high-pressure reaction chamber for XPS measurements capable of taking measuring at pressures up to 10 Torr. This chapter describes the STM chamber, the STM design, sample preparation, the UHV chamber and the instruments contained therein in detail, as well as the XPS chamber.

STM

3.1: UHV Chamber

The UHV chamber is a standard Varian surface analysis chamber equipped with a nitrogen cooling line for annealing, sputtering gun, electron beam heater, Auger spectroscopy, oxygen and argon gas inlets and mass spectrometry. The system is pumped by a turbomolecular pump (Pheiffer 60 L/sec), a 200 L/sec ion pump, and a titanium sublimation pump. During operation the base pressure of the system is $< 2 \times 10^{-10}$ Torr.

3.1.1 : Sample Preparation

The single crystal we used was platinum (111) cut within 0.3˚ of accuracy from Matek Corporation. The diameter of the crystal is 10mm and the thickness is 2mm. If need be, the crystal was mounted in Koldmount epoxy, and polished using Metadi diamond paste polishing compound on Buehler Microcloth polishing cloths. Decreasing grit size was used beginning at 15 micron down and finishing with 0.25 micron. Once the crystal had been satisfactorily polished it was sonicated in acetone to remove the epoxy and finally sonicated in methanol to remove any surface residue. Once the crystal was clean, it was etched in room temperature aqua regia to etch off surface defects caused by the polishing process. After sonicating in deionized water to remove residual aqua regia, the crystal was spot-welded to a tantalum disc with a diameter of 11-12 mm. Sample mounting was accomplished by tantalum pressure clamps holding the tantalum disc around the base of the single crystal.

Once the crystal has been mounted and inserted into the UHV preparation chamber, it was cleaned to remove surface contaminants by ion bombardment. Our ion gun is a Varian ion bombardment gun (model# 981-2043). In the process of ion bombardment, inert gas ions, usually neon or argon are created by collisional excitation with electrons from a hot filament. A continually pumped backpressure of inert gas allows for a steady supply of gas molecules for ionization as well as the removal of contaminant molecules that are sputtered off the surface. Gas pressures in the range of 1 x 10^{-5} Torr are generally used. Once the positive ions have been generated by the filament, they are focused and accelerated by an electrostatic lens system. The newly created beam of ions has energies generally ranging from 0.5 – 3 keV. In our studies 1keV was chosen as the ideal sputtering energy. Upon encountering the surface, these highly energetic ions cause the ejection of small clusters or atoms of surface material, thus removing the contaminant layer and exposing a clean but definitely not atomically flat underlying layer. Figure 3.2 displays the sputtering process.

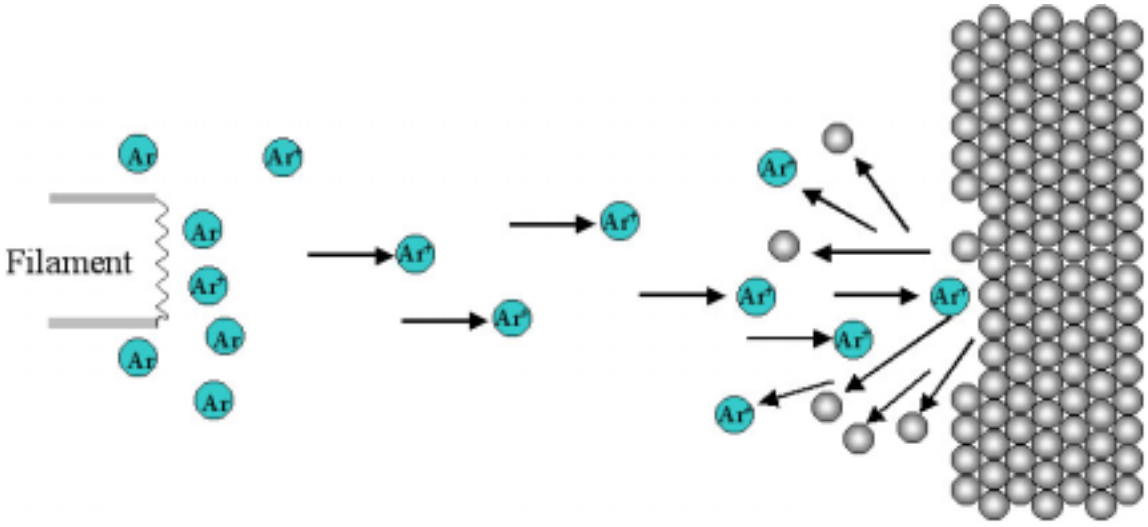

Figure 3.2 – Schematic of the ionization of the argon gas and the removal of the surface layers of a crystal through sputtering.

After ion bombardment, the sample is clean but no longer contains the large atomically flat terraces needed for STM and thus it must be annealed to recover the surface crystallinity. To accomplish the specific heating of the crystal, electron bombardment was chosen as the best technique for annealing. In electron bombardment, a tungsten wire is doped with thorium to lower the work function. The wire is then heated in vacuum by passing a current (typically ~2A) through the wire. The heating gives the valence electrons in the atoms in the wire enough thermal energy to overcome the work function of the metal, which creates an electron cloud around the filament. The filament is then biased negatively with respect to the chamber, which accelerates the electrons away from the filament towards the chamber around it. Typical electron energies are ~1.5keV. In our system the filament is enclosed in a ceramic tube with a small (0.5cm) opening at one end. The tube absorbs the ejected electrons and allows for the high-energy electron source to be directionalized. The opening of the tube is then placed directly behind the sample forcing the majority of the electrons to collide with the rear of our single crystal sample. The kinetic energy that is transferred to the sample heats it considerably and temperatures up to 1500°C can easily be reached. Our sample wa heated in to ~900˚C for about 5 minutes. The heating of the sample give the surface atoms sufficient thermal energy to diffuse readily around on the surface and reach their thermodynamically most stable positions which is that of the bulk crystal lattice. During annealing, the sample holder is held in contact with a liquid nitrogen cooled copper block to minimize the temperature of the sample holder. Depending on the level of sample cleanliness prior to our cleaning cycle, several cleaning cycles with varying sputtering

and annealing times may be used. Just prior to introduction to the STM chamber the sample is flashed back to annealing temperature for 1 minute to remove any contaminants that may have adsorbed during cooling. Sample STM images showing the resulting crystalline surface are shown in figure 3.3.

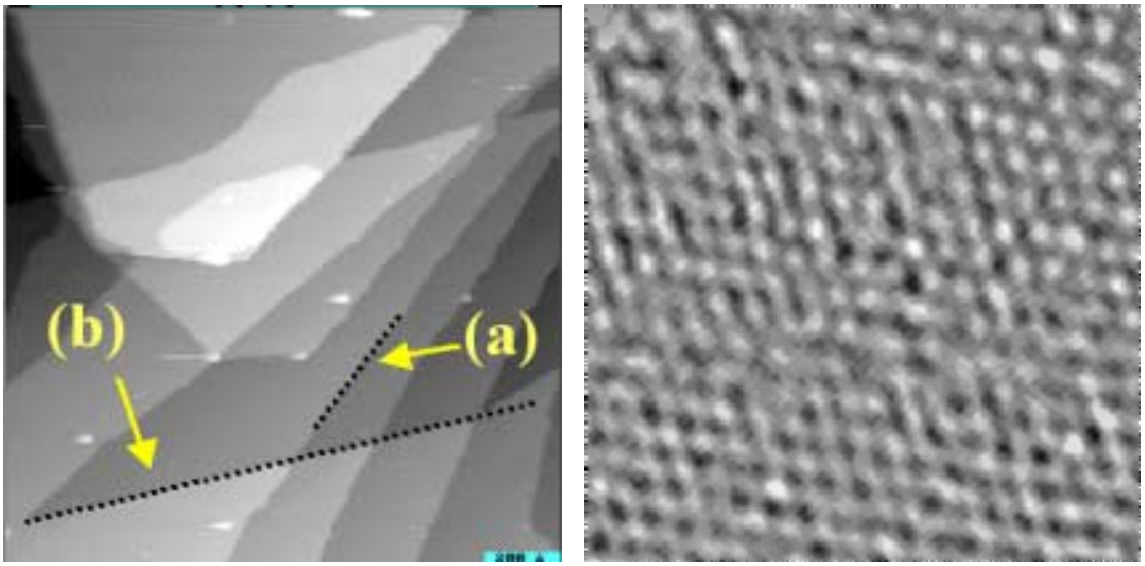

Figure 3.3 – Crystalline surface of Pt(111) after annealing (left) 1500Å x 1500Å STM image of Pt(111) at 300K. Atomic steps corresponding to both (a) crystal miscut of ~0.3º and (b) [110] dislocation planes, are resolved . (right) 50Å x 50Å image of Pt(111) in vacuum at 300K. Atomic periodicity is resolved

3.1.2 Mass Spectrometry

The UHV chamber is equipped with a Stanford Research Systems mass spectrometer for residual gas analysis. The system contains a quadrapole analyzer that covers a mass range from 2 to 100, and is sensitive down to partial pressures of ~$1x10^{-11}$ Torr. A sample mass spectrum of the background during a typical day is shown in figure

3.4. The major peaks present correspond to hydrogen (mass 2), water (mass 18), and carbon monoxide (mass 28). The mass spectrometer is used for leak checking the system with helium, analyzing the purity of the reactant gases, and also for analyzing gas samples leaked from the high-pressure STM chamber during reactions. A two-foot long stainless steel flex tube is connected from the STM chamber to the UHV chamber through a variable leak valve. By leaking small amounts (<1 x 10^{-6} Torr) of gas from the STM chamber to the UHV chamber, the gas phase products and reactants in our high-pressure chamber can be monitored as a function of time. From this we can obtain reaction rates, and by repeating our experiments over a variety of temperatures activation energies are calculated.

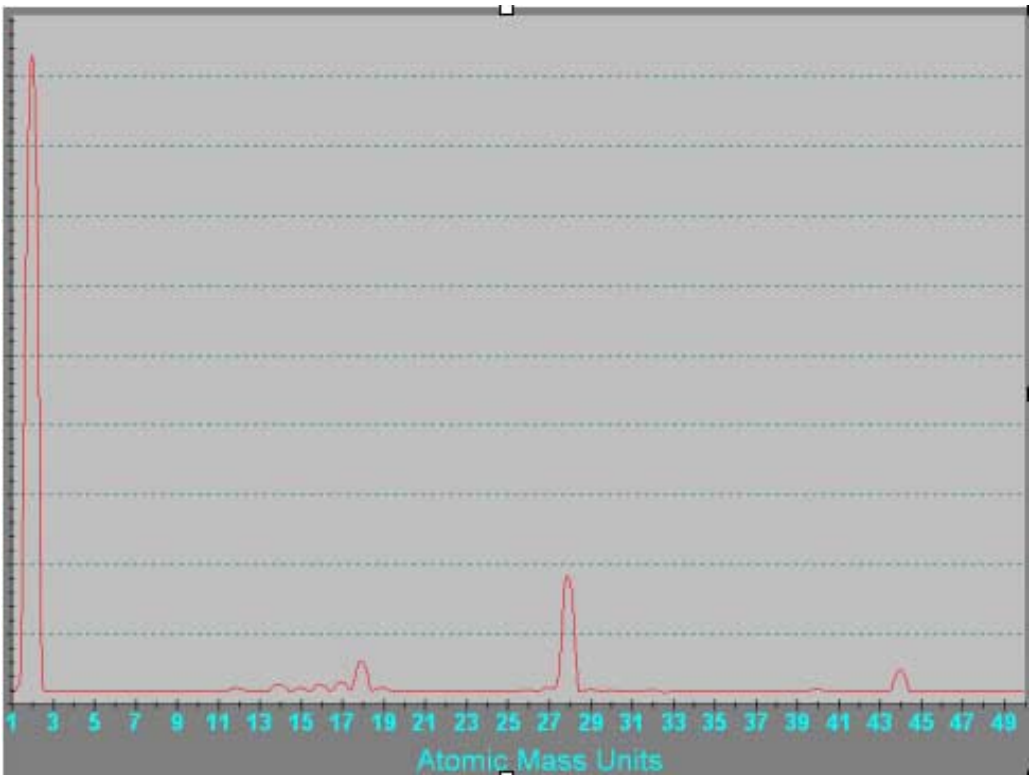

Figure 3.4 – Sample mass spectrum of UHV background. Peaks correspond to hydrogen (2), water (18), carbon monoxide (28), and carbon dioxide (44)

3.1.3 Auger Electron Spectroscopy

A Varian Auger electron spectroscopy (AES) system was also used in the UHV chamber to monitor the surface cleanliness of our sample. AES utilizes the Auger process to detect the atomic species that are present on a surface. This is accomplished by bombarding the sample surface with a high energy (3keV) electron beam. These incident electrons can cause a core electron from a surface atom to be ejected, thus leaving the atom in an energetically unstable state. The core electron vacancy can then be filled by an outer shell electron. This process lowers the energy of the atom and the energy can be released through the ejection of a valence shell electron. This ejected electron, called the Auger electron, has a characteristic kinetic energy (KE) that can be calculated from equation 3.1[5]:

Equation 3.1 $KE = E_a - E_b - E_c$

Ea = energy of the core electron that was removed

Eb = energy of the electron that fills the empty orbital

Ec = energy of the valence electron ejected

A schematic illustrating the Auger process is displayed in figure 3.5. Each element can undergo a variety of Auger transitions, and yields a characteristic Auger spectrum containing peaks for several different transitions. In total, three electrons have been used in the process, and the atom has been left in a doubly ionized state [6].

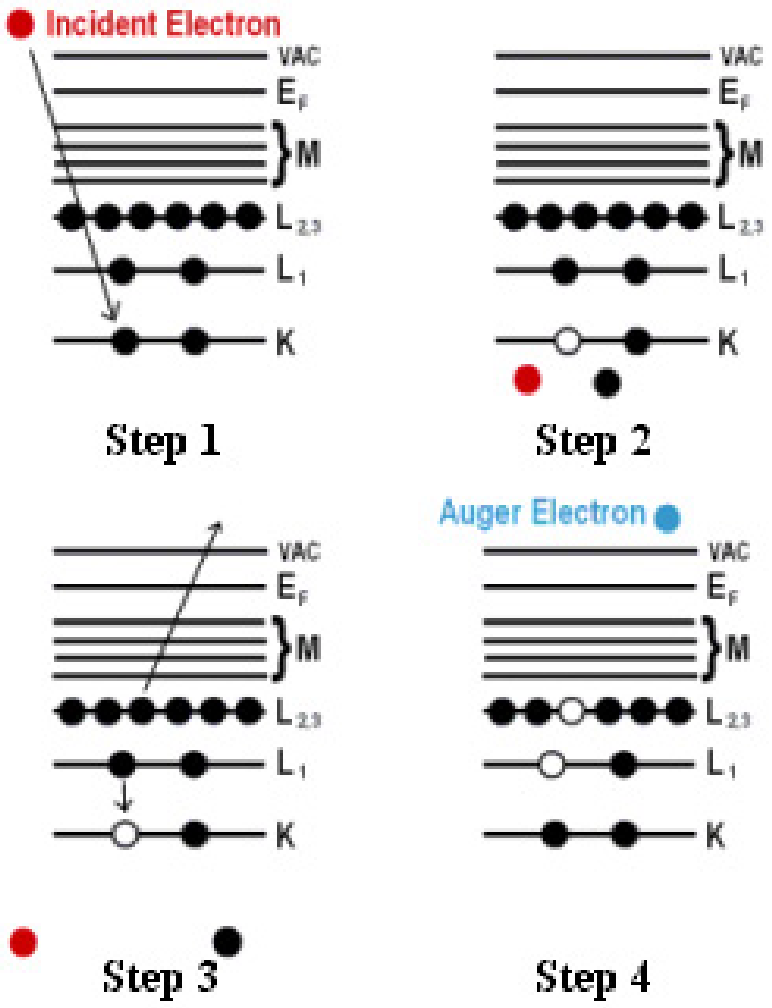

Figure 3.5 – Diagram of the four step Auger process. Step 1: High energy electrons hit the surface atoms. Step 2: Atomic ionization by the removal of a core electron. Step 3: Higher shell electron collapses down to fill core vacancy. Step 4: Energy released from collapse results in the emission of an outer shell electron (Auger electron).

Electron detection is accomplished with a cylindrical mirror analyzer (CMA), which is shown schematically in figure 3.6. In the CMA design, there is a concentric inner cylinder that is grounded, and an outer cylinder to which a negative scanning

potential is applied. Electrons emitted from the surface over a reasonable solid angle are passed through a fixed slit in the inner cylinder. As the particles experience the retarding field of the outer cylinder, if they have a kinetic energy within a specific narrow range, they are reflected back through a second set of slits in the inner cylinder and come to focus at the first dynode of an electron multiplier. Varying the potential on the outer cylinder can adjust the electron energy, which is allowed to pass.

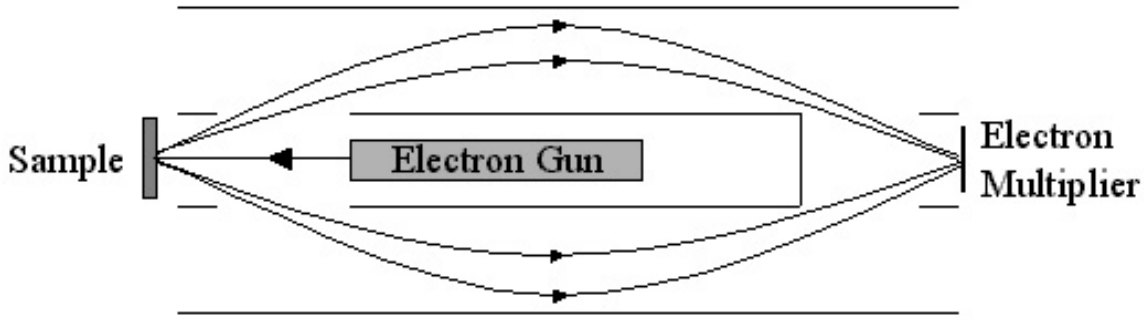

Figure 3.6 – Diagram of a cylindrical mirror analyzer. By applying a voltage between the inner and outer cylinders, only electrons of a very specific energy are allowed to pass between the two slits and reach the detector.

A representative Auger spectrum is displayed in figure 3.7, showing the surface before and after the sputtering and annealing cleaning procedure discussed previously. In figure 3.7a, a large peak corresponding to surface carbon, the most common contaminant, can be seen at 272 eV. After the cleaning procedure, this peak has been largely removed, and all that remains are the platinum peaks.

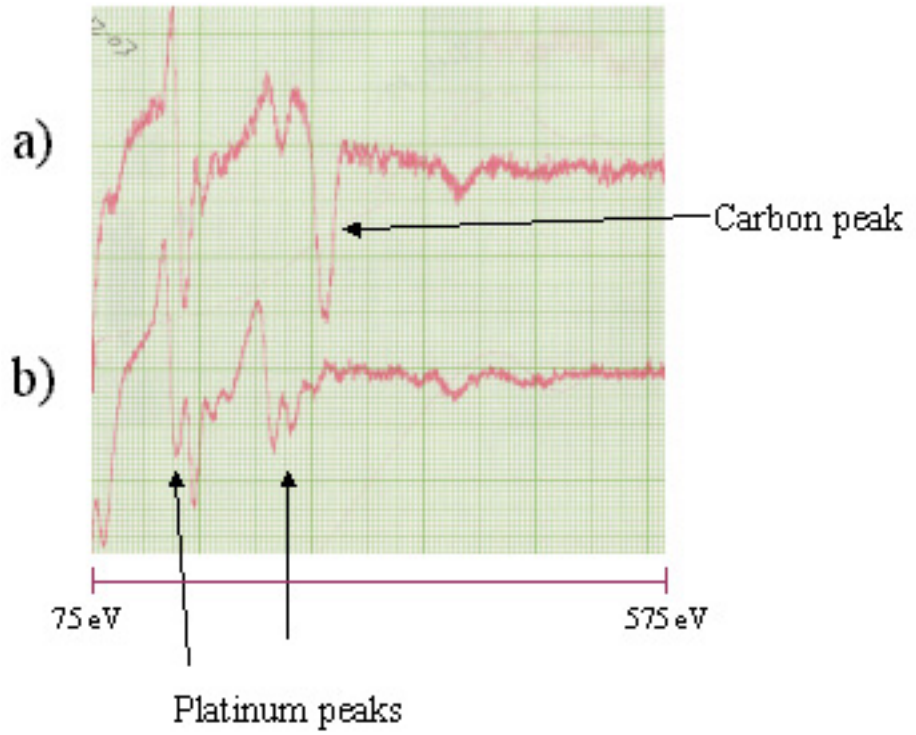

Figure 3.7 – Sample Auger spectra of platinum(111). The carbon peak that is clearly visible in spectrum a) is mostly removed after one cleaning cycle, as is observed in spectrum b).

3.1.4 Sample Manipulator

The sample manipulator used in the UHV chamber is a commercial X,Y,Z and θ manipulator manufactured by Thermionics Northwest. Inc. The sample is held on a vertical stainless steel fork such that the thermocouple leads point directly to the right and rest on thermocouple wires connected to an electrical feed through. Behind the sample is the previously discussed electron beam heater. The ceramic tube is inserted directly behind the sample to ensure the maximum current density at the rear of the sample. The ceramic tube is mounted in the center of a 0.5cm thick copper plate. The copper plate is

moved forward until it is flush with the base of the sample holder. The block is then cooled by nitrogen flowing through a liquid nitrogen dewar and then through copper coils within the chamber. The coils are connected to the copper plate through a copper braid. This provides a cold sink during annealing and decreases the amount of time needed for cooling back to room temperature after annealing, which reduces the amount of surface contamination.

3.2 Transfer System and Sample Holder

One of the most important features of any system is the ability to securely mount your specimen for analysis, as well the ability to move it from chamber to chamber without much inconvenience. This section discusses the transfer arm mechanism and the sample holder used in our system.

3.2.1 Magnetic Transfer Arm

The transfer system consists of a 36" long magnetic transfer arm with a fork at the end for holding the sample and tip exchanger. The arm has a low and high position setting for removal of both the sample and tip exchanger. At the fully retracted position, the fork at the end of the arm rests comfortably in the load lock portion of the system and can be isolated from the other chambers. At the full extended position, the forks rest at the sample manipulator in the UHV chamber. Between these positions, the arm can rest in the STM chamber.

3.2.2 Sample holder

The sample holder consists of two major parts and is made mostly of molybdenum. A schematic of the sample holder is shown in figure 3.8. The top portion of the sample holder consists of an inner ledge on which the sample is placed, and an outer ring separated into three identical ramps for coarse approach. At the base of each ramp is a tapped hole to which each of the tantalum pressure clamps is attached. Also on one of the ramps a hole is bored through allowing for a thermocouple to contact the sample and monitor its temperature during experiments and annealing. The lower portion of the sample holder has two parallel grooves on the outside that allow the forks on the transfer arm and wobble stick to securely hold the sample holder at one of two heights. The inside of the lower portion of the holder is hollow with a diameter of ~ 1.5cm. This allows room for the bulb needed for sample heating to be positioned as close to the sample holder as possible.

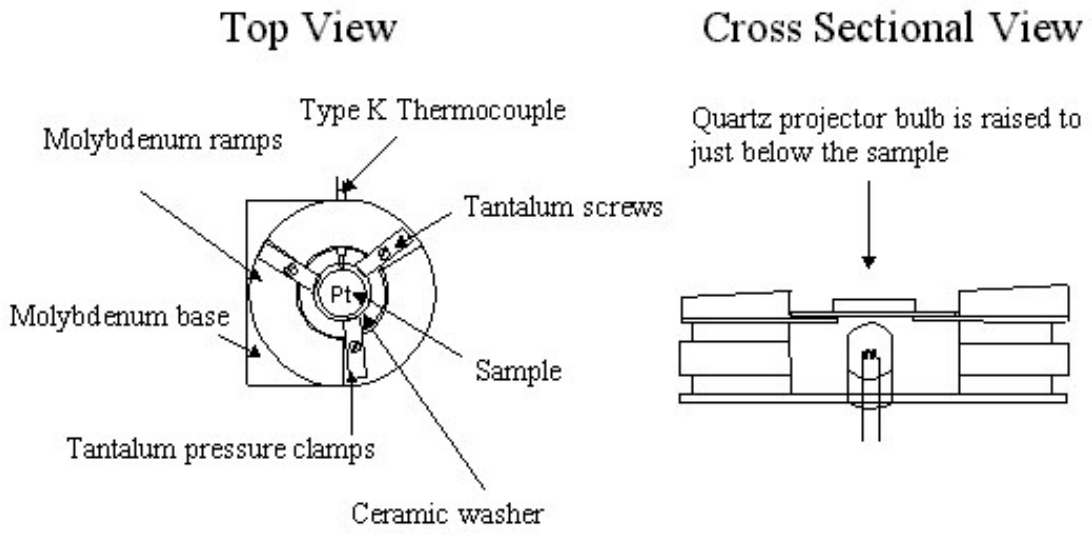

Figure 3.8 – Diagram of the sample holder.

3.2.3 Load Lock

The system also contains a small volume load lock (< 1L) for exchange of the sample and tip. During general operation, the tip is replaced as often as weekly or daily. The load lock allows for introduction of tips and samples without having to vent the entire chamber, which then requires several days of bakeout to reobtain its low base pressure. Once the sample or tip exchanger has been placed in the load lock, it is isolated by two gate valves and vented with dry nitrogen. The load lock can then be opened by removing a 2 3/4" flange. Once the tip and/or sample has been replaced the flanged is reattached and the load lock can be independently pumped by a mechanical/turbomolecular pump system to obtain a load lock pressure of ~1 x 10^{-8} Torr before introduction into the STM chamber.

3.3 High Pressure STM Chamber

The high pressure chamber contains the entire STM unit. It is pumped by a 60 l/s ion pump as well as a turbomolecular pump and has a working base pressure of ~5 x 10^{-10} Torr. Attached to the system are four leak valves which allow the introduction of mixtures containing up to four different gases and with a total pressure of about 1 atm. Of the four gas inlets, one contains an apparatus for introduction of liquid samples at pressures below their vapor pressure. This system is attached to a mechanical pump for freeze-pump-thaw purification of the samples. A Varian ionization gauge is used to monitor pressures up to 5 x 10^{-5} Torr, and the appropriate gas correction factor is used to calculate the pressure of each type of gas. An MKS Instrument Baratron model 722A is used for experiments involving pressures ranging from 0.1mTorr - 10 Torr and model

122A for experiments involving pressures from 10 - 1000 Torr. The chamber is equipped with a six inch window directly in front of the STM for easy viewing as well as a wobble stick for moving the sample to and from the stage, the sample holder and the magnetic transfer arm.

3.3.1 Scan Head

The microscope that was used for these studies is a beetle type design commercially available from RHK technologies. The STM head is composed of three outer piezoelectric tubes which are used for coarse movement of the tip and an inner piezoelectric tube that is used solely for the scanning of the sample. Figure 3.9 shows a picture of the scan head during approach. All of the piezos are composed of lead zirconate titanate (PZT). Zinc is coated on the inside and outside of each tube to create electrodes. The three outer tubes are significantly smaller than the inner tube ~0.5x the diameter. Each tube is divided lengthwise into four quadrants and the same or opposite voltages are applied to the quadrants to accomplish expansion, contraction, and bending of the tube. The scan tube which is larger than the three outer tubes contains a small opening at the end where the tip holder can be inserted and magnetically held in place.

The coarse approach of the tip is performed using solely the outer three piezos. Attached to the end of each of the outer piezos are three sapphire spheres. The entire scan head rests on the three piezoelectric legs which make contact with three molybdenum ramps of the sample holder through the sapphire balls. Each leg “walks” down the ramp during the approach until the tip is within tunneling range. The entire height of each ramp is 1mm, so the tip must be carefully inserted into the tip holder so the

total tip to sample distance is less than 1 mm. The walking is accomplished by slowly bending each tube down the ramp and then quickly bringing back to its equilibrium position. During the fast movement, the sapphire slips on the ramp and the head ends up slightly further down the ramp that where it began. Between each set of steps, the scan tube is extended to "look" for current. If no current is detected, it retracts and another step is taken. Upon reaching tunneling range, the central scan tube is used for local movements up to a total range of 5000 nm. During introduction of high pressures of gases, the tip can be brought back out of tunneling range using solely the scan piezo allowing for imaging of the same portion of the sample at various pressures, and protecting the tip in case the system is bumped while the gas is being added.

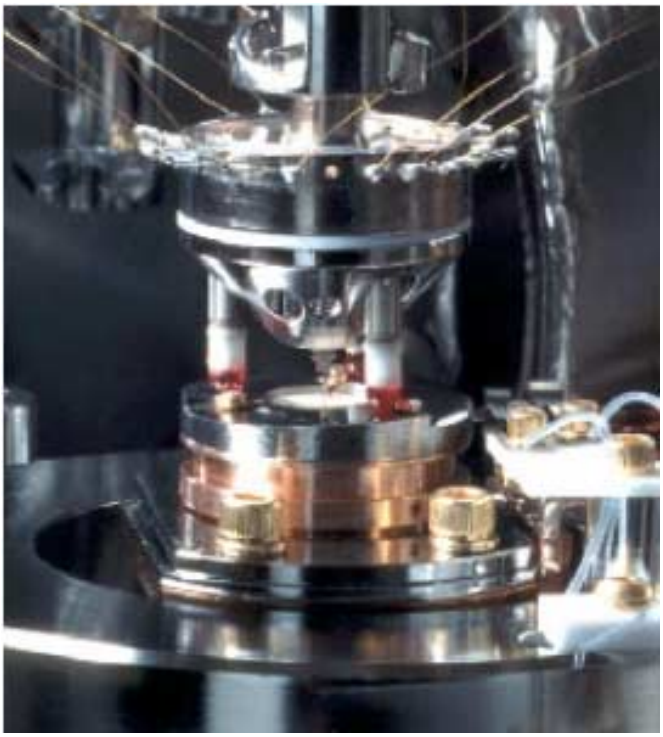

Figure 3.9 – Photograph of the "Johnny Walker" or "Beetle" type scan head during approach.

3.3.2 Sample Stage

The sample stage provides a stable place for the sample to be rigidly held while the experiments are being performed. It also contains infrastructure for heating of the sample for reaction studies as well a cooling system which can create a heat sink for reaction studies. The sample stage is supported on three Viaton rings which form a rigid support for the system but also dampen high-frequency vibrations from the rest of the system.

In order to heat our sample in the presence of high pressures of potentially reactive gases, the electron beam heater used in sample preparation cannot be used due to the low mean free path of electrons at high pressures. The electron beam heater has been replaced by a 360W, 80V, tungsten filament, halogen filled, quartz projector bulb. The bulb provides radiative heating of the sample without making mechanical contact. The bulb can be raised into position so it is directly below the sample and contained within a gold cylinder. Thus providing the most efficient heating possible, reaching sample temperatures up to 500 K. A variable auto transformer is used to control the power supplied to the bulb and thus the sample temperature. During heating, a water cooled copper block connected to the sample stage via a copper braid is used as a heat sink to minimize heating of the entire stage. Due to the expansion of the sample as it is heated, it is generally very difficult to remain in the same position on the sample over a range of temperatures. As a result, many portions of the sample must be imaged to gather a representative image of the surface structure.

3.3.3 Tips

One of the most crucial but also the most troublesome aspects of STM is the fabrication of reliable, robust tips capable of providing atomically resolved images. The two most common types of tip materials used today are platinum (or a platinum iridium alloy) and tungsten, and the two most common fabrication techniques are electrochemically etching of the tips and clipping or pulling tips with wire cutters.

In this work the choice of tip material was tungsten for a few reasons. Primarily, tungsten is known to provide stable imaging under high pressures of CO, NO, hydrocarbons, and hydrogen. These molecules represent all of the molecules that were used in our research, so the fact that some molecules such as oxygen can form insulating overlayer and damage tip performance was not of great concern to our research. Secondly, tungsten is very hard and is less susceptible to wear and blunting than other softer metal used for STM tips. Thirdly, tungsten is very easily etched providing a reliable and reproducible fabrication method. Finally tungsten was chosen as a tip material because it is relatively for the catalytic reactions we have studied. Platinum, which is the other largely used tip material would clearly create problems in our catalytic studies of reactions on platinum single crystals.

Due to the hardness of tungsten and its ease of etching, electrochemical etching was the obvious choice for tip preparation. The tips are prepared by creating a simple electrochemical cell consisting of two electrodes and represented graphically in figure 3.10. The working electrode is a piece of 10 mil tungsten wire which will eventually be our STM tip. The counter electrode is a platinum wire loop surrounding the tungsten wire. The platinum loop is dipped into a 2M KOH solution, which forms a film across

the loop that is about 1 mm thick. This film act as the electrolyte for the cell. Once created, the electrodes are connected to an external power supply and a voltage of ~2V is applied. The area of the tungsten that is in contact with the electrolyte is oxidized, and the newly created tungsten ions diffuse across the electrolyte and plate out on the platinum loop as tungsten metal. The etching of the wire, however, is not symmetric, and the lower portion has a taper much longer than the top portion. Since the longer the taper, the more susceptible a tip is to vibrational excitation, this is not desirable. To circumvent this problem, the tip is very nearly etched all of the way through and then flipped for the final stages of etching. This process was developed by Klein et al[7], and has been shown in our group to provide reliable reproducible tips.

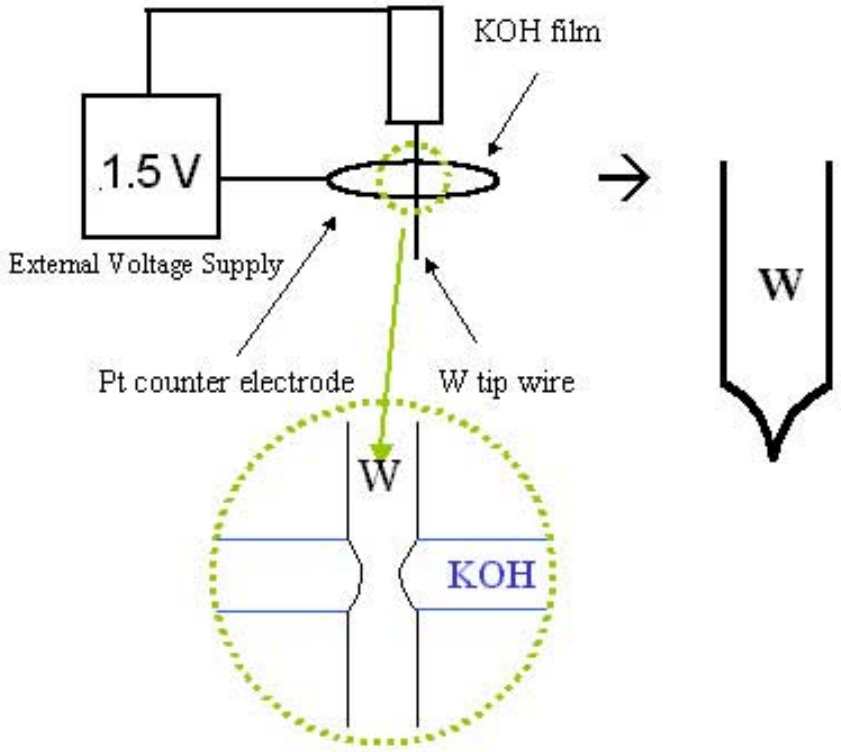

Figure 3.10 – Electrochemical cell used to etch tungsten tips

3.3.4 Tip Exchanger

In STM experiments in general, and especially high-pressure and high-temperature STM, tip lifetimes can be very short. Thus it is important to have an easy, reliable method for exchanging tips that causes as little disruption to the system as possible. The previously discussed load lock allows for exchange without requiring venting the entire system. The tip exchange mechanism discussed below necessitates that only the tip itself and a small tip holder be removed from the chamber.

The tip exchanger is shown in figure 3.11. When the tip requires changing, the sample is removed from the stage and the tip exchanger unit is inserted into the sample holder position on the stage. The STM scan head is then lowered down onto the tip exchanger unit. Three polymer posts identical in height to the STM piezoelectric legs extend upward from the tip exchanger. These legs serve to align the scan head by sliding into three depressions located on the scan head. Not only does this align the scan head and tip exchanger, but also prevents the head from being lowered too far, resulting in an inadequate amount of pressure being applied to the piezos. Also upon lowering, the tip holder (shown in figure 3.11c) slides into a hole in the tip exchanger. Once fully lowered, a wire in the tip exchanger can be bent to slide into a small notch in the tip holder locking the tip holder in place. Thus the tip holder has gone from that shown in 3.11a to 3.11b. Retracting the scan head results in the tip holder and tip remaining in the exchanger.

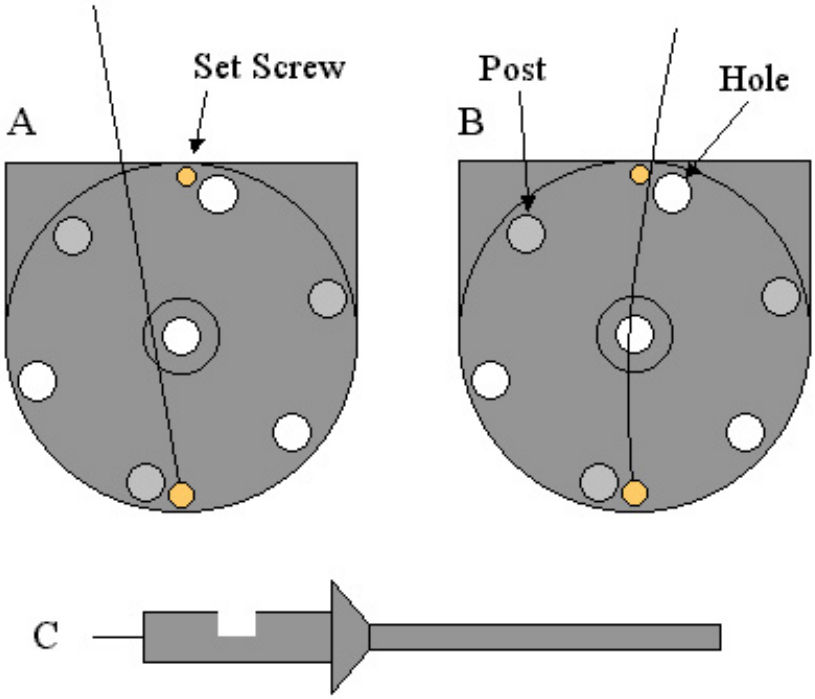

Figure 3.11 – Diagram showing tip exchanger in open (A) and locked (B) positions, as well as the tip holder (C)

Upon removing the tip exchanger from the system through the load lock, the tip holder is removed from the exchange unit. The tip is held in the tip holder simply by bending the tungsten wire tip and sliding into the hollow tip holder. The spring of the bent wire being inserted into the straight tube of the tip holder is sufficient to securely hold the tip in place. Once the tip has been adjusted to the correct exposed length, the entire process is repeated in reverse and the new tip is ready to be tested.

XPS

3.4 UHV Chamber

The UHV chamber of the system is a standard surface analysis chamber equipped with mass spectrometry, low energy electron diffraction (LEED), ion sputtering, and button heater annealing. The system is pumped by a turbomolecular pump and an ion pump to reach a working base pressure of $1x10^{-9}$ Torr. The chamber is connected to the high-pressure XPS cell via a leak valve so samples of gas from the high pressure chamber can be monitored during experiments. It is also connected to an independently pumped transfer chamber for moving the sample into and out of the chamber without venting. Since mass spectrometry and ion sputtering have been discussed in detail previously, this portion of the chapter will focus on LEED.

3.4.1 Low Energy Electron Diffraction (LEED)

Another surface characterization technique commonly used is low energy electron diffraction (LEED). LEED provides a method to study ordered substrate surfaces as well as ordered adsorbed monolayers under high vacuum conditions. It can provide information about the adsorbate unit cell, how stepped the surface is, and if substrate reforming is induced by adsorbed molecules. LEED uses the fact that electrons are scattered strongly by their interactions with the charges of electrons and nuclei of the surface[8]. It also exploits the fact that electrons behave as both particles and waves and follow Bragg's Law. By using electrons above a specific energy, their wavelengths become short enough to undergo diffraction by a periodic array of atoms. In LEED a

crystal surface is bombarded with monoenergetic low energy electrons (<500eV). Many of these electrons are elastically backscattered and collide with a phosphorescent screen. In order to screen out electrons that are scattered inelastically, a screen with a potential just below that of the elastically scattered electrons is placed directly in front of the phosphorescent screen. Thus the only electrons reaching the phosphorescent screen are elastically scattered. Due to the wavelength of the electron beam being of the same order as the surface lattice constant, the beam forms a diffraction pattern of the surface. In addition, the fact that the mean free path of an electron in a solid is only about 1 nm, and that the electron must not only penetrate into the sample but also escape once scattered. This means that LEED is highly surface sensitive. In practice only the top 2 or 3 layer of surface atoms contribute to the diffraction pattern [9]. Figure 3.12 represents Bragg's law pictorially.

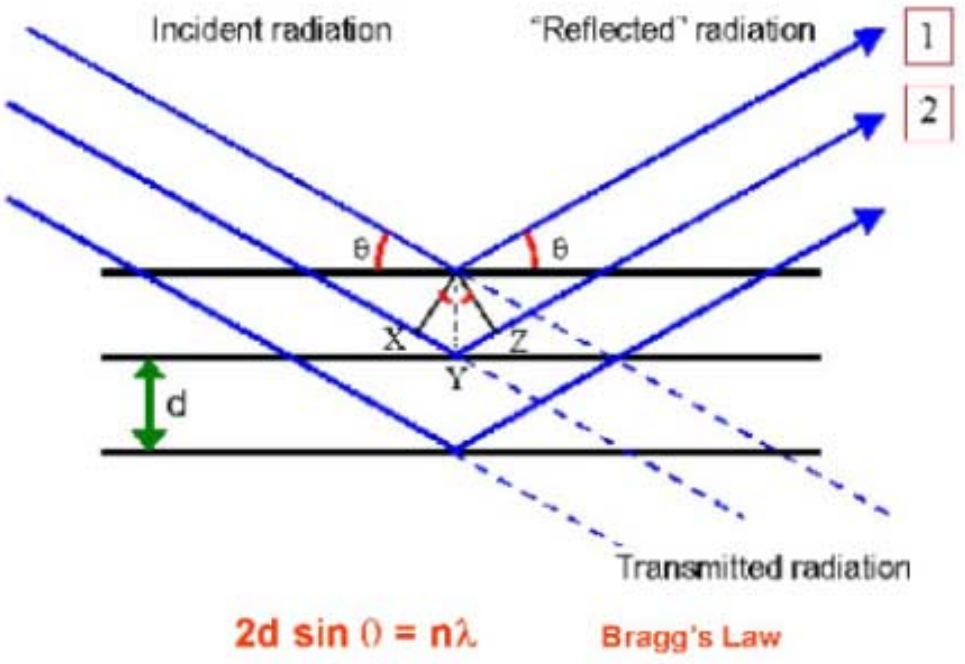

Figure 3.12 – Bragg's law. In LEED the difference in path lengths of two scattered particles must be an integer of their wavelength.

The diffraction pattern formed from LEED is related to the reciprocal space structure corresponding to the surface periodicity. LEED utilizes that fact that the electron waves once scattered will interfere both constructively and destructively upon reaching the phosphorescent screen. The diffracted electrons follow the conditions of Bragg's Law in that the difference in distance traveled of an electron reaching the screen must be an integer factor of the wavelength for constructive interference. Thus, by tuning the energy/wavelength of the incident electron, different unit cells on the surface will yield diffraction patterns. A sample LEED diffraction pattern corresponding to the Pt(111) surface is displayed in figure 3.13.

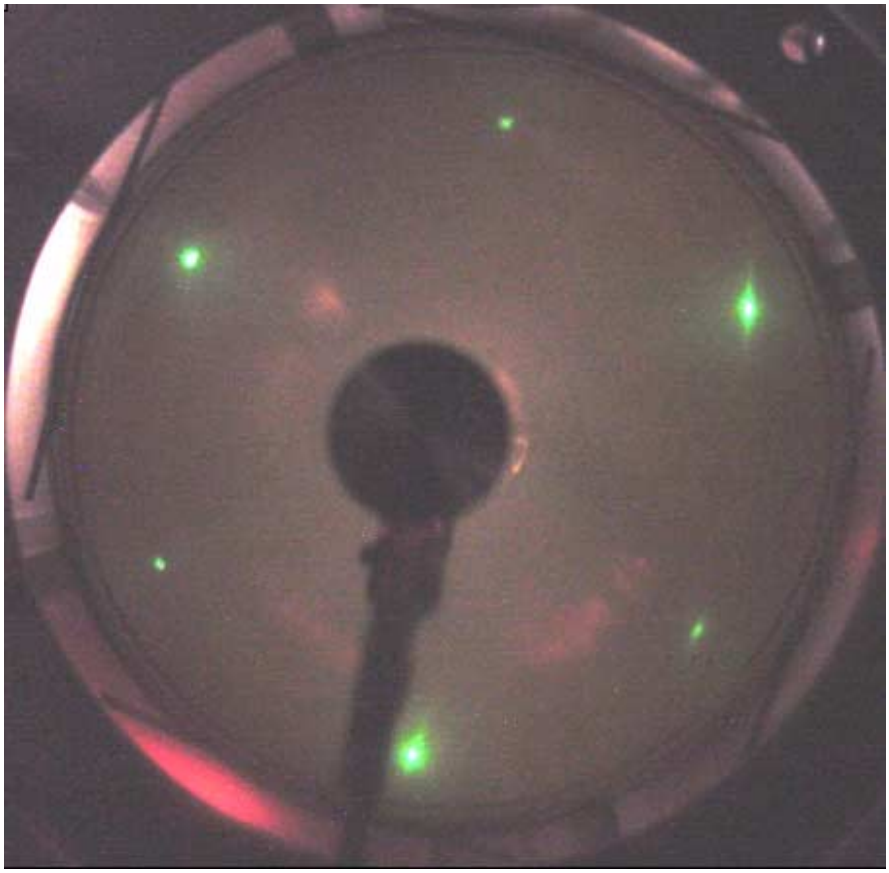

Figure 3.13 – LEED pattern from a Pt(111) surface

3.5 High Pressure Reaction Cell and Detector

The high pressure reaction cell is a standard stainless steel chamber pumped by a turbomolecular pump and an ion pump to reach a working base pressure of ~1 x 10^{-9} Torr. It is connected to several leak valves which allow for the introduction of any mixture of gases up to a total pressure of 10 Torr. Also connected to the chamber is a differentially pumped electrostatic lens system leading to a concentric hemispherical analyzer (CHA) and a synchrotron x-ray source. These three features will be discussed in detail below.

3.5.1 Differentially Pumped Electrostatic Lens System

The differentially pumped electrostatic lens system is designed to transfer photoemmitted electrons from the high pressure chamber to the concentric hemispherical analyzer (CHA) that is located in UHV. The system consists of four main parts, an exchangeable nozzle with a diameter of 0.1 – 1.0 mm, and three differentially pumped sections. The size of the aperture in the nozzle is of particular importance because it determines the fraction of the photoelectrons that are collected. It also, however, determines how much gas from the high pressure chamber escapes into the first of the three differentially pumped stages. A nozzle size of ~0.6 mm has been found to work well to balance each of these needs and is pictured in figure 3.14. The position of the nozzle with respect to the sample is also important due to the low mean free path of electrons in high pressures of gases. For example, for a 500 eV electron, the mean free path at 4 Torr is ~ 1 mm but at 40 Torr is only ~0.1 mm [10]. In general, during operation the gap between the sample and nozzle is on the order of 0.5 mm.

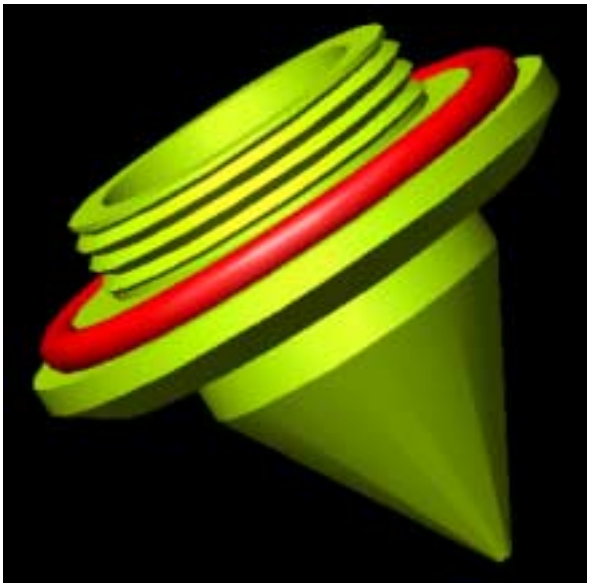

Figure 3.14 – Computer representation of the nozzle separating the differential pumping system and the high-pressure chamber. [10]

The differentially pumped electrostatic lens system is shown in figure 3.15. It is composed of three sections that are connected by apertures about 0.3 mm in diameter. Each section is designed to lower the pressure about three orders of magnitude from the previous section through turbomolecular pumping. Each section also contains a series of potentials designed to focus the stream of electrons entering the chamber through the aperture connected to the next chamber. This allows for very little loss of signal, while providing only a small aperture through which the gas can pass.

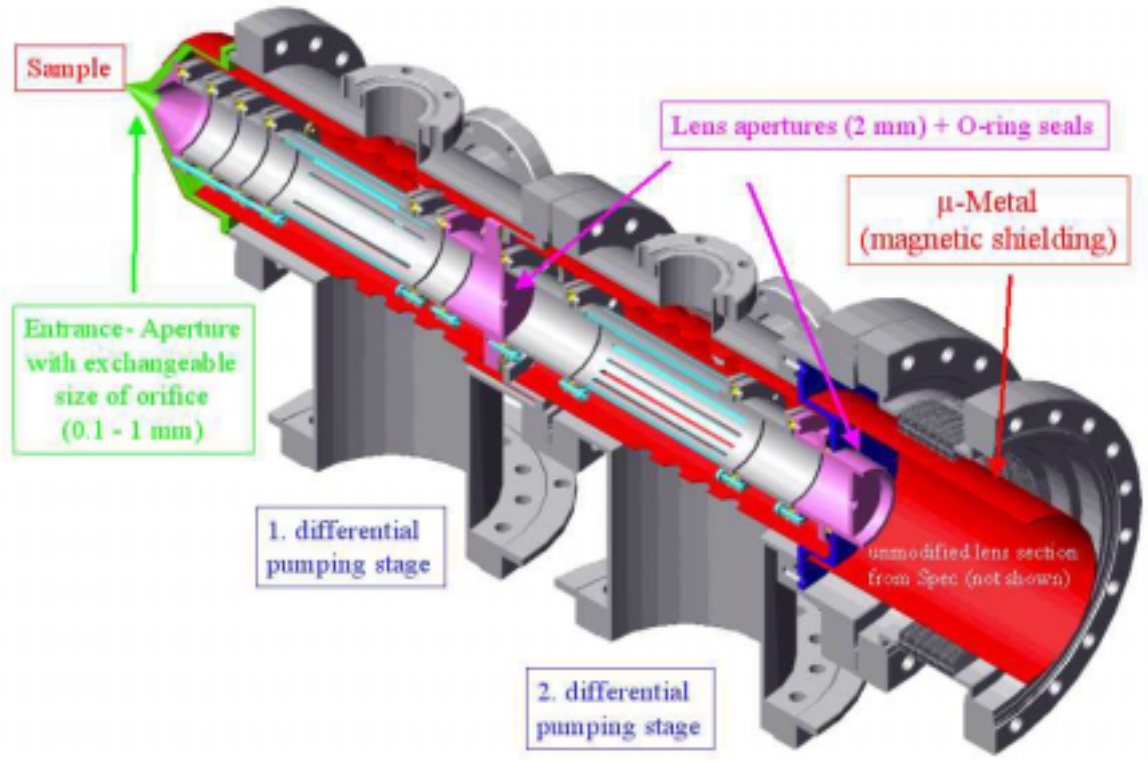

Figure 3.15 – Diagram showing the differential pumping electrostatic lens system.

3.5.2 Concentric Hemispherical Analyzer

The kinetic energies of the photoelectrons are analyzed using a concentric hemispherical analyzer (CHA). A CHA, also referred to as a Hemispherical Deflection Analyzer (HDA), consists of two metal hemispheres. One of the hemispheres is smaller than the other and the two are positioned concentrically. A schematic illustrating the relative position of the two hemispheres is shown in figure 3.16. Different voltages are placed on each hemisphere such that there is an electric field between the two hemispheres. Electrons that have traveled through the 3-stage differentially pumped system are injected into the gap between the hemispheres. Electrons with a kinetic energy too high will impinge on the outer hemisphere. Electrons with a kinetic energy that is too low will be attracted to the inner hemisphere. Only electrons in a narrow

energy region (called the pass energy) succeed in getting all the way round the hemispheres to the detector without colliding with the wall. Through changing the potentials on the two hemispheres, a range of electron energies can be analyzed.

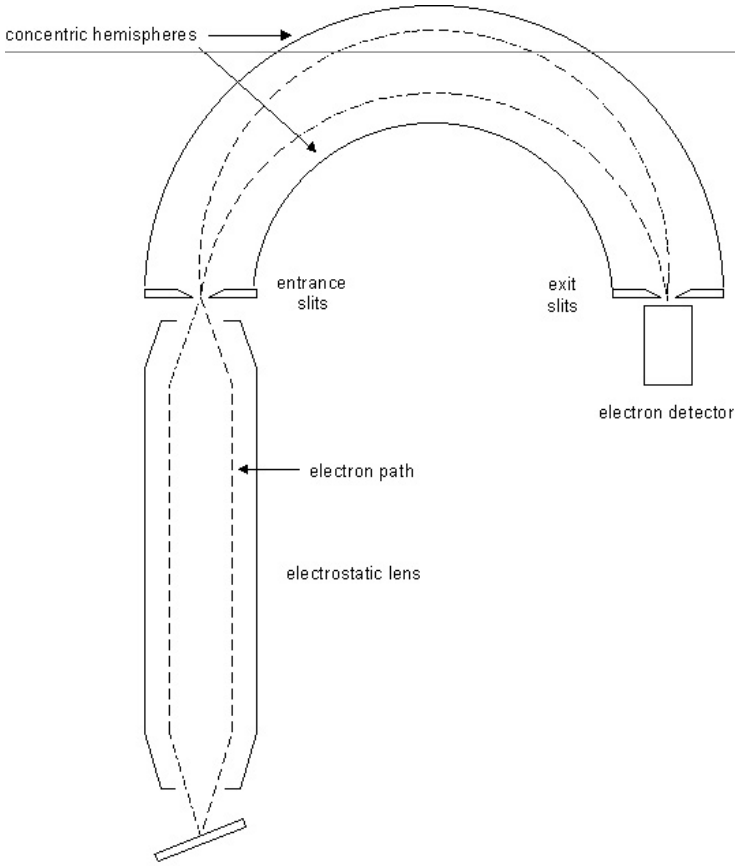

Figure 3.16 – Diagram of concentric hemispherical analyzer (CHA). Only electrons with very specific energies can pass through both the entrance and exit slits.

3.5.3 Synchrotron X-ray Source

High pressure x-ray photoelectron spectroscopy necessitates a high intensity source to ensure a large initial signal. A synchrotron radiation source meets this need. All XPS experiments in this thesis were performed at beamline 11.0.2 at the advanced

light source in Berkeley, California. X-rays with energies of 95-2000 eV can be used. The spot size of the beam is 6 x 11 μm with a photon flux of 10^{12}-10^{13} photons/s. The monocrometer used is a variable-included-angle PGM. The resolving power for the photons used is our experiment is ~0.1eV. The ring current of the synchrotron is resupplied three times daily with an initial current of 400 mA that decays to around 200 mA prior to refilling. A schematic of the ring current over an average day is shown in figure 3.17. All measurements must take into account the relative ring current, as it affects the signal intensity.

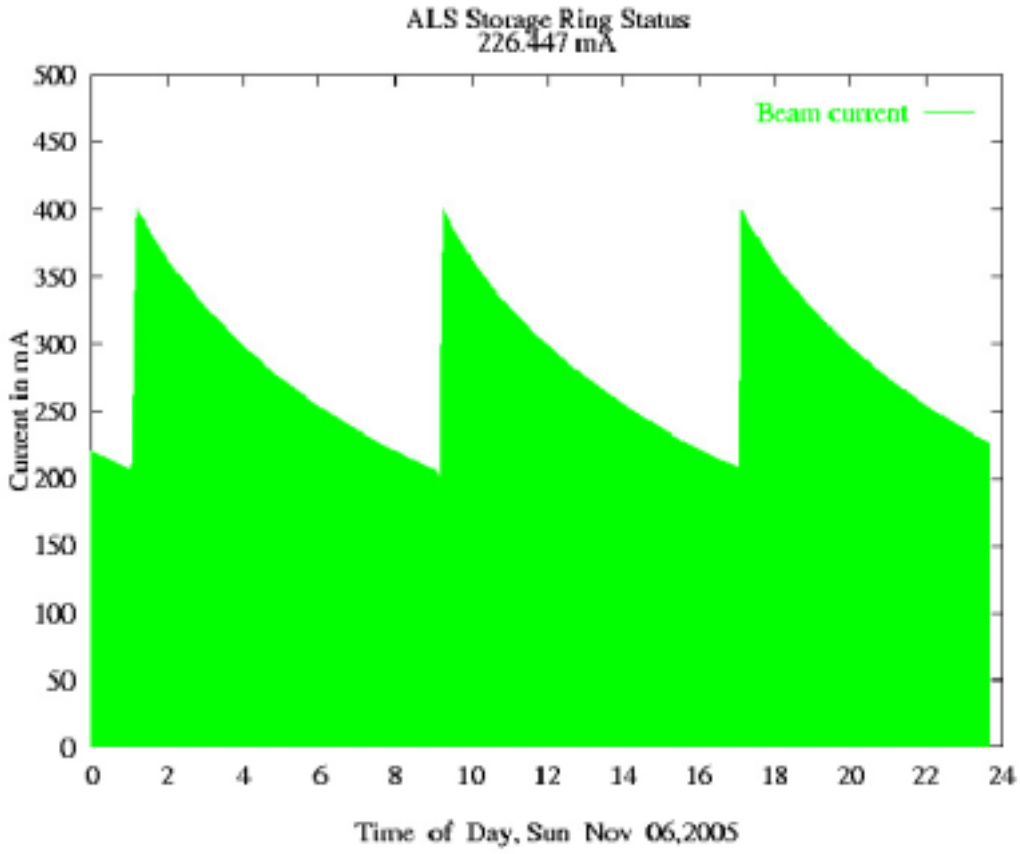

Figure 3.17 – Graph of the decay of the synchrotron ring current over time for a typical day.

Briefly, a synchrotron radiation source uses the fact that radiation is emitted when a fast electron is accelerated. A magnetic field in an area an electron is traveling in will cause the electron to change direction by exerting a force on it perpendicular to the direction the electron is moving. As a result, the electron will be accelerated, causing it to radiate electromagnetic energy. This is called bremsstrahlung or synchrotron radiation (after radiation observed from particle accelerators by that name). If the electrons and the magnetic field are energetic enough, the emitted radiation can be in the form of x-rays. A schematic of a synchrotron source is shown in figure 3.18.

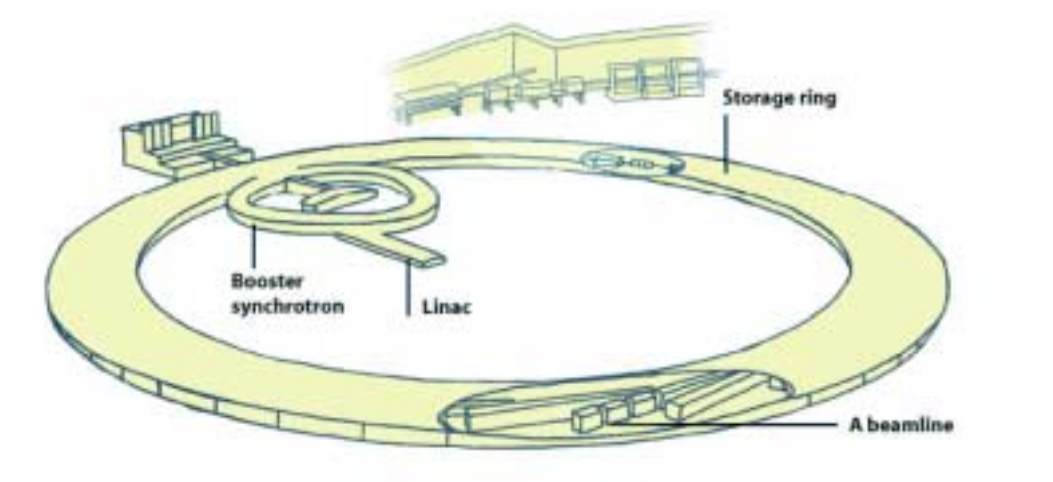

Figure 3.18 – Map of a synchrotron radiation source.

References

[1] McIntyre, B. J.; Salmeron, M.; Somorjai, G. A. *Review of Scientific Instruments* **1993**, *64*, 687.

[2] Jenson, J. A.; Rider, K. B.; Chen, Y.; Salmeron, M.; Somorjai, G. A. *Journal of Vacuum Science and Technology B* **1999**, *17*, 1080.

[3] Hwang, K. H. *Ph.D. Thesis, University of California* **2002**.

[4] Ogletree, D. F.; Bluhm, H.; Lebedev, G.; Fadley, C. S.; Hussain, Z.; Salmeron, M. *Review of Scientific Instruments* **2002**, *73*, 3872.

[5] Tang, D. C. *Ph.D. Thesis, University of California* **2005**.

[6] Strobel, H. A.; Heineman, W. R. *Chemical Instrumentation: A Systematic Approach;* 3rd ed.;John Wiley and Sons Inc. New York, **1989**.

[7] Klein, M.; Schwitzgebel, G. *Review of Scientific Instruments*, **1997**, *68*, 3099.

[8] Atkins, P.; *Physical Chemistry*; 6th ed.; W. H. Freedman and Company, New York, **1998**.

[9] Somorjai, G. A.; *Introduction to Surface Chemistry and Catalysis*; John Wiley and Sons Inc. New York, **1994**.

[10] Hebenstreit, E. L. D.; Ogletree, D. F.; Salmeron, M.; Bluhm, H.; Kleimenov, E.; Schlogl, R.; Shuh, D. K.; Tyliszczak, T.; Gilles, M. K. *A New Endstation for Beamline 11.0.2 High Pressure Photoelectron Spectroscopy (HPPES)* **2002**

Chapter 4: Low Pressure STM Surface Structure Study of Cyclic C_6 Hydrocarbons adsorbed to Pt(111)

This chapter discusses STM studies of the low pressure (10^{-6} Torr) adsorption structures of cyclic C_6 hydrocarbon monolayers on the platinum (111) crystal surface. Upon adsorption at 5 x 10^{-6} Torr on Pt(111) both cyclohexane and cyclohexene produce the same structure, which corresponds to the partially dehydrogenated π-allyl (C_6H_9) as studied by spectroscopic methods [1-3]. 1,3-cyclohexadiene and benzene appear to yield molecular benzene structures. 1,4-cyclohexadiene forms a structure very different from the other two and is most likely molecular 1,4-cyclohexadiene. Increasing the backpressure of cyclohexene from 5 x 10^{-6} Torr up to 10 Torr, results in no surface structure change until 10 Torr. At this point, a structure similar to that observed for 1,4-cyclohexadiene is observed.

4.1 Introduction

Catalysis is, and will most likely remain a massive contributor to the world economy. In the production of virtually all industrial chemicals, the refinement of petroleum products, the fabrication of polymers, and the production of fertilizers, catalysis is necessary. In fact, the catalytic production of ammonia on iron based catalysts was recently named the most important technological achievement of the 20th century [4] due to the fact that it allows food for literally billions of people to be

produced at a reasonable price. Despite this huge importance to our economy and our society in general, the knowledge of the catalytic process is far from complete.

One method to further elucidate the catalytic process is to study common or model adsorbates at low pressures. Investigating what types of surface species form from a particular gas, and how this may change with the back-pressure level or chemical composition can yield information about what types of stable surface intermediates are favored on a particular catalyst surface. This can tell you if the catalyst preferentially supports certain reaction pathways, and thus enhances selectivity. Cyclic C_6 hydrocarbons are of particular industrial importance due to the petroleum industry. The refining of crude oils and the production of high octane fuels both involve catalytic hydrocarbon reaction on platinum based catalysts. Understanding how these organic molecules interact with a catalyst surface is crucial to obtaining a complete molecular level understanding of catalysis.

Here we report the low pressure structures formed from cyclohexane, cyclohexene, 1,3-cyclohexadiene, 1,4-cyclohexadiene, and benzene on the platinum (111) surface. Also we investigate how the low pressure structure observed from the presence of background cyclohexene changes as the pressure is raised from 5×10^{-6} Torr up to 10 Torr.

4.2 Experimental

All experiments were performed in a high pressure, high temperature STM that has been described in detail elsewhere [5]. The system combines a UHV surface analysis/preparation chamber with a variable temperature (298K – 675K) and pressure

(10^{-10} – 10^{3} Torr) scanning tunneling microscope (RHK Technology, Model VT-UHV 300). The base pressure of the system was 1 x 10^{-10} Torr with a background mostly made up of H_2, CO and H_2O. Using three gate valves, the STM chamber can be isolated from the rest of the system and filled with any gas mixture. Leaking the gas to a mass spectrometer located in the UHV chamber monitored the composition of the gas. (Stanford Research Systems, RGA 200)

All experiments were carried out using a platinum single crystal of (111) orientation with a miscut angle of $\leq 0.3^{\circ}$. The crystal was polished using diamond grit down to a grit size of .25 μm. Before each experiment the sample was sputtered in 5 x 10^{-6} Torr O_2 for 15 minutes. The ion energy was 400 eV and the current was ~4 μA. The sample was then heated with an electron beam heater to 1123 K for 5 min and briefly flashed back to 1123K for 1 minute just prior to being transferred to the STM chamber. Sample cleanliness was monitored using Auger electron spectroscopy and checked with STM prior to gas introduction.

During STM experiments, the STM chamber was isolated from the rest of the system while cyclohexane, cyclohexene, 1,4-cyclohexadiene, 1,3-cyclohexadiene or benzene was introduced. The cyclic C_6 liquids (99.5%, Fluka) were purified by freeze-pump-thaw treatment before being introduced.

All images were taken using electrochemically etched tungsten tips etched with a technique developed by Klein et. al. [6]. STM settings during image acquisition were I=0.05 - 0.2 nA and V= 50 – 100 mV. A pressure transducer was used to monitor the chamber pressure during experiments. A Varian ionization gauge model UHV-24 was used to monitor pressures up to 5 x 10^{-5} Torr and the appropriate gas correction factor

was used to calculate the pressure of each type of gas. MKS Instrument Baratron model 722A was used for experiments involving pressures ranging from .1mTorr – 10 Torr and model 122A was used for experiments exceeding 10 Torr.

4.3 Results/Discussion

Low Pressure Studies

The structures formed by exposing Pt(111) to low pressures (2×10^{-6} Torr – 1×10^{-5} Torr) of cyclohexene and potential intermediates cyclohexane, 1,4-cyclohexadiene, 1,3-cyclohexadiene and benzene were studied. Preparing the platinum sample by the method discussed above results in a clean stepped surface. Scanning smaller areas we were occasionally able to resolve the periodicity of the (111) platinum surface. In addition to verifying sample cleanliness, this was used for piezo calibration. Imaging large areas can display steps produced by dislocation planes crossing the surface. These steps are aligned along the compact [110] type direction and provide an internal calibration of the crystal orientation for comparison with the molecular images. Exposing the clean platinum surface to 2×10^{-6} Torr of cyclohexene at 300K reveals the stable surface structure seen in figure 4.1a. The cyclohexene molecules form a surface structure with hexagonal symmetry and a periodicity of ~7 Å. In one of the directions, the individual molecules are more difficult to resolve suggesting that the molecules may overlap differently in that direction. The structure is rotated with respect to the platinum by ~18-20˚, which indicates that it may be a ($\sqrt{7} \times \sqrt{7}$) R19.1˚ structure. SFG, high resolution electron energy loss spectroscopy (HREELS), bismuth post dosing thermal desorption mass spectroscopy, and theoretical studies performed have determined that the

species present at room temperature is the partially dehydrogenated π-allyl C_6H_9 [1-3]. Using the 3-fold hollow adsorption site calculated in previous studies by density functional theory [7] a surface model of this molecular structure is displayed in figure 4.1c. The geometry of the π-allyl molecule when adsorbed to the platinum surface is a chair configuration and is displayed in figure 4.1b.

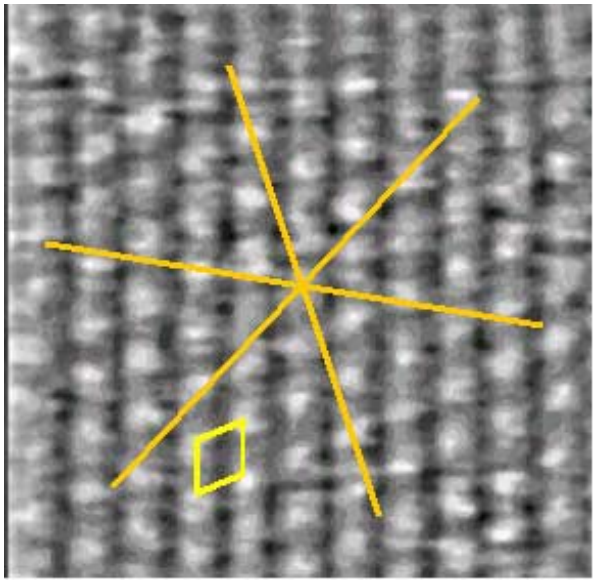

a)

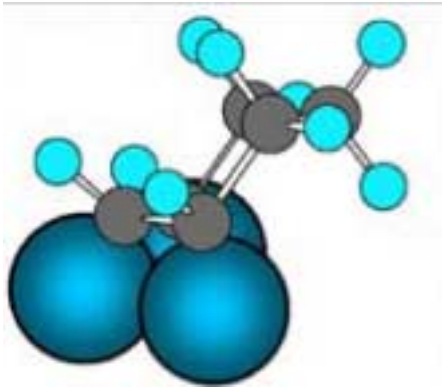

b)

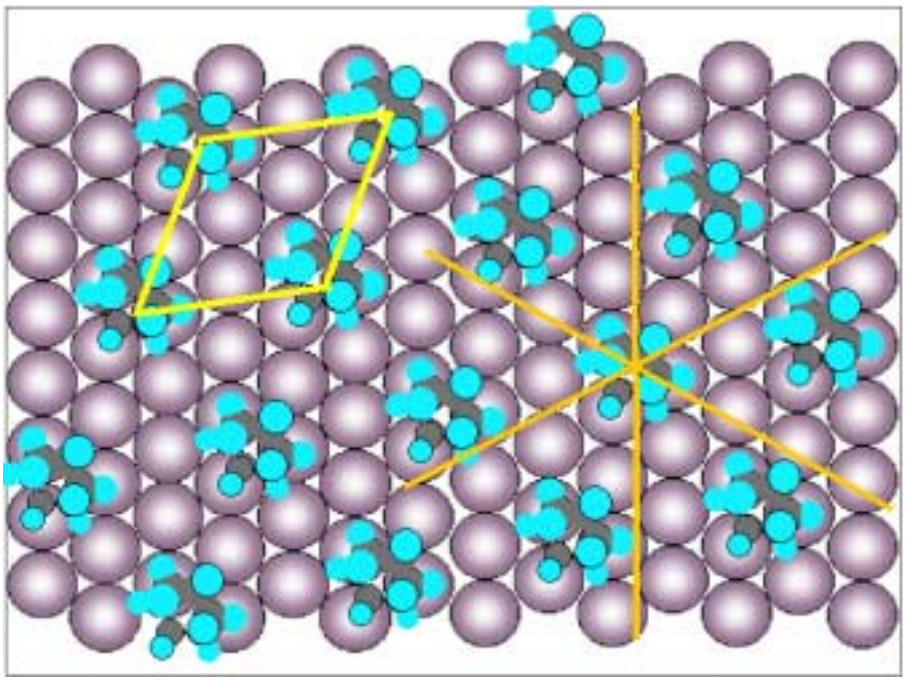

c)

Figure 4.1 – a) 60Å x 60Å STM image of Pt(111) in the presence of 2×10^{-6} Torr cyclohexene at 300K. A hexagonal arrangment of spots is observed with a periodicity of ~6.5Å. Spectroscopy studies have found the surface species to be π-allyl. Lines represent [110]-directions of underlying platinum. A unit cell of the adsorbate structure is drawn. b) Schematic of the bonding structure of π-allyl. c) Diagram of the proposed (√7 x √7) R19.1° model for the π-allyl structure in figure 4.1a.

To confirm that the cyclohexene had not further dehydrogenated to 1,4 or 1,3-cyclohexadiene or benzene, or hydrogenated to cyclohexane, the sample was independently exposed to all four species in an attempt to characterize their respective low pressure surface structures. Figures 4.2, 4.3a, 4.4 and 4.5a show the Pt(111) exposed to 2×10^{-6} to 1×10^{-5} Torr of each species at 300K. Figures 4.3b, and 4.5b show the

accepted bonding geometry. Figures 4.3c, and 4.5c show the proposed bonding structures.

The platinum surface when exposed to cyclohexane forms an ordered structure very similar to that formed from exposure to cyclohexene (Figure 4.2). This is unlikely to be molecular cyclohexane, since a quick calculation of the residence time using ΔH_{ads} = -58.1 kJ/mol [2] and equation 4.1 [8]

Equation 4.1 - $\tau = \tau_o \cdot e^{\left(\frac{\Delta H_{ads}}{RT}\right)}$

τ = residence time,

$\tau_o = 10^{-12}$ sec,

ΔH_{ads} = heat of adsorption,

R = gas constant,

T = temperature (K)

results in a residence time of about .015 sec. The flux of molecules striking the surface at this pressure is around 2 collisions/surface atom/sec. From this one can easily calculate the surface coverage using a Langmuir adsorption isotherm equation 4.2 [18]

Equation 4.2 – $\sigma = \frac{\sigma_o F\tau}{\sigma_o + F\tau}$

σ = coverage

F = Flux

σ_o = coverage of a complete layer

τ = residence time,

gives a coverage of ~0.01 monolayers. Our STM is able to take an image in slightly less than 1 minute, so many molecules have adsorbed diffused and desorbed over the course of taking one image. This very low coverage, rapid adsorption/desorption as well as the surface diffusion these vacancies allow make resolving the surface structure of the intact cyclohexane molecule difficult. Higher pressure sum frequency generation studies by Yang et. al. [9] have shown that at 1.5 Torr cyclohexane and at 310K the adsorbed cyclohexane does indeed partially dehydrogenate on the Pt(111) surface to form the π-allyl overlayer. Low coverage studies [10,11] also show that cyclohexane forms the π-allyl but begins to dehydrogenate to benzene between 270 – 290K. This small temperature discrepancy can be explained by the competition for vacant sites needed for hydrogen abstraction that occurs at saturation coverages. The images show that the π-allyl again forms the (√7 x √7) R19.1° that it forms from exposure to cyclohexene.

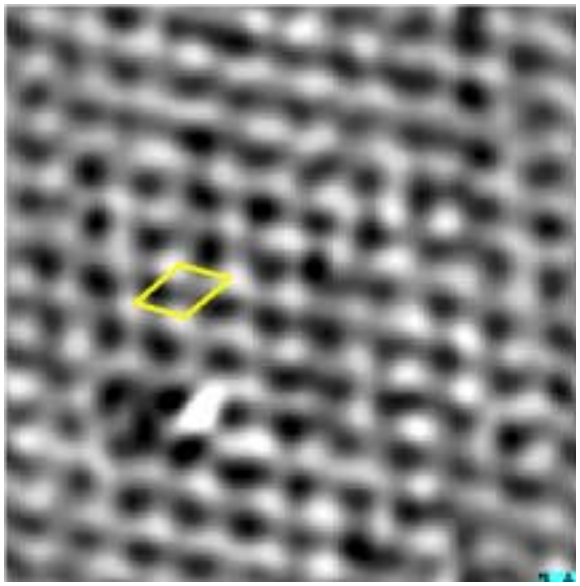

Figure 4.2 – 75Å x 75Å STM image of Pt(111) in the presence of 2 x 10^{-6} Torr cyclohexane at 300K. Periodicity of ~ 7Å. Spectroscopic studies suggest that the surface species is π-allyl.

When the clean platinum surface is exposed to $1x10^{-5}$ Torr of 1,4-cyclohexadiene the platinum surface exhibits a complicated surface structure with six member rings forming from individual 1,4-cyclohexadiene molecules. (Figures 4.3a). The rows of hexagons are rotated ~10˚ with respect to the underlying platinum. The intermolecular distance is 9.8 $\pm$ .7 Å while the distance between rings composed of 6 molecules is 18.4 $\pm$ 1.1 Å. DFT calculations by Saeys et. al. [12] show that the bridge site in which the molecule forms four sigma bonds and the 3-fold hollow in which the molecule forms two sigma and one pi-bond, have essentially equal adsorption energies of 145.6 kJ/mol and 141.6 kJ/mol respectively. Using the 3-fold hollow site with the bonding geometry shown if figure 4.3b a (√43 x √43) R7.6° surface model is proposed (Figure 4.3c). This model gives intermolecular distances of 9.9 Å and interring distances of 18 Å. Both of these values are well within the experimental error of observed values. In addition, this model helps to explain why we do not observe a center bonded 1,4 –cyclohexadiene molecule. As can be observed from the structure, the center bonding site is different from the outer 6 which may provide weaker surface interactions and thus a residence time that is too short to image with the STM. Also, the molecule may adsorb on an identical site to the other six that is slightly off center, and as the adsorbed molecules moves easily from site to site, its electron density is spread out sufficiently to appear significantly lower than its outer six counterparts.

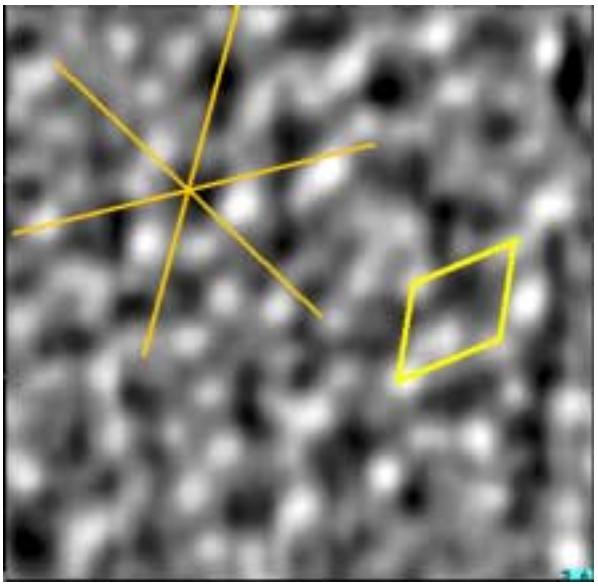

a)

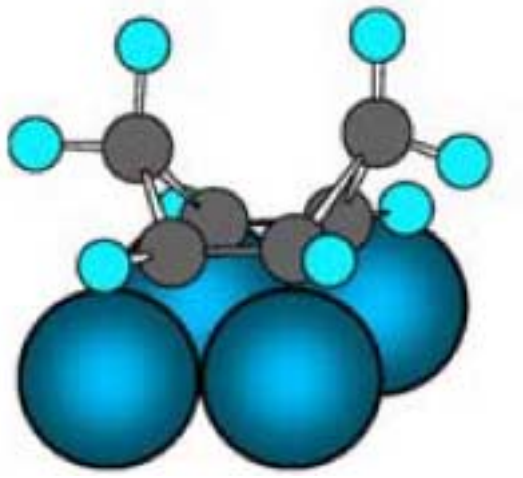

b)

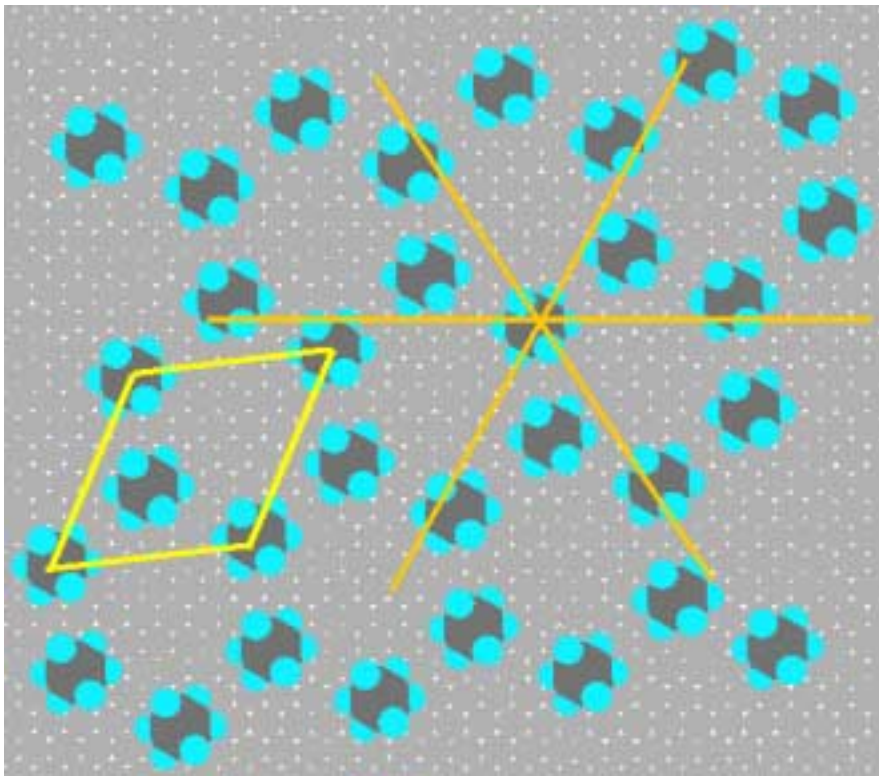

c)

Figure 4.3 – a) 50Å x 50Å STM image showing the structure formed by 1,4 – cyclohexadiene on Pt(111) at 1x 10^{-5} Torr and 300K. Lines in the [110]-type directions of the underlying platinum lattice are drawn. The surface species form hexagonal units in domains containing a few unit cells and in antiphase relationship to each other. The periodicity and rotation suggest a (√43 x √43) R7.6º structure b) Model of the bonding geometry of adsorbed 1,4- cyclohexadiene. c) Diagram of the proposed (√43 x √43) R7.6º 1,4-cyclohexadiene structure.

Exposure to 1 x 10^{-5} Torr of 1,3-cyclohexadiene shows an ordered structure as well, but in this case it has hexagonal symmetry with periodicity of 9.4 Å $\pm$ .3, 9.9 Å $\pm$.3, and 10.2 Å $\pm$ .2 for the 3 axes of symmetry (Figure 4.4). The rotation with respect to the underlying platinum surface was ~30˚ . This species is thought to be benzene as is discussed below.

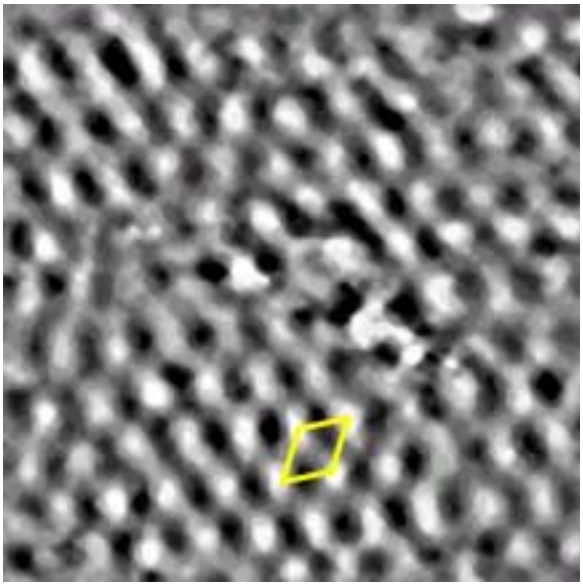

Figure 4.4 – 100Å x 100Å image of Pt in the presence of 1x 10^{-5} Torr 1,3 – cyclohexadiene at 300K. The surface structure, (2√3 x 2 √3) R30.0º, is similar to that formed by benzene.

Finally when exposed to 1 x 10^{-5} Torr of benzene a surface structure essentially identical to that of 1,3-cyclohexadiene is observed with a periodicity of 8.9 Å $\pm$ .5, 8.6 Å $\pm$.6, and 8.9 Å $\pm$ .5 for three axes of symmetry (Figure 4.5a) and is rotated 30˚ with respect to the underlying platinum. The structure we propose based on periodicity and rotation relative to the underlying platinum is (2√3 x 2√3) R30.0˚. DFT calculations [13,14] have shown that the most favored adsorption site is the bridge bonded rotated 30˚ as is displayed if figure 4.5b. With this a bonding model has been created and is displayed in Figure 4.5c. Since adsorbed benzene remains molecular benzene in our experimental conditions, and the periodicities are very similar one can conclude that upon adsorption to the platinum substrate at 300K, the 1,3-cyclohexadiene dehydrogenates to benzene. These studies correlate with a thermal desorption mass spectroscopy study performed by the Campbell group[15]. This study showed that the dehydrogenation of 1,3-cyclohexadiene to benzene at low coverages occurs between 20-30K lower temperature than for the 1,4-cyclohexadiene. Bismuth post dosing thermal desorption spectroscopy reveals dehydrogenation temperatures of ~230K and 260K respectively while thermal desorption spectroscopy shows H_2 evolution beginning at ~280K and 300K. Our studies indicate temperatures similar to the latter, but are performed at saturation coverages, which may lead to competition for the vacant sites needed for hydrogen abstraction. This site blocking effect at saturation coverages leading to higher

dehydrogenation temperatures has been observed in the case of cyclohexene dehydrogenation as a function of temperature [16]. The 1,3 cyclohexadiene appears dehydrogenated to benzene, while the 1,4-cyclohexadiene has either remained entirely intact or just begun to dehydrogenate resulting in a coadsorption structure.

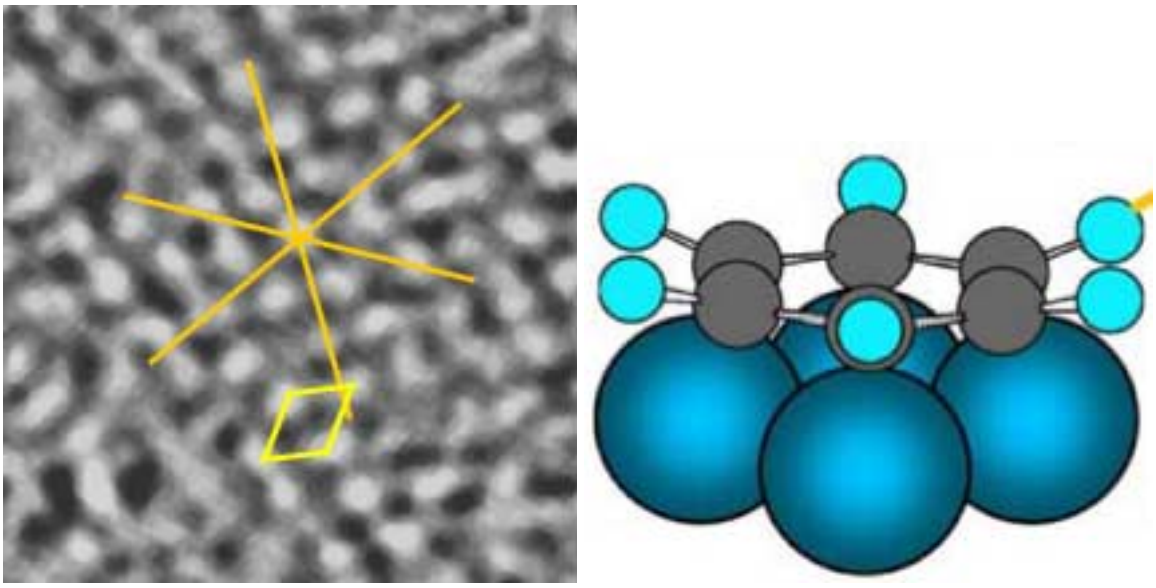

a) **b)**

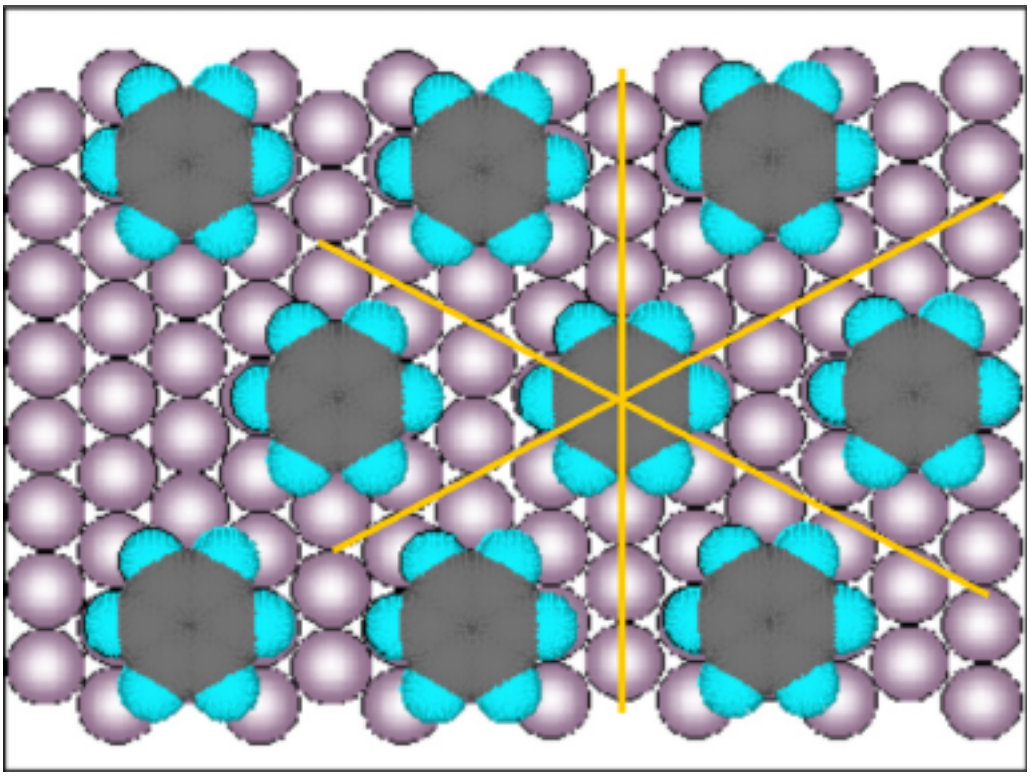

c)

Figure 4.5 – a) 80Å x 80Å STM image of Pt in the presence of 1.2 x 10^{-5} Torr benzene at 300K. Species is molecular benzene. Lines in the [110]-type directions of the underlying platinum lattice, and a unit cell of the adsorbate structure have been drawn. b) Model of the accepted bonding site and geometry. c) Diagram of proposed (2 √3 x 2 √3) R30.0º benzene structure.

The structures observed from benzene 1,3 and 1,4 –cyclohexadiene are entirely different than the one observed when the surface was exposed to purely cyclohexene, while the one observed from exposure to cyclohexane is very similar to that detected in the presence of cyclohexene. This leads one to conclude that no further dehydrogenation

has occurred and that the structure observed in Figure 4.1a is indeed the π-allyl proposed by others.

Cyclohexene Pressure Study

The effect on the back pressure of cyclohexene gas on the surface structure of the adsorbed molecules on Pt(111) was studied. Initially the surface was exposed to ~2L of cyclohexene and imaged in vacuum. As can be seen in figure 4.6a, areas of rows very similar to those observed under saturation coverage are observed, as well as areas that appear to still be the clean platinum surface. The similarities to the higher pressure structure and previous spectroscopic studies indicate that the surface species is the partially dehydrogenated π-allyl. Upon introducing 1 x 10^{-5} Torr of cyclohexene, the surface become fully covered, and the (√7 x √7) R19.1º π-allyl structure observed previously is clearly seen. The back pressure is then increased to 100 mTorr and then 1.53 Torr. In each case a surface structure corresponding to the (√7 x √7) R19.1º is observed (figures 4.6c and 4.6d). After increasing the back pressure to 10 Torr some surface changes are seen. Although there are some areas that remain unchanged (figure 4.6e), some areas have converted to a new surface species as is clearly seen in figure 4.6f. This larger ring like structure is very similar to that seen on the surface from the presence of 1,4-cyclohexadiene, but with slightly lower resolution. SFG studies have shown that at around 2 Torr there is a surface chemistry change that corresponds to the dominant surface species becoming 1,4-cyclohexadiene from the π-allyl. A sample SFG spectrum is shown in figure 4.7.

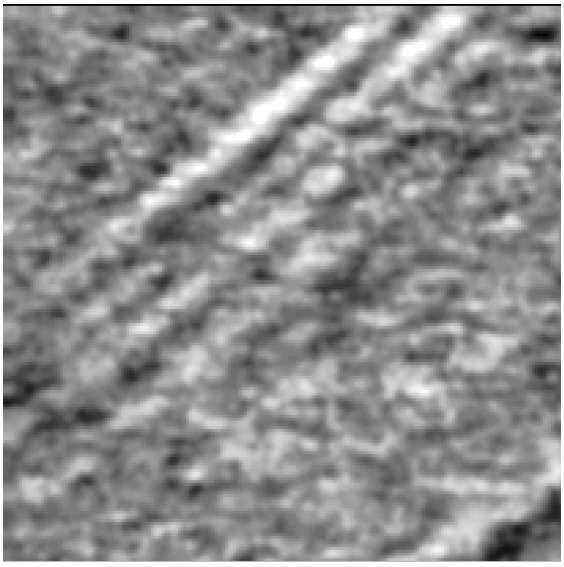

a)

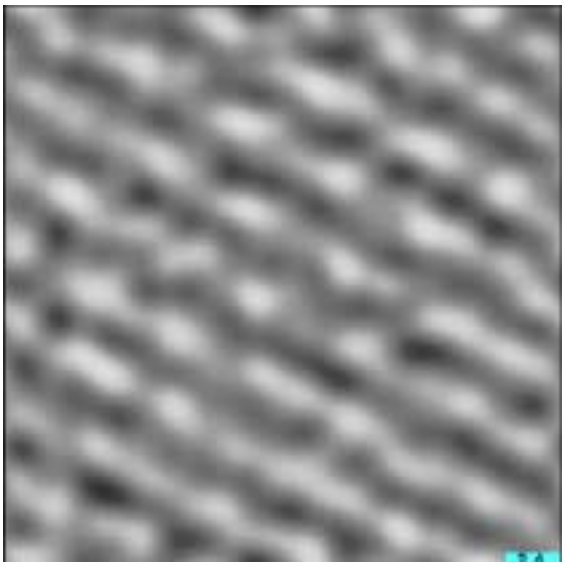

b)

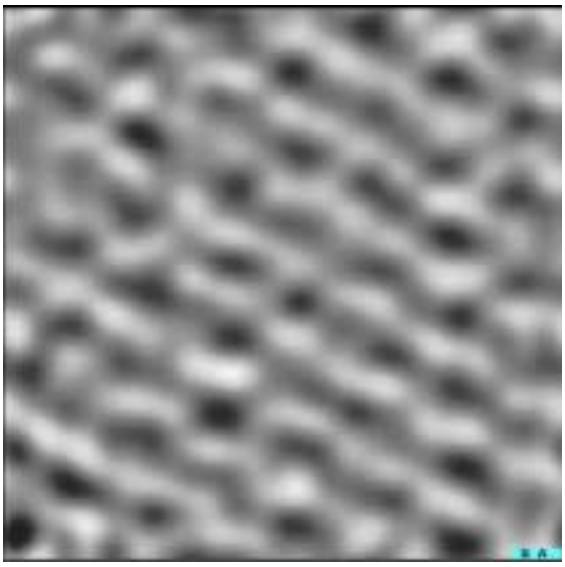

c)

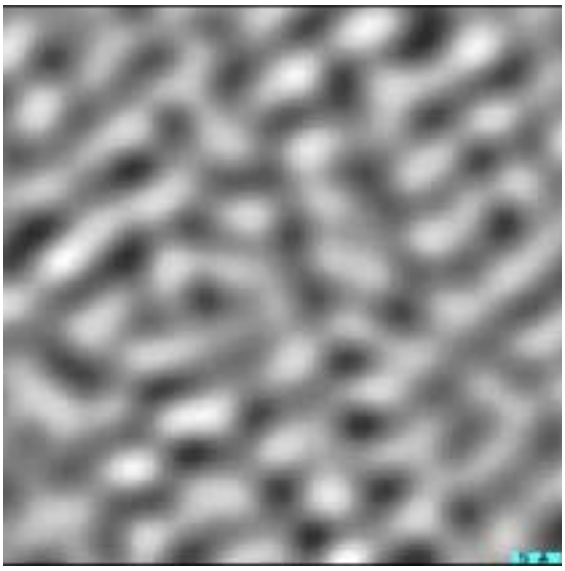

d)

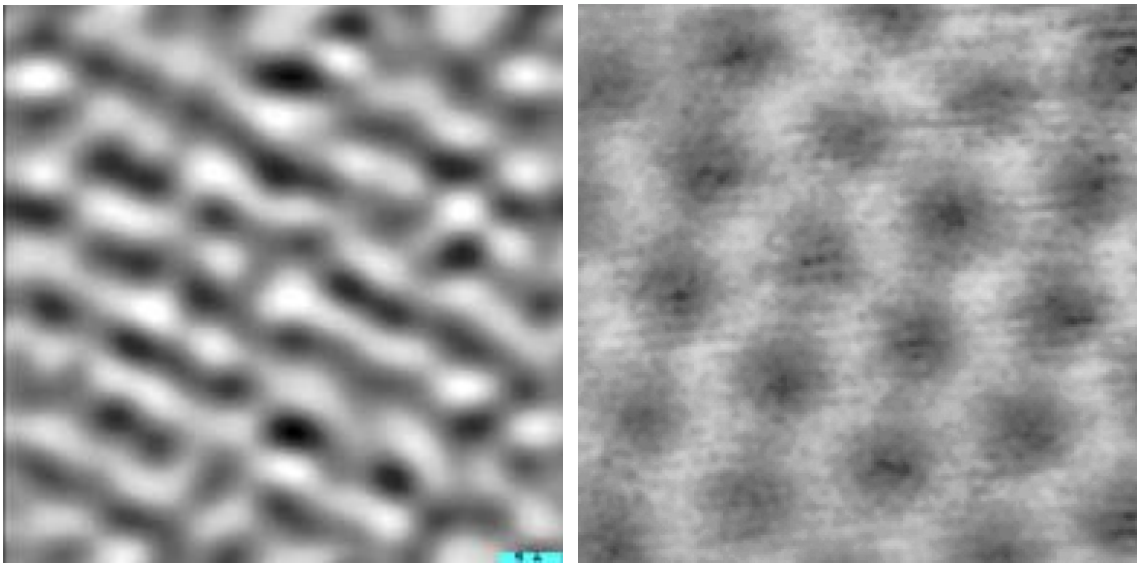

e) f)

Figure 4.6 – Series of STM images of cyclohexene adsorbed to Pt(111) as the back pressure of gas is increased. The pressure is: a) 2 L (70Å x 70 Å), b) 1 x 10^{-5} Torr (40 Å x 40 Å), c) 100 mTorr (42 Å x 42 Å), d) 1.5 Torr (50 Å x 50 Å), e) (35 Å x 35 Å)and f) 10 Torr (65 Å x 65 Å). The structure observed remains the same up until 10 Torr when it starts to change. Data suggests it is changing from the (√7 x √7) R19.1º π-allyl structure to a (√43 x √43) R7.6º 1,4- cyclohexadiene structure.

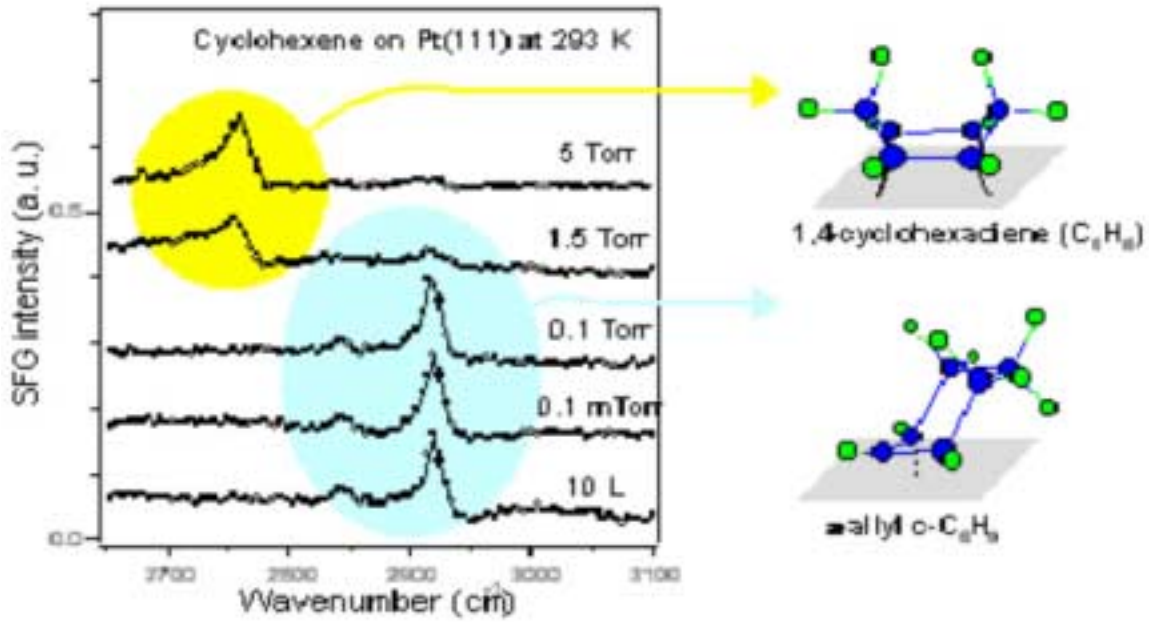

Figure 4.7 – Sample sum frequency generation vibrational spectroscopy spectra of Pt(111) in the presence of increasing pressures of cyclohexene. As can be observed, the dominant surface species converts to 1,4-cyclohexadiene from the π-allyl at around 2 Torr.

4.4 Conclusions

At 300K and at low pressures we have identified three stable surface structures formed from cyclic C_6 hydrocarbons. Both cyclohexane and cyclohexene partially dehydrogenate to form an ordered π-allyl overlayer with a surface structure of (√7 x √7) R19.1˚. Benzene and 1,3-cyclohexadiene both form a (2√3 x 2√3) R30.0˚ structure, which consists of molecular benzene. Finally 1,4-cyclohexadiene forms a structure very different from the first two. This (√43 x √43) R7.6 structure is either pure 1,4-cyclohexadiene or a coadsorption structure containing other partially dehydrogenated species.

The pressure dependent surface structure of cyclohexene on Pt(111) revealed that from doses to $1x10^{-5}$ Torr up to 1 Torr the surface structure remains the π-allyl (√7 x √7) R19.1˚ structure observed at low pressures. Further increasing the pressure to 10 Torr, however, shows a surface phase change to a structure similar to the (√43 x √43) R7.6° structure of 1,4-cyclohexadiene. Sum frequency generation studies support that this phase change occurs at a similar pressure.

References

[1] Yang, M.; Chou, K. C.; Somorjai, G. A. *Journal of Physical Chemistry B* **2004**, *107*, 14766.

[2] Koel, B. E.; Blank, D. A.; Carter, E. A.; *Journal of Molecular Catalysis A*, **1998**, *131*, 39.

[3] Henn, F. C.; Diaz, A. L.; Bussell, M. E.; Hugenschnidt, M. B.; Domagala, M. E.; Campbell, C. T. *Journal of Physical Chemistry* **1992**, *96*, 5965.

[4] Smil, V.; *Nature* **1999**, *400*, 415.[5] Jenson, J. A.; Rider, K. B.; Chen, Y.; Salmeron, M.; Somorjai, G. A. *Journal of Vacuum Science and Technology B*, **2003**, *204-205*, 499.

[6] Klein, M.; Schwitzgebel, G. *Review of Scientific Instruments*, **1997**, *68*, 3099.

[7] Yang, M.; Dunietz, B.; Head-Gordon, M.; Somorjai, G. A. *To be Published*

[8] Somorjai, G.; A. *Introduction to Surface Chemistry and Catalysis*, John Wiley and Sons, New York, NY 1994.

[9] Yang, M.; Somorjai, G. A. *Journal of the American Chemical Society* **2003**, *125*, 11131.

[10] Bussell, M. E.; Henn, F. C.; Campbell, C. T. *Journal of Physical Chemistry* **1992**, *96*, 5978.

[11] Pansoy-Hjelvik, M. E. Schnabel, P.; Hemminger, J. C. *Journal of Physical Chemistry* B. **2000**, *104*, 6554.

[12] Saeys, M.; Reyniers, M. F.; Marin, G. B.; Neurock, M. *Surface Science* **2002**, *513*, 315.

[13] Sautet, P.; Bocquet, M. L. *Surface Science* **1994**, *304*, L445.

[14] Saeys, M.; Reyniers, M. F.; Marin, G. B.; Neurock, M. *Journal of Physical Chemistry B*. **2002**, *106*, 7489.

[15] HugenSchmidt, M. B.; Diaz, A. L.; Campbell C. T. *Journal of Physical Chemistry* **1992**, *96*, 5974.

[16] Su, X.; Kung, K.; Lahtinen, J.: Shen, R. Y.; Somorjai, G. A. *Catalysis Letters* **1998**, *54*, 9.

Chapter 5: Combined STM Surface Structure and Reaction Rate Studies of Cyclohexene Hydrogenation/Dehydrogenation and Its Poisoning by Carbon Monoxide on the Pt(111) Crystal Surface

This chapter details the use of HPSTM to study the hydrogenation/ dehydrogenation of cyclohexene on platinum(111). Catalytic reactions of cyclohexene were studied on platinum in the presence of hydrogen at mTorr pressures in the 300K – 350K temperature range. The surface structures were monitored by STM during the reaction and in the presence of CO that poisons the reactions. Reactivity was monitored by a mass spectrometer.

When 20 mTorr of H_2 and 20 mTorr of cyclohexene are introduced at 300K the surface forms the same structure seen at low pressures of pure cyclohexene. No gaseous cyclohexane or benzene is observed. Heating to 350K disorders the surface but the catalyst remains inactive as the surface becomes covered with benzene and other dehydrogenated carbonaceous fragments. When a pressure of H_2 of 200 mTorr is used at 300K with 20 mTorr cyclohexene, the surface is disordered and both cyclohexane and benzene gaseous products can be detected as they are formed by continuous catalytic reaction. Adding 5 mTorr of CO stops all catalysis and orders the surface. Repeating

this experiment at 350K yields the same result of poisoning the reaction except the surface stays disordered upon addition of CO. Lowering the temperature to 325K recovers the ordered CO structure. Using higher pressures of gases (1.5 Torr cyclohexene, 15 Torr H_2 and 1 Torr CO) also yields a disordered surface during catalysis, and an ordered surface upon introducing CO at 300K that poisons the reaction. Again the CO structure disorders when heated to 350K.

5.1 Introduction

High pressure scanning tunneling microscopy (HPSTM) has proven to provide the means of monitoring the structure of the metal surface during catalytic turnover [1,2]. The technique is able to detect molecular surface structures that are present at high pressures. It can also monitor the mobility of adsorbates and metal atoms if motion occurs in the range of the scan rate ~ 100Å/msec. This ability to detect surface dynamics is rather unique in the repertoire of surface techniques that provide molecular information under reaction conditions. Most spectroscopic techniques yield time-averaged information of structure and bonding. In prior studies we utilized the HPSTM (which was built for the first time in our laboratory) [3,4] to study ethylene hydrogenation and it's poisoning by carbon monoxide using the (111) crystal faces of platinum and rhodium [5,6]. It was found that the surface monolayers of adsorbates, mostly ethylidyne (C_2H_3) and hydrogen in this case are mobile and disordered while the catalytic turnover proceeds at a steady and sustainable rate. Upon the introduction of carbon monoxide the reaction stops and ordered domains form that are co-adsorbed ethylidyne and CO on the platinum and rhodium. The conclusion of these studies was that adsorbates on the catalytically

active metal surface must be mobile. This permits active metal sites where reaction events occur to become temporarily available as the adsorbates leave the site. This is made possible by the low activation energy for surface diffusion (~0.1 eV) as compared to the heat of desorption of strongly bound adsorbates.

In this chapter I report combined HPSTM and reaction turnover studies of the hydrogenation and dehydrogenation of cyclohexene to cyclohexane and benzene, respectively. This reaction has been studied extensively in the 300K – 450K region on the Pt(111) surface using sum frequency generation (SFG) – vibrational spectroscopy in the presence of excess hydrogen as well as gas chromatography (GC) [7-9,17]. SFG surface spectroscopy was also carried out at low and high reactant pressures (10L to 5 Torr) as a function of temperature to monitor the surface species [8]. At 300K and 1.5 Torr cyclohexene, 1,4-cyclohexadiene and some 1,3-cyclohexadiene form on the surface. As the temperature is increased these species convert to the π-allyl (C_6H_9) at about 320K as detected by SFG, this species remains on the surface until about 420K where it further dehydrogenates to benzene. At room temperature and cyclohexene pressures below 1 Torr however it has been shown that the π-allyl is the only significant surface species [10]. The presence of hydrogen changes somewhat the reactions that occur. At room temperature with 1.5 Torr cyclohexene and 15 Torr hydrogen again 1,4-cyclohexadiene is the dominant species. As before at 320K it converts to the π-allyl. At around 400K, it converts to 1,3 cyclohexadiene before fully dehydrogenating to benzene.

Our HPSTM studies support the SFG findings of the formation of the π-allyl species from cyclohexene at low pressures on the Pt(111) crystal face at 300K. As the pressure of hydrogen is increased the steady state production of both cyclohexane and

benzene is detectable and there is an absence of ordered surface structures. The STM images are diffuse indicating surface mobility of the adsorbed species that is faster than the scan rate of the STM, just as it was found in previous studies of ethylene hydrogenation. Increasing the temperature in the absence or at low pressures of hydrogen (20 mTorr) yields an immobile carbonaceous overlayer as a result of rapid dehydrogenation. At higher hydrogen pressures the surface remains disordered and catalytically active. When carbon monoxide is introduced at 300K, catalytic turnover stops, the reaction is poisoned. Simultaneously an ordered surface structure can be detected with STM that proved to be the ($\sqrt{19}$ x $\sqrt{19}$)-CO structure that has also been identified in previous HPSTM studies [11,12]. Repeating this experiment at 350K yields similar results. When the reaction is poisoned with CO turnover stops, but in this case the surface remains disordered. Reducing the temperature to 330K reestablishes the CO order.

5.2 Experimental

All experiments were performed in a high pressure, high temperature STM that has been described in detail elsewhere [4]. The system combines a UHV surface analysis/preparation chamber with a variable temperature (298K – 675K) and pressure (10^{-10} – 10^{3} Torr) Scanning Tunneling Microscope (RHK Technology, Model VT-UHV 300). The base pressure of the system was 1 x 10^{-10} Torr with a background mostly made up of H_2, CO and H_2O. Using three gate valves, the STM chamber can be isolated from the rest of the system and filled with any gas mixture. Leaking the gas to a mass

spectrometer monitored the composition of the gas. (Stanford Research Systems, RGA 200)

All experiments were carried out using a platinum single crystal of (111) orientation. The crystal was polished using diamond grit down to a grit size of .25 μm. Before each experiment the sample was sputtered in 5 x 10^{-6} Torr O_2 for 15 minutes. The ion energy was 400 eV and the current was ~4 μA. The sample was then heated with an electron beam heater to 1123 K for 5 min and briefly flashed back to 1123K for 1 minute just prior to being transferred to the STM chamber. Sample cleanliness was monitored using Auger electron spectroscopy and checked with STM prior to gas introduction.

During STM experiments, the STM chamber was isolated from the rest of the system while various combinations of hydrogen, cyclohexene, and carbon monoxide were introduced. Hydrogen was always introduced first followed by the cyclohexene and then CO (if necessary). The hydrogen and CO were of ultrahigh purity grade, while the cyclohexene (99.5%, Fluka) were purified by freeze-pump-thaw treatment before being introduced. If the experiment involved CO it was introduced after the sample had reached experimental temperature. In order to heat our sample in the presence of high pressures of potentially reactive gases, a 150 W, tungsten filament, halogen filled, quartz projector bulb was used. The bulb provided radiative heating without making mechanical contact and could be raised into position so it was directly below the sample providing the most efficient heating possible. A type K thermocouple spot-welded to the side of the crystal monitored sample temperature. The sample was always allowed to equilibrate at least 5 min prior to imaging. All images were taken using electrochemically etched tungsten tips etched with a technique developed by Klein et. al. [13]. STM settings

during image acquisition were I=0.05 - 0.2 nA and V= 50 – 100 mV. A pressure transducer was used to monitor the chamber pressure during experiments. A Varian ionization gauge model UHV-24 was used to monitor pressures up to 5 x 10^{-5} Torr and the appropriate gas correction factor was used to calculate the pressure of each type of gas. MKS Instrument Baratron model 722A was used for experiments involving pressures ranging from .1mTorr – 10 Torr and model 122A was used for experiments exceeding 10 Torr.

5.3 Results/Discussion

Exposure to 20 mTorr of cyclohexene and 20 mTorr of hydrogen

The Pt(111) surface in the presence of cyclohexene and hydrogen was studied with STM and mass spectrometry. The surface structure in the presence of 20 mTorr of H_2 and 20 mTorr of cyclohexene at 300K is shown in Figure 5.1. As can be seen, the structure formed is ($\sqrt{7}$ x $\sqrt{7}$) R19.1˚ structure identical to that formed by pure cyclohexene at lower pressures [14]. Thus the presence of hydrogen at this pressure is not sufficient to prevent the formation of the partially dehydrogenated π-allyl. It also does not weaken the Pt-π-allyl surface bond enough to allow for room temperature mobility that is faster than our STM is capable of imaging. An analysis of the bulk gas with a mass spectrometer however shows no significant production of either cyclohexane or benzene. When the temperature is increased to 350K there is still no cyclohexane or benzene detected but the surface disorders (Figure 5.2). This is not entirely surprising however. As has been shown previously [7,9], the increase in temperature also leads to an increase in benzene production, which is significantly less mobile than cyclohexane

and has a very low desorption probability. The surface may become covered with the benzene product potentially leading to self-poisoning. The higher temperatures also can lead to decomposition and dehydrogenation of adsorbed benzene, eventually leading to the formation of an immobile carbonaceous overlayer. In an effort to further understand how benzene behaves on the surface, we exposed the (111) platinum surface to 2 x 10^{-6} Torr of pure benzene at 298K and then heated the sample to 350K as was done in the previous experiment. As was observed in the reaction studies, an ordered surface at room temperature (Figure 5.3a) disordered at 350K (Figure 5.3b) further leading us to believe that the catalyst surface in the previous experiment was poisoned by benzene and other dehydrogenated species.

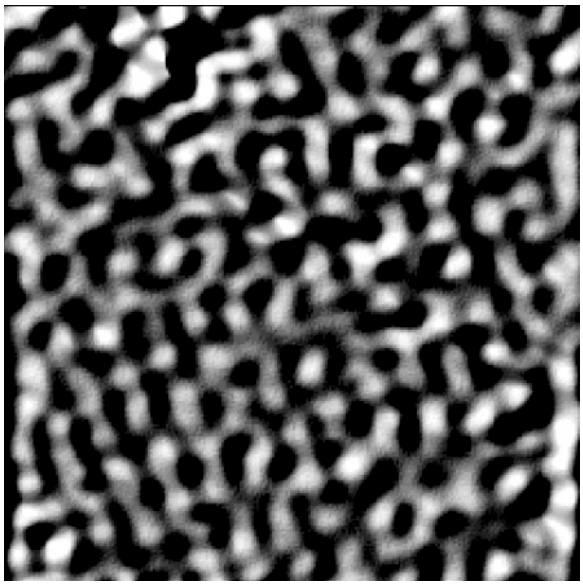

Figure 5.1- 100 Å x 100Å image of Pt(111) at 25C in the presence of 20 mTorr of hydrogen and 20 mTorr of cyclohexene. Surface structure formed is the ($\sqrt{7}$ x $\sqrt{7}$) R19.1˚ composed of the π-allyl species.

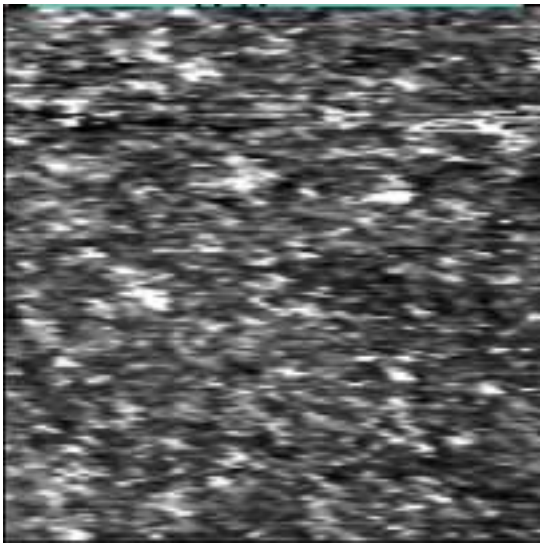

Figure 5.2 - 100Å x 100Å image of Pt(111) at 350K in the presence of 20 mTorr hydrogen and 20 mTorr cyclohexne. No surface order can be discerned, but mobile adsorbate species are present that give rise to streaks as they are partially imaged by the scanning

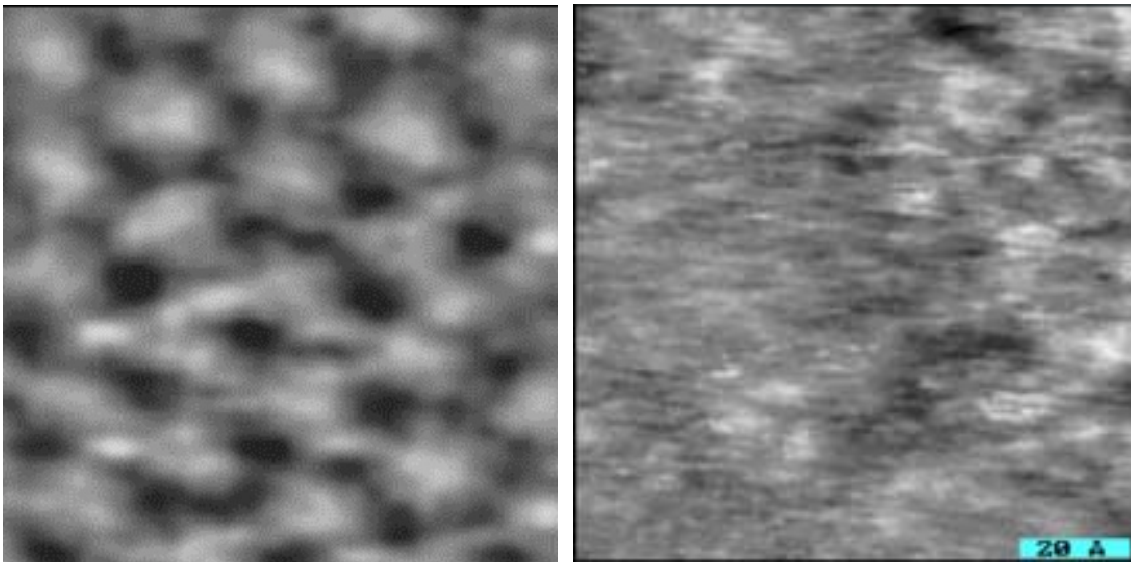

a) **b)**

Figure 5.3 – a)50Å x 50Å STM images of Pt(111) at 300K in the presence of 2 x 10^{-6} Torr benzene. Surface orders at room temp. b) 100Å x 100Å of the same surface heated up to 350K. All surface order is lost.

High pressure studies under catalytic reaction conditions (20 mTorr cyclohexene, 200 mTorr hydrogen. Effect of CO poisoning.

a) Room temperature

When the Pt(111) sample was exposed to 200 mTorr of hydrogen and 20 mTorr of cyclohexene at 298K no surface ordering could be detected by STM (Figure 5.4). This suggests rapid diffusion and low residence time of adsorbed reactant molecules as well as the formed products cyclohexane and benzene. Mass spectrometry data shows that the surface is catalytically active producing mostly cyclohexane. A sample graph from the mass spectrometry study is shown in figure 5.5. This preference for the cyclohexane product has been previously found at higher pressures but at the same H_2/C_6H_{10} ratio [7,9]. When 5 mTorr of CO is introduced, cyclohexene and benzene production is stopped as detected by mass spectrometry. This ceasing of catalytic activity corresponds to the formation of an ordered surface overlayer (Figure 5.6). The structure in figure 5.6 is the only structure observed and appears similar to the saturated CO ($\sqrt{19} \times \sqrt{19}$) R23.4° structure reported earlier by Besenbacher et. al[11,12] and also observed in our system when the crystal was exposed to 5 Torr of pure CO (Figure 5.7). In our reaction images the periodicity observed is from the ($\sqrt{19} \times \sqrt{19}$) R23.5˚ unit cell CO structure and individual molecules within the unit cell are not resolved.

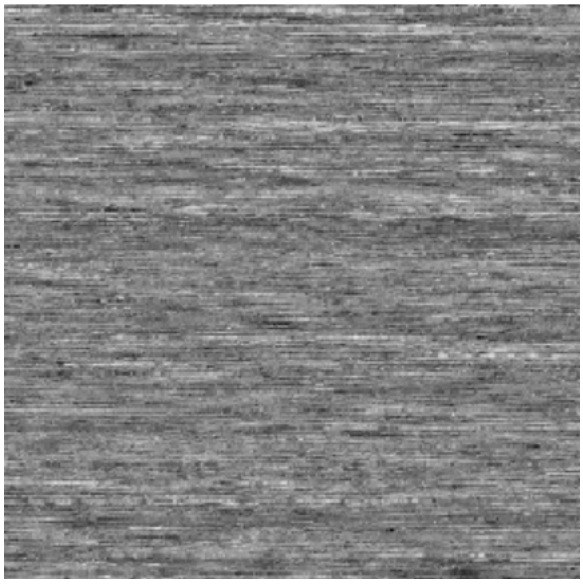

Figure 5.4 - - 75Å x 75Å STM image of Pt(111) at 300K in the presence of 200 mTorr H_2 plus 20 mTorr cyclohexene. No discernable order or surface structure is observed.

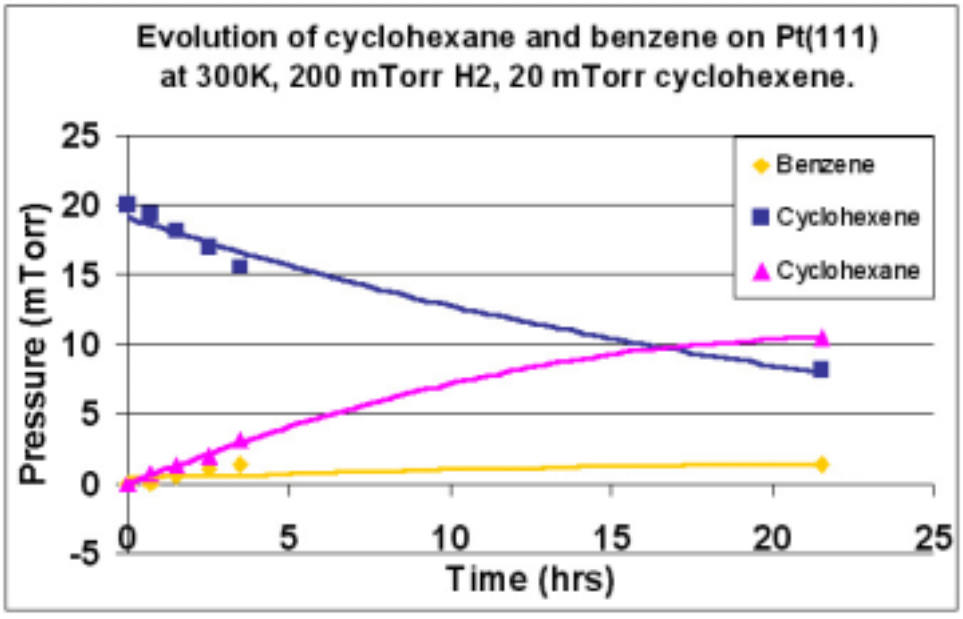

Figure 5.5 - Mass spectrometer study showing the evolution of the reaction products (cyclohexane and benzene) at 300K resulting from cyclohexene hydrogenation and dehydrogenation

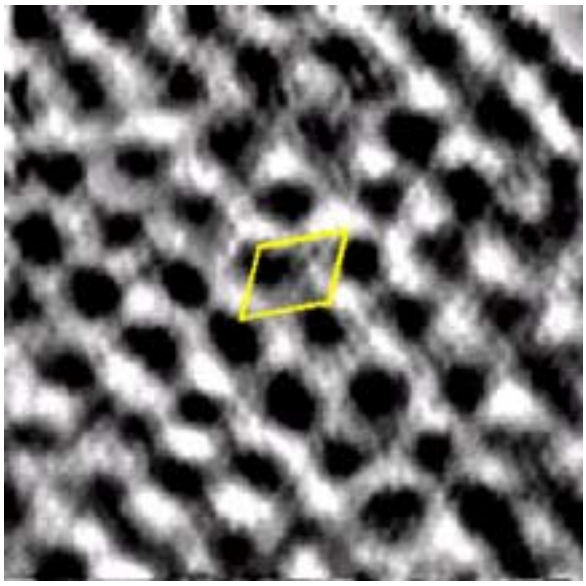

Figure 5.6 - 90Å x 90Å STM image of Pt(111) at 300K in the presence of a mixture of 200 mTorr H_2, 20 mTorr of cyclohexene, and 5 mtorr CO. Periodicity of ~13Å corresponds to structure seen for pure CO. A unit cell has been drawn.

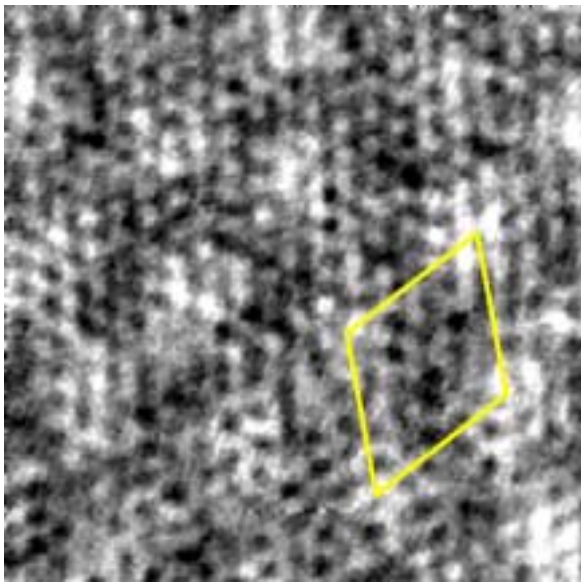

Figure 5.7 - 50Å x 50Å STM image of Pt(111) in the presence of 5 Torr CO at 300K. A large (√19 x √19) R23.4° unit cell is marked. The Moire structure is due to the incommensurability of CO-CO and Pt-Pt distances.

b) Temperature increased to 353K

The same experiment was repeated at a temperature of 353K. At this temperature and higher pressures the surface is known to favor dehydrogenation. Our mass spectrometer experiments confirm this result. Again as in the room temperature case, STM images show a surface with no discernable surface order in figure 5.8a. This can once again be attributed to the high mobility of surface species as well as low residence times. When 5 mTorr of CO is introduced once again all catalytic activity ceases as is evidenced from mass spectrometry. STM however still shows a disordered surface (Figure 5.8b) indicating fairly mobile surface species. This is not entirely surprising. Calculating the residence time of pure CO on Pt(111) using Equation 5.1 [15]

Equation 5.1- $\tau = \tau_o \cdot e^{\left(\frac{\Delta H_{ads}}{RT}\right)}$

τ = residence time,

$\tau_o = 10^{-12}$ sec,

ΔH_{ads} = heat of adsorption,

R = Gas constant,

T = temperature

and a saturation binding energy of 80 kJ/mol [16] a residence time of roughly 2 seconds is obtained. The time to acquire an image is roughly 1 minute so the short residence time alone would make it difficult to image the CO structure. In addition, due to the high mobility of CO [18,19] neighboring molecules can quickly move to fill these sites before a molecule from the gas phase adsorbs resulting in a highly mobile surface as well.

Although resolving periodicity should still be possible as CO molecules will spend a disproportionate amount of time on preferred adsorption sites resulting in increased electron density, the corrigation will be significantly reduced and we were never able to resolve the structure. Increasing the pressure of CO would increase the flux of CO hitting the surface and as is shown in equation 5.2 [15]

Equation 5.2 - $\sigma = F\tau$

σ = coverage,

F = flux and

τ = residence time.

also increasing the coverage. Although the increase in coverage will not increase the residence time, and will in fact most likely decrease it, it will reduce the probability that neighboring molecules will fill the vacant site before a gas molecule, thus lowering the mobility and potentially making imaging at this temperature possible. The explanation for the lack of catalytic activity can be due to several factors. First the surface is simply dominated by CO resulting in a very low coverage of the π-allyl or other necessary intermediates. Also since vacant sites are needed for hydrogen bond cleavage and formation [15], in order for reaction to occur, cyclohexene must not only adsorb when CO molecules vacate the necessary number of sites, but also encounter another empty site before it desorbs. This theory of a mobile CO covered surface is supported by the fact that if we then cool the sample down to 325K resulting in a calculated residence time of 35 seconds, a clearly ordered overlayer corresponding to the ($\sqrt{19}$ x $\sqrt{19}$) R23.4° CO structure is observed (Figure 5.9).

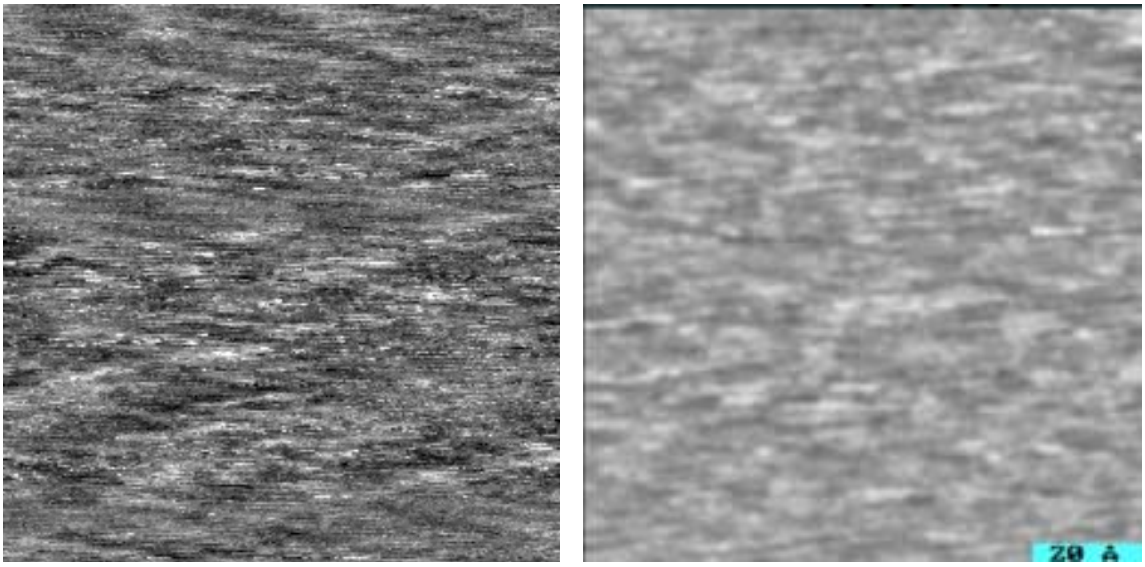

a) **b)**

Figure 5.8 - 100Å x 100Å STM images of Pt(111) at 80C in the presence of a) 200 mTorr H_2, 20 mTorr of cyclohexene, and b) 200 mTorr H_2, 20 mTorr of cyclohexene, and 5 mTorr CO. No order is seen despite the lack of catalytic activity and the introduction of CO.

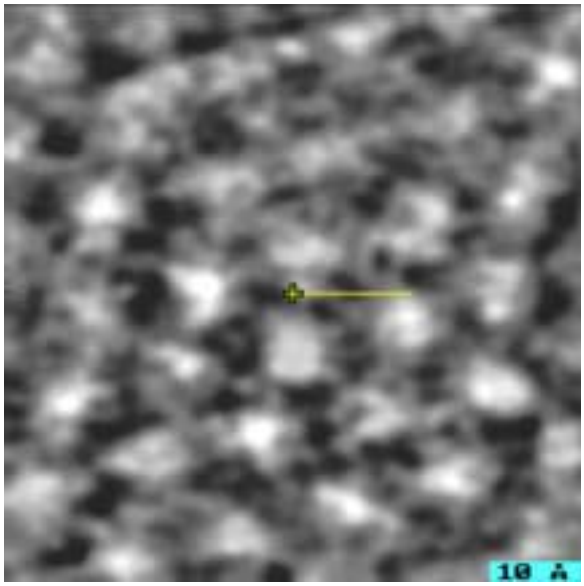

Figure 5.9 - 70Å x 70Å image of Pt(111) in the presence of 200 mTorr H2, 20 mTorr of cyclohexene heated to 80ºC, 5 mTorr CO added cooled to 50ºC

c)Higher pressures (> 10 Torr) of cyclohexene, hydrogen and CO

The effect of CO poisoning on Pt(111) catalyzed hydrogenation/dehydrogenation of cyclohexene at 298K and pressures in the Torr regime was also studied. The mass spectrometer used in this study is unable to detect small amounts of product in large excesses of reactants, so data from previous gas chromatography studies was used [20]. When exposed to 15 Torr H_2 and 1.5 Torr of cyclohexene the platinum surface is markedly different from the lower pressure experiments. SFG studies done by Yang et. al. [8] have shown that the dominant surface species is no longer the π-allyl but is now 1,4-cyclohexadiene. This study also shows that the surface is catalytically active in the hydrogenation of cyclohexene. STM reveals a disordered surface that indicates the cyclohexadiene species is also mobile at room temperature with an excess of hydrogen. When 1 Torr of CO was introduced the result was similar to the lower pressure study. An ordered CO array could be easily seen everywhere on the surface (Figure 5.10). This formation of an ordered surface overlayer also coincides with the ceasing of all catalytic activity observed by Yang at lower CO partial pressures. As was in the case for our lower pressure study as well, the CO ordering disappeared when the sample was heated to 350K and reappeared upon cooling back to 300K.

Figure 5.10 - 100Å x 100Å image of Pt(111) at 25ºC in the presence of 15 Torr H_2, 1.5 Torr of cyclohexene and 1 Torr CO

5.4 Conclusions

The adsorbed monolayer that is produced during cyclohexene hydrogenation/ dehydrogenation on the catalytically active surface is disordered. These results are the same as those found for ethylene hydrogenation in prior studies [6]. Thus, surface mobility is an important feature of the catalytically active metal surface. Poisoning the reaction by the introduction of carbon monoxide produces an ordered surface overlayer at 300K that becomes disordered at 350K but orders again when the temperature is brought back below 325K. Thus the CO induced reduction of mobility in combination with site blocking poison the catalytic reaction. These findings bring into focus the importance of adsorbate mobility and site competition on the crowded surface during catalytic turnover.

The activation energy for ethylene hydrogenation on the CO poisoned Pt(111) surface increased to 20 kcal/mol as compared to the 9.7 kcal/mol for the reaction in the

absence of CO [5]. The heat of desorption of CO at high coverages is about 20 kcal/mol [16] which indicates that the reaction can only take place on the CO poisoned surface if the CO molecules desorb. Studies by Yang [20] indicate similar changes in the activation energy for cyclohexene hydrogenation/dehydrogenation in the presence of carbon monoxide. Apparent activation energies for hydrogenation and dehydrogenation in the absence of CO are 8.6 kcal/mol and 17.9 kcal/ mol respectively. These activation energies increase to 16.1 kcal/mol and 24.8 kcal/mol after CO is introduced.

SFG studies by Yang on Pt(111) at pressures ranging from 10L – 100 mTorr of cyclohexene indicate the presence of a π-allyl (C_6H_9) species at room temperature. The π-allyl is also observed at 1.5 Torr of cyclohexane at 310K. The ordered ($\sqrt{7}$ x $\sqrt{7}$) R19.1˚ structure we see by STM at 20mTorr of hydrogen and 20 mTorr of cyclohexene can be assigned to the π-allyl molecule. As the temperature is increased we see a disordered overlayer that corresponds to the presence of mobile benzene and potentially other dehydrogenated products which results in a catalytically inactive surface. Upon the addition of excess hydrogen at room temperature, STM images show a disordered overlayer and simultaneously we detect the onset of catalytic turnover for both hydrogenation and dehydrogenation of cyclohexene.

The addition of CO causes all catalytic activity to cease. The fact that CO also forms ordered ($\sqrt{19}$ x $\sqrt{19}$) domains at 300K, which remain ordered to 323K, but disorder at 353K reflects the higher activation energy for the mobility of adsorbed CO on the Pt(111) surface as compared to cyclohexene and other cyclic C_6 species in the presence of >20mTorr of hydrogen under reaction conditions at 300K.

References

[1] Hendriksen, B. L. M.; Frenken, J. L. M. *Physical Review Letters*. **2002**, 89, 046101.

[2] McIntyre,B. J.; Salmeron, M.; Somorjai, G. A. *Journal of Catalysis*. **1996**, *164*, 18.

[3] McIntyre,B. J.; Salmeron, M.; Somorjai G. A. *Review of Scientific Instruments*, **1993**, *64*, 687.

[4] Jenson, J. A.; Rider, K. B.; Chen, Y.; Salmeron, M.; Somorjai, G. A. *Journal of Vacuum Science and Technology B*, **2003**, *204-205*, 499.

[5] Hwang, K. S.; Yang, M.; Zhu, J.; Grunes, J.; Somorjai, G. A. *Journal of Molecular Catalysis A.* **2003**, *204-205*, 499.

[6] Tang, D. C.; Hwang, K. S.; Salmeron, M.; Somorjai, G. A. *Journal of Physical Chemistry B*. **2004**, *108*, 13300.

[7] Su, X.; Kung, K.; Lahtinen, J.: Shen, R. Y.; Somorjai, G. A. *Catalysis Letters* **1998**, *54*, 9.

[8] Yang, M.; Chou, K. C.; Somorjai, G. A. *Journal of Physical Chemistry B* **2003**, *107*, 5267.

[9] McCrea, K. R.; Somorjai, G. A. *Journal of Molecular Catalysis A.* **2003,** *163***,** 43**.**

[10] Yang, M.; Chou, K. C.; Somorjai, G. A. *Journal of Physical Chemistry B* **2004**, *108*, 14766.

[11] Vestergaard, E. K.; Thostrup, P.; An, T.; Laesgsgaard, E.; Stensgaard, I.; Hammer, B. Besenbacher, F. *Physical Review Letters*, **2002**, *88*, 259601.

[12] Longwitz, S.R; Schnadt, J; Kruse Vestergaard, E; Vang, R.T; Laesgsaard, E; Stensgaard, I; Brune, H; Besenbacher, F *Journal of Physical Chemistry B* **2004,** *108*, 14497.

[13] Klein, M.; Schwitzgebel, G. *Review of Scientific Instruments*, **1997**, *68*, 3099.

[14] Montano, M; Salmeron, M; Somorjai, G.A; *Surface Science* **2006** (To Be Published)

[15] Somorjai, G. A.; *Introduction to Surface Chemistry and Catalysis*, John Wiley and Sons, New York, NY **1994**.

[16] Ertl, G.;Neumann, M.; Street, K. M.; *Surface Science*, **1977**, *64*, 393.

[17] Yang, M. Somorjai, G. A.; *Journal of the American Chemical Society*, **2003**, *125*, 11131.

[18] Croci, M.; Felix, C.; Vandoni, G,; Harbich, W.; Monet, R.; *Surface Science*, **1993**, *290*, L667.

[19] Ma, J.; Xioa, X.; Dinardo, N. J.; Loy, M. M. T. *Physical Reviews B* **1998**, *58*, 4977.

[20] Yang, M.; Rioux, R.; Somorjai, G. A. *Journal of Catalysis*, **2006**, 237, 255 [15] 1992) 5978.

Chapter 6: Hydrogen and Deuterium Exchange on Pt (111) and Its Poisoning by Carbon Monoxide Studied by Three Surface Sensitive High-Pressure Techniques.

This chapter discusses catalytic hydrogen/deuterium exchange on a platinum (111) single crystal and its poisoning with carbon monoxide studied using scanning tunneling microscopy (STM), X-ray photoelectron spectroscopy (HPXPS), sum frequency generation vibrational spectroscopy (SFG) and mass spectrometry, under reaction conditions at pressures in the mTorr range. At 298K and in the presence of 200 mTorr of hydrogen and 20 mTorr of deuterium the surface is catalytically active for HD production with activation energy of ~5.3 kcal/mol. Addition of 5 mTorr of CO stops the reaction and STM reveals an ordered surface structure of chemisorbed CO. At 353K addition of 5 mTorr of CO to the same system, slows the reaction considerably but HD production continues with activation energy of 17.4 kcal/mol. XPS and SFG indicate that the amount of adsorbed CO is only ~10% less than at room temperature. Changes in the adsorption site of CO as the coverage changes during reaction are detected by SFG and XPS. From these data, a CO dominated, mobile and catalytically active surface model is proposed.

6.1 Introduction

The nature of the poisoning of catalysts under reaction conditions is a problem that, despite huge economic and environmental importance, is still not understood completely. Poisoning is a complex phenomenon involving a variety of effects. The simplest one is site blocking, where the strongly bound poison prevents adsorption of the reactants. However site blocking is rarely complete and numerous vacancies are still present on the catalyst surface. These residual vacancies however, may form ensembles that are too small to allow adsorption of reactants or the formation of reaction intermediates. In that case, mobility of the poison species at sufficiently high temperatures might unblock the catalyst surface by allowing poisons and reactants to diffuse and vacancies to aggregate into sufficiently large ensembles. This is a most interesting situation since the poison becomes either a simple passive spectator species or it might generate patterns of vacancies with special geometries. It might also control, through its diffusion parameters, the rate and selectivity of the reaction. To investigate these interesting issues a molecular scale investigation of the structure of the surface during reaction is required. Until recently most molecular scale surface science studies have been performed at low pressures because the techniques used to obtain such information cannot operate under the high-pressure conditions required for catalysis.

This situation has changed dramatically in recent years due to the development of microscopy and spectroscopy techniques that can operate under realistic pressure and temperature conditions. Here we have employed three such techniques: high-pressure scanning tunneling microscopy (HPSTM), high-pressure X-ray photoelectron spectroscopy (HPXPS) and sum frequency generation vibrational spectroscopy (SFG) to

study a catalytic system near ambient conditions. HPSTM has been shown to be able to provide atomically resolved images at high-pressures and temperatures [1-3] which provide information about the dynamics and structure of the adsorbed monolayer. HPXPS can yield quantitative chemical information and specific binding sites at pressures currently up to 5 Torr [4]. SFG, a non-linear optical technique, provides vibrational spectra and reveals chemical environmental changes in adsorbate structure. The use of these three powerful surface sensitive techniques while concurrently monitoring the activity of the catalyst can give a comprehensive view of the structure of active and poisoned catalyst surfaces.

6.2 Experimental

High-pressure STM experiments were performed in an instrument that has been described in detail elsewhere [5,6]. The system combines a UHV surface analysis/preparation chamber with a variable temperature (298K - 675K) and pressure (10^{-10} - 10^{3} Torr) chamber housing an STM head from RHK (model VT-UHV 300). The base pressure of the system was 1 x 10^{-10} Torr with a background mostly made up of H_2, CO and H_2O. Using three gate valves, the STM chamber can be isolated from the rest of the system and filled with any gas mixture. A mass spectrometer (Stanford Research Systems, RGA 200) connected to the chamber by a leak valve was used to monitor the gas composition.

The sample was a platinum single crystal of (111) orientation from Matek Corporation with a miscut angle of < 0.3˚. Before each experiment the sample was sputtered with Ar ions for 15 minutes at an energy of 500 eV and current of 4 μA. After

sputtering, the sample was heated with an electron beam to 1073 K for 10 min. This process was repeated a few times before transferring the sample to the reaction chamber. The surface composition was monitored by Auger electron spectroscopy and checked with STM prior to gas introduction.

During experiments the STM chamber was isolated from the rest of the system while various combinations of hydrogen, deuterium and carbon monoxide were introduced. Hydrogen was always introduced first followed by CO and deuterium. To heat our sample in the presence of reactive gases, a 150 W projector bulb was used to radiatively heat the sample without making mechanical contact. A type K thermocouple spot-welded to the side of the crystal monitored sample temperature. The sample was always allowed to equilibrate at least 5 min prior to imaging. Blank experiments were run under identical conditions (by removing the crystal) in order to check for background reactions. A sample rate study and the blank study are shown in figures 6.1 a and b respectively. STM images were taken with electrochemically etched tungsten tips, following the technique described by Klein et. al [7]. STM settings during image acquisition were I = 0.05 - 0.2 nA and V = 50 - 100 mV. An MKS Instrument Baratron model 722A was used to monitor chamber pressure.

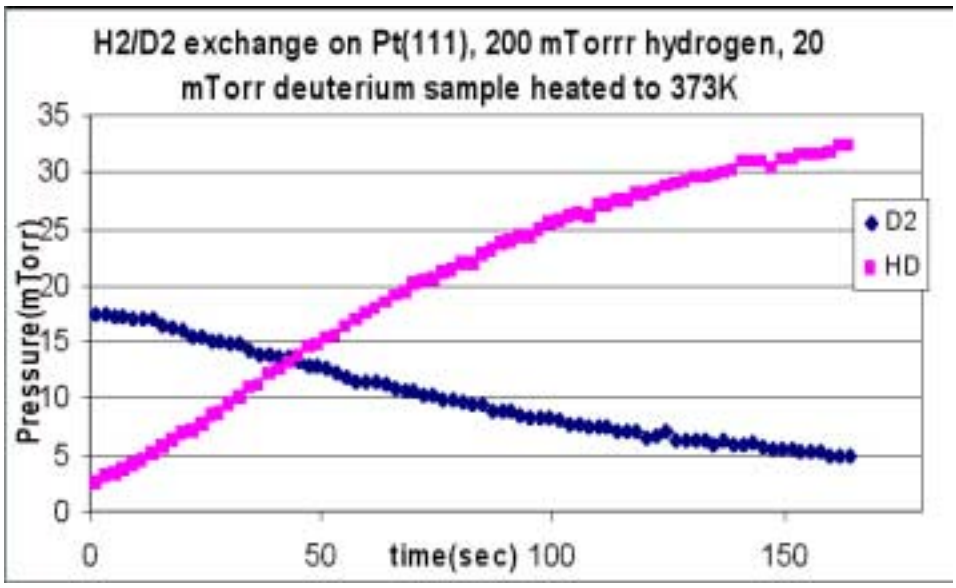

a)

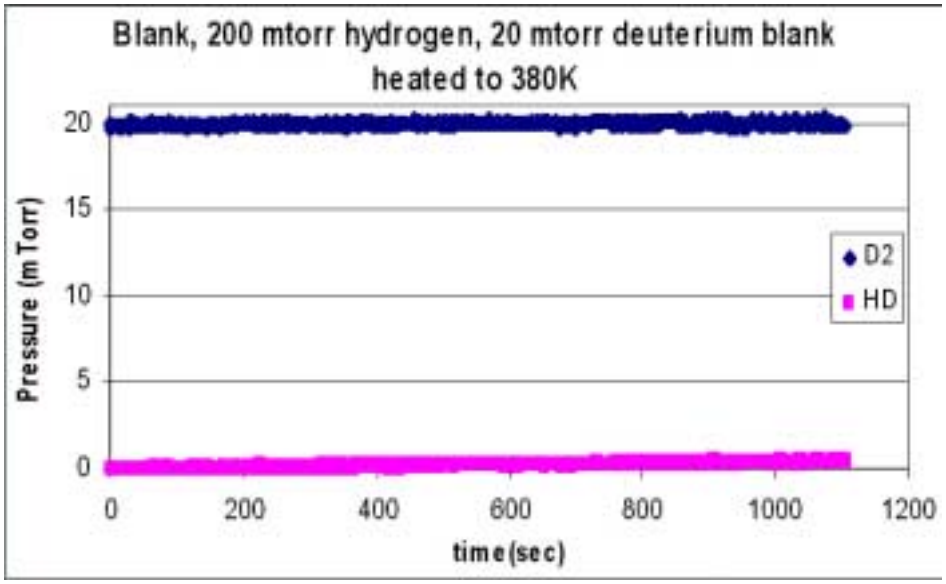

b)

Figure 6.1 – a) Sample graph of H_2/D_2 exchange on platinum (111) showing the evolution of HD and the consumption of D_2. b) Crystal has been removed and replaced with ceramic disc. No HD production can be detected.

The high-pressure x-ray photoelectron spectroscopy experiments were performed at beamline 11.0.2 at the Advanced Light Source in Berkeley. The system uses a differentially pumped electrostatic lens system that has had a prototype described previously [8]. It is also decribed in detail in the beamline manual [9] The platinum 4f, carbon 1s, and oxygen 1s peaks were recorded at incident photon energies of 230eV, 450eV, and 690eV respectively in order that the photoelectron kinetic energy, and therefore their surface sensitivity, is the same. After normalization the peak areas were used to monitor surface coverage of CO. The hydrogen, deuterium and carbon monoxide flows were regulated with three leak valves, which continuously replenished the gases lost through the aperture. Sample heating was accomplished using a button heater directly beneath the sample, which was turned off during measurement.

The sum frequency generation experiments were performed by Katie Bratlie in a system consisting of a UHV chamber with base pressure of 2×10^{-9} Torr and a high-pressure cell isolated from the UHV chamber by a gate valve. Two CaF_2 windows on the HP cell allow transmission of infrared (IR), visible (VIS), and sum frequency radiation for SFG experiments.

A Nd:YAG laser produced 1064 nm photons in 20 ps pulses and 20 Hz repetition rate. This was used to create a tunable IR (1800-4000 cm^{-1}) and a second harmonic VIS (532 nm) beam. The VIS (200 μJ) and the IR (200 μJ) beams were spatially and temporally overlapped on the Pt(111) surface with incident angles of 55º and 60º, with respect to the surface normal. All spectra were taken using a ppp polarization combination (SFG, VIS, and IR beams were all p-polarized). The generated SFG beam was sent through a monochromator and the signal intensity was detected with a

photomultiplier tube and a gated integrator as the IR beam was scanned over the range of interest. The spectra were curve fit using a previously reported procedure [10,11] to a form of the equation 6.1

$$\textbf{Equation 6.1 - } I_{SFG} \propto \left| \chi_{NR}^{(2)} e^{i\phi_{NR}} + \sum_q \frac{A_q}{\omega_{IR} - \omega_q + i\Gamma_q} e^{i\gamma_q} \right|^2$$

where $\chi_{NR}^{(2)}$ is the nonresonant nonlinear susceptibility, $e^{i\phi_{NR}}$ is the phase associated with the nonresonant background, A_q is the strength of the qth vibrational mode, ω_{IR} is the frequency of the incident infrared laser beam, ω_q is the frequency of the qth vibrational mode, Γ_q is the natural line width of the qth vibrational transition, and $e^{i\gamma_q}$ is the phase associated with the transition. Detailed descriptions on the system can be found elsewhere.[12-15]

6.3 Results/Discussion

Scanning Tunneling Microscopy studies

The catalytic activity for H_2/D_2 exchange on the Pt(111) crystal was studied in the presence and absence of CO over a temperature range of 298K – 480K. It was found that at room temperature and in the presence of 200 mTorr of H_2 and 20 mTorr of D_2 the surface is catalytically active producing HD at a rate of ~4.3 mol/site/sec. STM images show a surface with no discernable order (Fig. 6.2a) as the adsorbate species are diffusing much faster than the scanning rate of our instrument (~10 nm/msec). Upon introduction of 5 mTorr of CO the production of HD dropped below the detection limits of our mass spectrometer and no products could be detected over the course of 1.5 days. STM images

of the surface show an ordered surface with hexagonal symmetry (Fig 6.2b). The structure corresponds to an incommensurate CO overlayer similar to the one observed previously for pure CO on Pt(111) [3]. It has a coverage of about 0.6 monolayers. A schematic of the structure is shown is figure 4a. At 345K, the turnover frequency in the absence of CO was measured to be 39.1 mole/site/sec. Once again the STM images revealed the lack of order characteristic of rapidly mobile adsorbates. Addition of 5 mTorr of CO at 353K decreased the reactivity dramatically. Unlike the room temperature case however, catalytic activity was still observed at the rate of 0.03 mol/site/sec. Imaging the surface with STM revealed that the CO overlayer is very mobile so that no periodic structure could be resolved. Cooling the sample back to room temperature restores the previously observed ordered structure (Fig. 6.3).

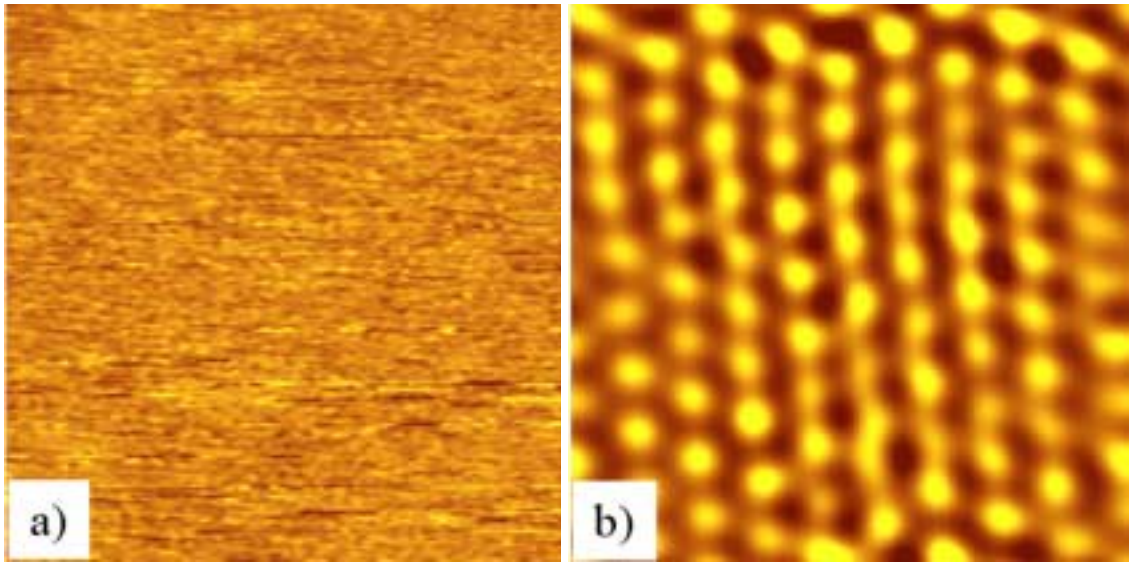

Figure 6.2- 90Å x 90Å STM images of Pt (111). a) in the presence of 200 mTorr H_2 and 20 mTorr D_2. Catalyst is actively producing HD. b) in the presence of 200 mTorr H_2, 20

mTorr D_2 and 5mTorr CO. Catalyst has been deactivated. Structure is high coverage CO forming an incommensurate structure.

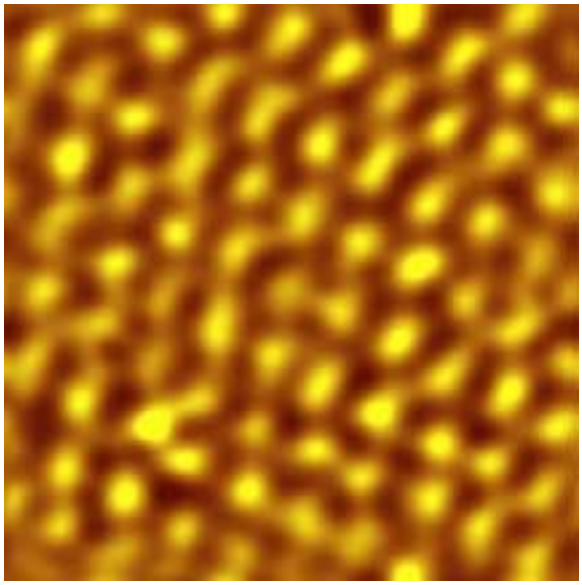

Figure 6.3 - 90Å x 90Å image of Pt(111) in the presence of 200 mTorr H_2, 20 mTorr D_2 heated to 353K, 5 mTorr CO added and cooled to 298K. No products detected

In previous studies of hydrogenation /dehydrogenation of cyclohexene under similar conditions [16] we have shown that although the surface disorders, no products were observed. Similarly, higher pressure studies of ethylene hydrogenation showed no formation of products until the temperature was near 400K [17,18]. The fact that catalytic activity is still observed for H_2/D_2 exchange, suggests that a smaller size of vacancy aggregates are needed for the dissociative adsorption of hydrogen and deuterium than for the larger cyclohexene and ethylene reactants. The larger vacancy ensembles are more difficult to produce on the CO crowded surface.

X-ray Photoelectron Spectroscopy studies

HPXPS spectra of the C1s and O1s peaks from adsorbed CO at 298 K in equilibrium with gas at a pressure of 200 mTorr H_2, 20 mTorr D_2, and 5 mTorr CO are shown in figure 6.4. Under these conditions the surface structure is the same incommensurate structure observed under identical conditions with STM (figure 6.2b). Two peaks in the C1s spectrum can be resolved, at 286.8 eV and 286.1 eV. Analysis of the O1s spectrum also shows clear splitting of the peaks. Similar values for the C1s peaks were obtained in low-pressure studies at 200K [19,20] for the c(4x2) CO on Pt(111) structure. The peaks were assigned to top (286.8 eV) and bridge site adsorption (286.1eV). In the c(4x2) structure however, each CO molecule is bound to a pure atop or bridge site, while under our higher pressure conditions, the surface structure is an incommensurate as shown in figure 6.5a. The observation of two clearly resolved XPS peaks is surprising. This suggests that the CO molecules might not be rigidly constrained to occupy the exact position shown in the schematics and that small lateral displacements are present that bring them closer to the ideal top and bridge sites. It is also possible that the bonding interactions do not change dramatically when small displacements from the ideal positions occur. This might result in core level binding energy shifts very similar to those of the pure top and bridge positions.

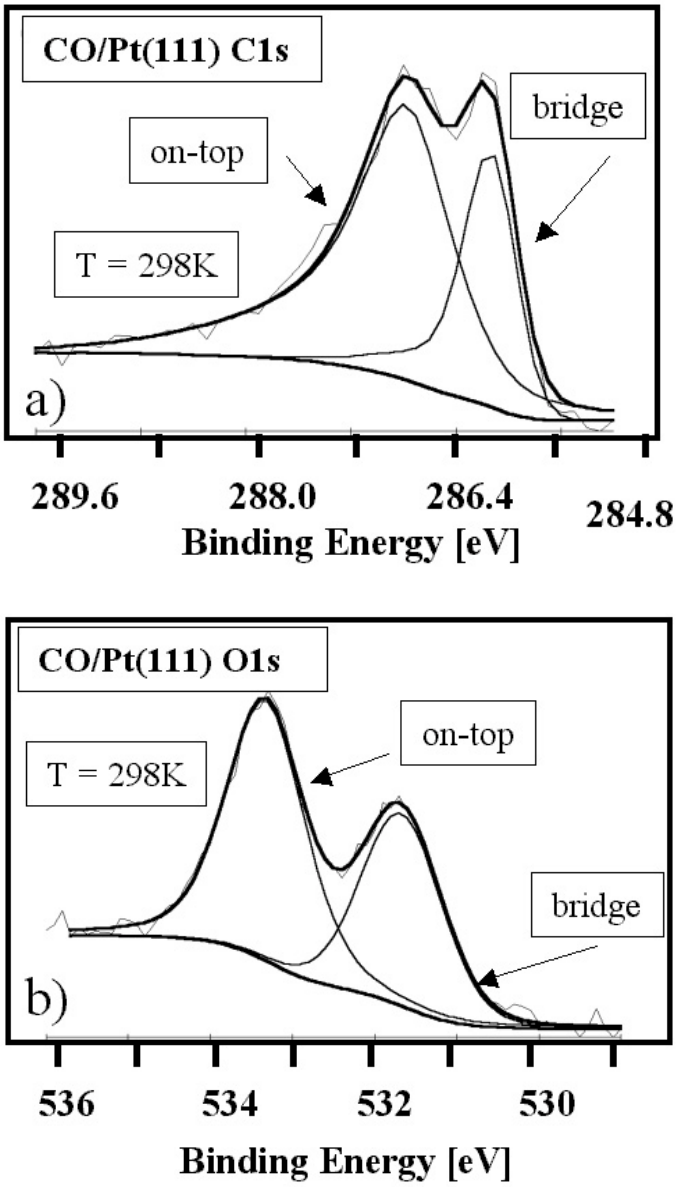

Figure 6.4 - Sample XPS spectra of Pt(111) at 298K exposed to 200 mTorr H_2, 20 mTorr D_2 and 5 mTorr CO. a) CO peaks from C1s orbital. b) CO peaks from the O1s

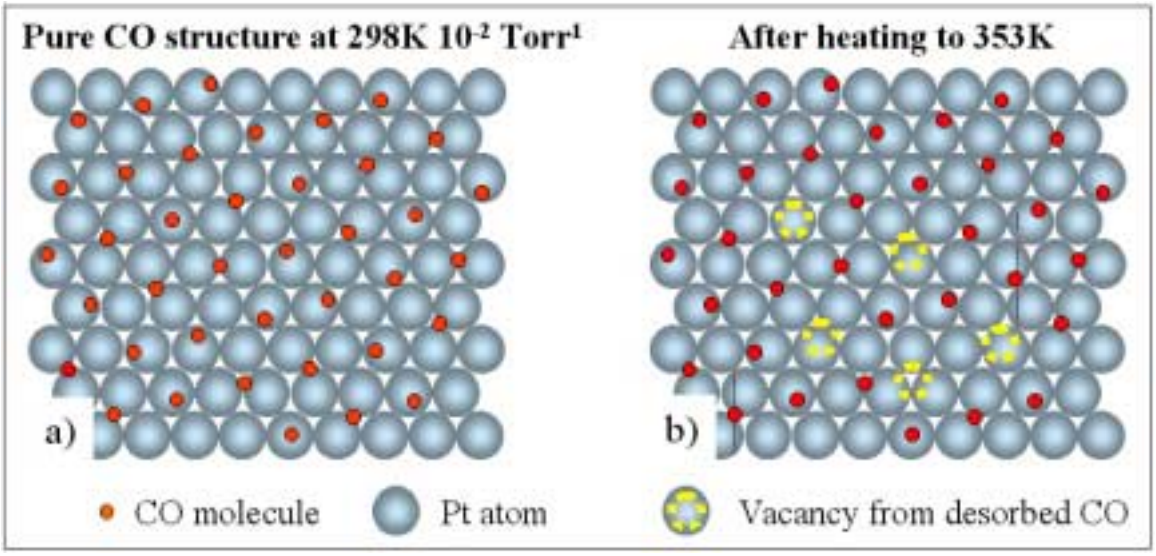

Figure 6.5 - – Diagram showing the proposed structure of CO on the Pt(111) surface with a CO backpressure of 5 mTorr a) at 298 K b) at 353K.

The intensity of the XPS peaks, as well as the total for both the C1s and O1s were monitored as the surface temperature was increased from 298K to 480K in the presence of 200 mTorr H_2, 20 mTorr D_2 and 5 mTorr CO. The C1s and O1s peaks were first normalized to the known starting coverage of 0.6 of a monolayer of CO, and then averaged. The resulting data are plotted in figure 6.6. As the temperature is increased, the total coverage decreases approximately linearly from a coverage of 0.6 at 298K to 0.39 at 480K. The increase in temperature from 298K to 353K, results in only about 11% of the surface CO desorbing. Despite the removal of a relatively small fraction of CO, the surface reactivity increases from being below the detection limits, to a sustainable 0.03 mol/site/sec. This suggests that the creation of a dynamic mobile surface is one of the crucial factors in allowing catalysis. As should also be noted, after the addition of CO to the unpoisoned system, reactivity fell by much more than would be predicted by a simple site blocking mechanism. If one takes the concentration of surface free sites on a

clean platinum surface to be 1, and the concentration of free sites for the incommensurate CO structure to be 0, then the concentration at 353K is ~0.11. The activity of the surface, however fell by more than three orders of magnitude (from 39.1 to 0.03 mol/site/sec). One possible explanation is that multiple free sites must congregate for dissociative hydrogen adsorption. It has been observed at low temperatures for CO on palladium that ensembles of three free sites are necessary [21]. If this was the case, the probability of ensembles of three vacancies forming on the surface would increase cubically with number of free sites. Another possible explanation is that the coadsorbed CO limits the ability of adsorbed H_2 and D_2 to diffuse across the surface and encounter one another. Optical diffraction studies of the independent diffusion of hydrogen atoms and CO molecules on Pt(111) give low coverage diffusion constants for hydrogen which are more than three orders of magnitude higher than for CO [22,23]. Clearly a hydrogen atom adsorbed on a surface of 90% CO will have its ability to diffuse severely hindered.

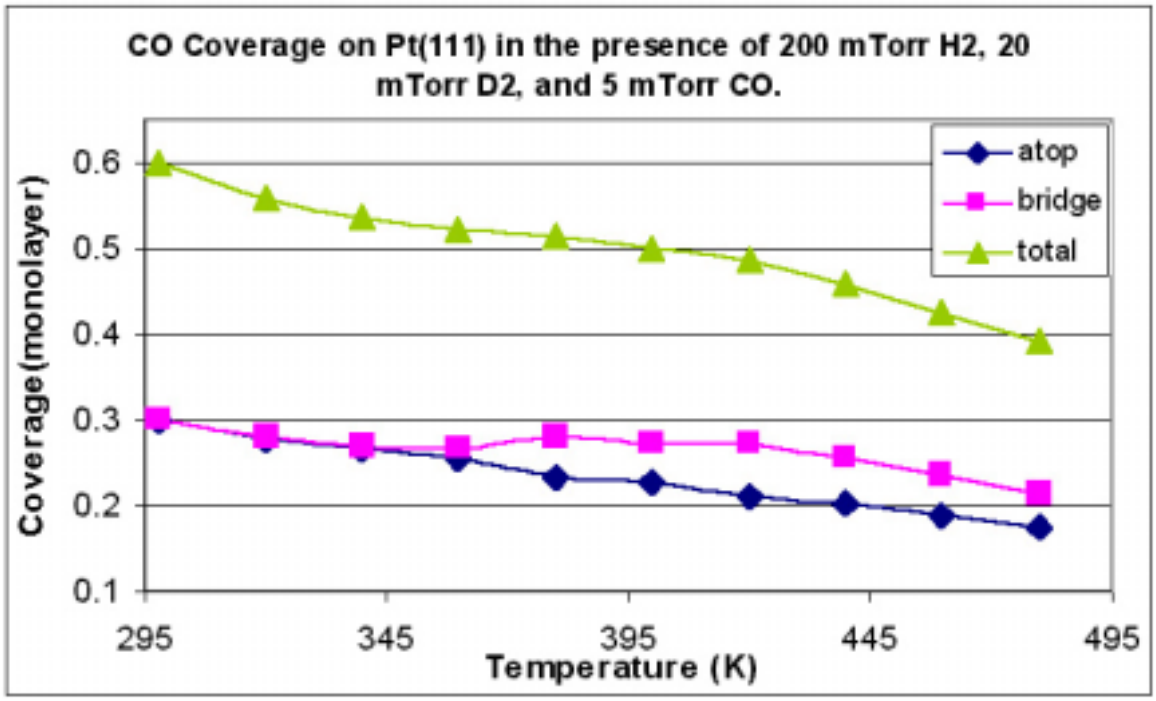

Figure 6.6 - CO coverage on Pt(111) in the presence of 200 mTorr H_2, 20 mTorr D_2 and 5 mTorr of CO. Coverage decreases as a function of temperature. Coverage calculated from average XPS peak intensity of O1s and C1s peaks.

The ratio of atop to bridge CO molecules was also studied as the temperature was raised, and is plotted in figure 6.7. The initial ratio at 298K was ~1.7. The incommensurate surface structure that is known to exist has a ratio of unity if all molecules are classified as either atop or bridge. The difference in ratios can be explained by photoelectron diffraction effects, which can cause peaks from different adsorption sites to appear with different intensities. This effect has been observed previously for CO on Pt(111).[19,20] At room temperature the diffraction effects were observed to be constant over a range of incident photon energies of 410 – 490 eV.

Scaling factors were calculated by assuming a 1:1 ratio of adsorption sites for the total coverage of 0.6 monolayers.

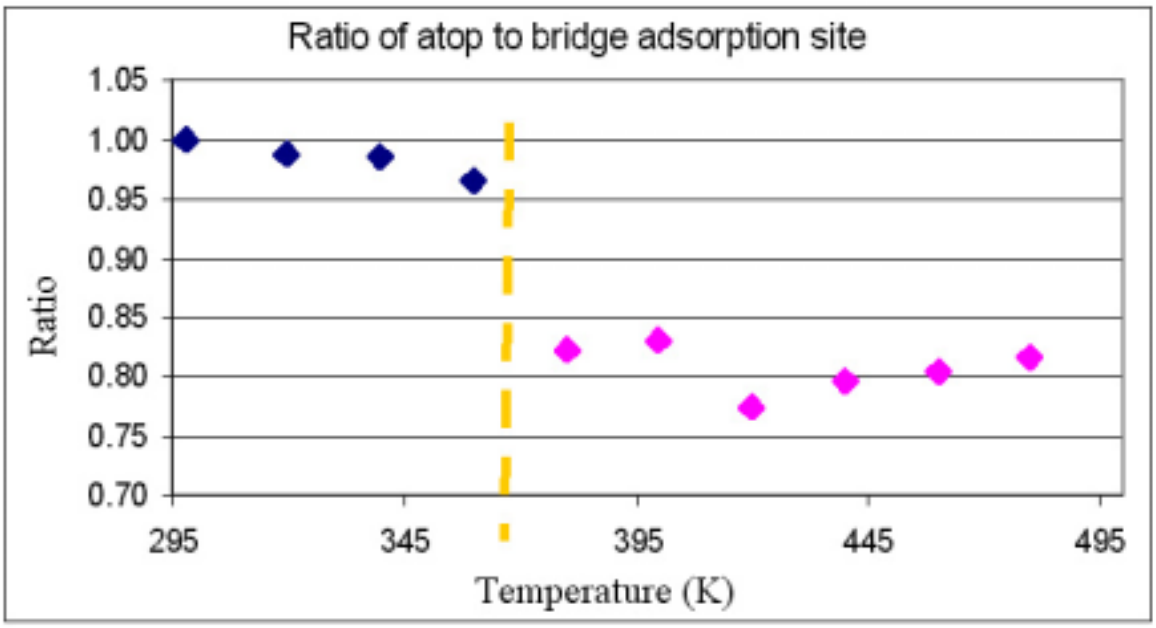

Figure 6.7 - Ratio of on top to bridge bound surface CO molecules as a function of temperature. Ratio abruptly changes from 1.0 to 0.8 around 370K Dashed orange line indicates transition period.

The ratio initially stays relatively constant from 300K up to 360K at a value of ~1. Heating the sample to 380K, however, results in the ratio quickly dropping to ~0.8 where it remains from 380K to 480K. The sudden change in adsorption site ratio suggests a surface phase change from the incommensurate structure known to initially exist, to a new structure. This structure could very well be the lower coverage c(4x2) that is known to exist at coverages near 0.5 monolayers. This structure has a 1:1 site ratio, but diffraction effects may cause this to change. In fact, in the previous studies investigating

this system, the bridge site peak has been observed to have a higher intensity despite equal populations of adsorption sites. The new structure is believed to contain coadsorbed hydrogen, deuterium and CO. Studies by Salmeron et. al.[**REF**] of CO and H_2 coadsorption on Pd(111) have shown that the two species segregate on the surface and form islands of each adsorbed species. This appears not to be the case for our studies, as large patches of adsorbed H_2 and D_2 would allow for isotope exchange rates that directly corresponded to the fraction of open sites generated by heating the sample. As can be seen from Table 1, exchange rates are well below what would be predicted by this model. Also previous studies of cyclohexene hydrogenation/dehydrogenation under identical conditions at 353K show no reaction [16]. Large patches of H_2 would clearly allow this reaction to proceed, albeit at a lower rate. Cooling the sample back to room temperature restores the original peaks indicating that the phase change is reversible.

Sum Frequency Generation Vibrational Spectroscopy

Sum frequency generation was also employed to investigate the same system as discussed above. Figure 6.8 shows a series of SFG spectra of the Pt(111) surface exposed to 200 mTorr of H_2, 20 mTorr of D_2, and 5 mTorr of CO. The resonant contribution to the SFG spectrum originating from adsorbed CO can be fit to eqn. 1. In figure 9, the position of the vibrational mode, ω_{CO}, and the amplitude of the transition, A_{CO}, are plotted against the metal surface temperature. The peak located at 2097 cm^{-1} corresponds to the atop bound CO molecule [25]. As the temperature is raised from 300K to 320K and then 340K there is no discernable shifting of the peak and only a slight decrease in intensity is observed. Upon heating to 360K, the peak red shifts by 1-2 cm^{-1}.

Heating above 360K results in a very noticeable shift, as seen in figure 9(a), and broadening of the peak, which corresponds to the same temperature at which HPXPS indicates a surface phase change. This has been previously observed on Pt(111) in the presence of CO as it is heated at a pressure of 40 Torr [26]. In the higher-pressure case, the same phenomenon of red shifting and broadening was observed but did not take place until higher temperatures. This is understandable as the higher backpressure allows for a much higher surface coverage at increased temperatures. UHV studies have revealed a similar trend in resonant mode shifting, peak broadening, and amplitude reduction.[27] The temperature dependence of the peak width is explained by a dephasing model in which a rapid energy exchange between low-frequency modes of the metal surface and low-frequency modes of the adsorbate, which are anharmonically coupled to the higher frequency mode investigated in this study. However, comparison of the peak widths obtained in this study, ~15 cm^{-1}, to that of CO adsorbed on a well ordered Pt(111) surface, ~8 cm^{-1}[28] implies significant inhomogeneous broadening. This broadening can be attributed to the creation of defect sites from sputtering procedures. Furthermore, step-site vibrations have been assigned to 2065 - 2078 cm^{-1}[29]. In both our current study and the previous high pressure study, cooling the sample back to room temperature returned the initial spectrum indicating, as did STM, that the initial incommensurate CO structure is restored.

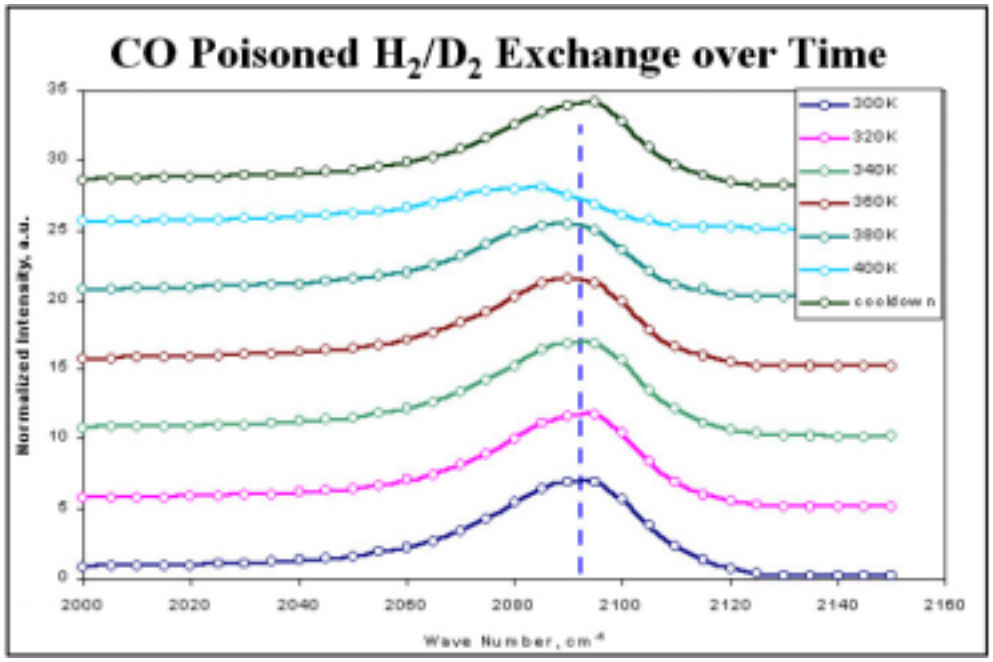

Figure 6.8 - Series of sum frequency generation (SFG) spectra showing Pt(111) in the presence of 200 mTorr H_2, 20 mTorr D_2, and 5 mTorr CO. CO peak at 2097 cm^{-1} remains the same up to 360K at which point it begins to shift. Markers represent experimental data and solid lines represent the curve fits.

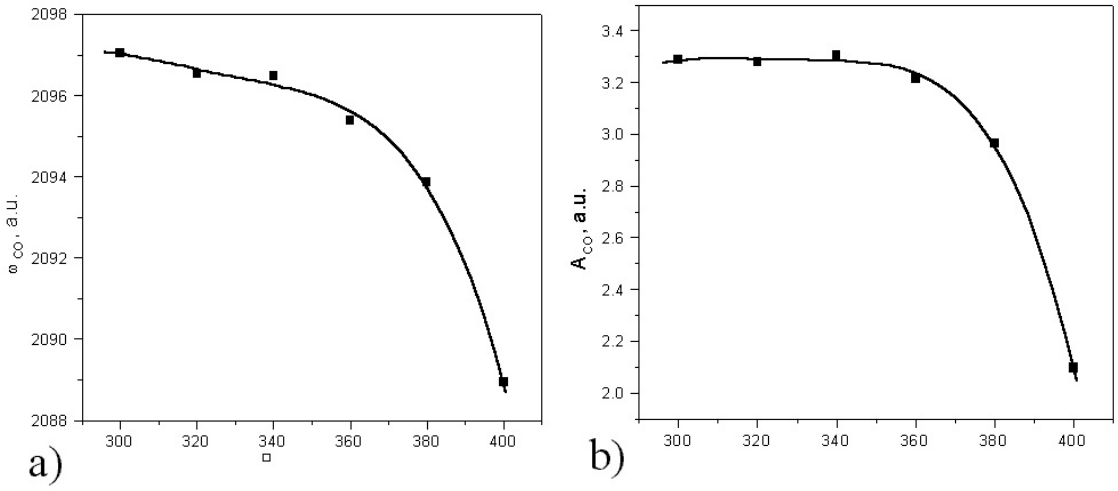

Figure 6.9 - . (a) CO vibrational resonance frequency, ω_{CO}, and (b) amplitude of the resonant contribution, A_{CO}, plotted against the metal surface temperature. Solid lines are drawn for visual aides

Turnover rates for HD production with and without CO for a variety of temperatures from 298K to 480K are shown in table 6.1 and Arrenius plots are displayed in figure 6.10. Activation energy for the H_2/D_2 exchange reaction in the absence of CO is 5.3 kcal/mol, slightly above the low pressure values obtained for Pt(111) [30] and on par with low-pressure polycrystalline studies [31]. The introduction of CO into the system causes the activation energy to more than triple to a value of 17.4 kcal/mol. A similar result was obtained for the poisoning of ethylene hydrogenation on Pt(111). In this case the activation energy increased from an unpoisoned value of 9.6 kcal/mol to 20.2 kcal/mol for CO poisoned ethylene hydrogenation [32,33]. The increase in activation energy for H_2/D_2 exchange of 12.1 kcal is slightly larger than increase seen for ethylene hydrogenation of 10.6 kcal/mol, and can potentially be explained by the fewer number of vacancies necessary for H_2/D_2 exchange. The reaction rates for the poisoned and unpoisoned surface initially differing by more than three orders of magnitude, begin to approach each other at the highest temperature studied.

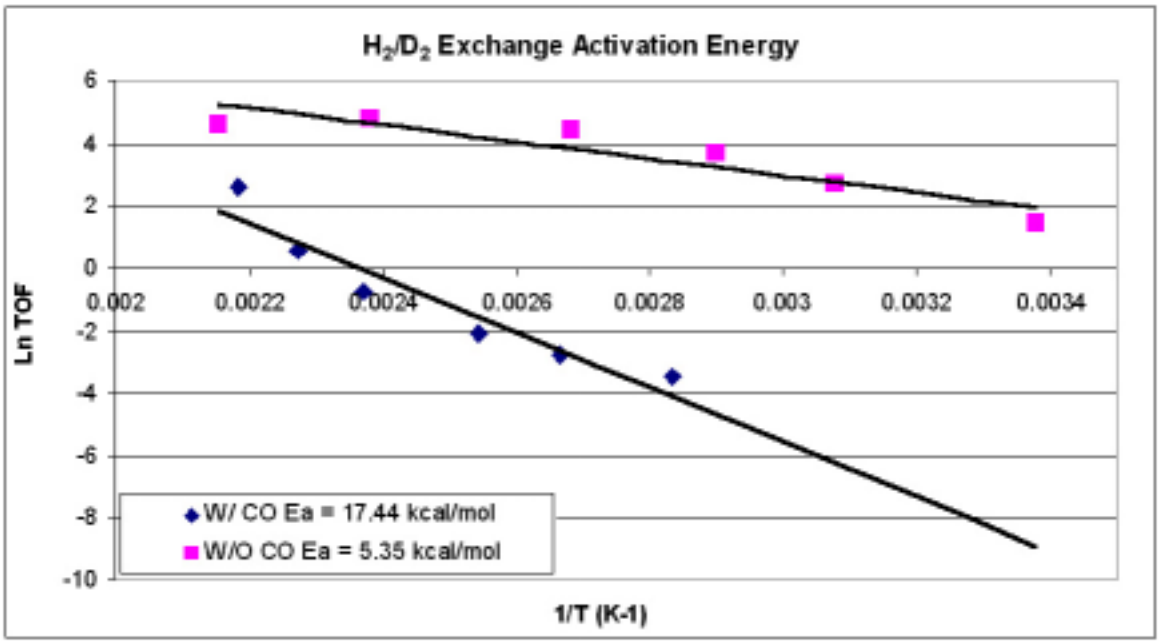

Figure 6.10 - Arrenius plot for H_2/D_2 exchange both with and without CO. Activation energy increases from 5.35 kcal/mol to 17.44 kcal/mol upon the addition of CO.

Temperature (K)	CO coverage (monolayers)	Surface Mobile?	H_2/D_2 exchange rate (mol/site/sec)
298	0.6	N	Below Detection Limits
353	0.53	Y	0.031
375	0.51	Y	0.064
393	0.49	-	0.125
422	0.47	-	0.478
440	0.44	-	1.775
458	0.41	-	13.17

a)

Temperature (K)	Surface Mobile?	H_2/D_2 exchange rate (mol/site/sec)
298	Y	4.3
325	Y	15.0
345	-	39.1
373	-	83.6
420	-	122.4
464	-	100.9

b)

Table 1 - Turnover frequencies for H_2/D_2 exchange on Pt(111) over a range of temperatures a) for the unpoisoned catalyst, b) for the poisoned catalyst

6.4 Conclusions

Overall, the poisoning of the H_2/D_2 exchange with CO increases the activation energy for reaction from ~5.3 kcal/mol to 17.4 kcal/mol and drastically reduces the reactivity similar to studies with CO poisoned ethylene hydrogenation. As the temperature is raised the reactivity under CO poisoned conditions approaches that of the unpoisoned system.

The only condition studied in which catalytic H_2/D_2 exchange was not detected was at room temperature in the presence of 200 mTorr of H_2, 20 mTorr D_2, and 5 mTorr of CO. These conditions also correspond to the only instance in which the adsorbed monolayer of molecules was static and immobile as detected by STM. The immobile structure was identified as an incommensurate structure composed of pure CO.

Removing only a small fraction (~11%) of the CO layer via heating the sample allowed the surface to become mobile and also catalytically active. The surface structure remains the same as that at room temperature but now contains some vacancies, which allow for surface mobility of the adsorbed CO and adsorption of gaseous H_2 and D_2 reactant molecules. Once adsorbed and dissociated, these atoms can diffuse due to the mobility of the surface and eventually encounter other hydrogen or deuterium atoms. The large extent of poisoning by CO can be explained by either ensembles of three or more vacancies being necessary for dissociative hydrogen and deuterium adsorption, or by a reduction in mobility of adsorbed reactant atoms.

The surface concentration of CO as detected by HPXPS decreases relatively linearly, as the Pt(111) surface was heated from 298K to 480K, from an initial coverage of 0.6 monolayers to a final coverage of 0.39 monolayers. At temperatures above 370K a surface phase change was observed from the initial incommensurate structure to an unknown phase consisting of CO, hydrogen and deuterium. This phase change was detected by an abrupt change in CO atop to bridge ratio, as well the onset of shifting and broadening of the SFG peak corresponding to the atop bound CO molecule. All techniques indicated that the mobility and surface phase changes incurred from heating the sample were reversible upon cooling back to room temperature.

References

[1] Hendriksen, B. L. M.; Frenken, J. W. M Physical Review Letters, 2002, 89, 046101.

[2] McIntyre, B. J.; Samleron, M.; Somorjai, G. A. Journal of Catalysis, 1996, 164, 18.

[3] Longwitz, S.R; Schnadt, J; Kruse Vestergaard, E; Vang, R.T; Laesgsaard, E; Stensgaard, I; Brune, H; Besenbacher, F *Journal of Physical Chemistry B* **2004,** *108*, 14497.

[4] Bluhm, H.; Havecker, M; Knop-Gericke, A.; Kleimenov, E.; Schlogl, R; Teschner, D.; Bukhtiyarov, V. I.; Ogletree, D. F.; Salmeron, M. *Journal of Physical Chemistry B* **2004**, *108*, 14340.

[5] McIntyre, B. J.; Samleron, M.; Somorjai, G. A. *Review of Scientific Instruments* **1993**, *64*, 687.

[6] Jenson, J. A.; Rider, K. B.; Chen, Y.; Salmeron, M.; Somorjai, G. A. *Journal of Vacuum Science and Technology B* **1999**, *17*, 1080.

[7] Klein, M.; Schwitzgebel, G. *Review of Scientific Instruments*, **1997**, *68*, 3099.

[8] Ogletree, D. F.; Bluhm, H.; Lebedev, G.; Fadley, C. S.; Hussain, Z.; Salmeron, M. *Review of Scientific Instruments* **2002**, *73*, 3872.

[9] Hebenstreit, E. L. D.; Ogletree, D. F.; Salmeron, M.; Bluhm, H.; Kleimenov, E.; Schlogl, R.; Shuh, D. K.; Tyliszczak, T.; Gilles, M. K. *A New Endstation for Beamline 11.0.2 High Pressure Photoelectron Spectroscopy (HPPES)* **2002**.

[10] Bain, C. D.; Davies, P.B.; Ong, T.H.; Ward, R.N.; Brown, M.A., *Langmuir* **1991,** *7*, 1563.

[11] Moore, F. G., Becraft, K.A., Richmond, G.L., *Applied Spectroscopy.* **2002,** *56*, 1575.

[12] Bratlie K. M.; Flores, L.D.; Somorjai, G.A., *Surface Science* **2005,** *599*, 93.

[13] Kung, K. Y.; Chen, P.; Wei, F.; Rupprechter, G.; Shen, Y. R.; Somorjai, G. A., *Review of Scientific Instruments* **2001,** *72*, 1806.

[14] Yang, M.; Tang, D. C.; Somorjai, G. A. *Review of Scientific Instruments* **2003,** *74*, 4554.

[15] Shen, Y. R., *The Principles of Nonlinear Optics*; Wiley: New York, 2003.

[16] Montano, M; Salmeron, M; Somorjai, G.A; *Surface Science* **2006** (To Be Published)

[17] Chen, P.; Westerberg, S.; Kung, K. Y.; Zhu, J.; Grunes, J.; Somorjai, G. A. *Applied Catalysis A*. **2002**, *229*, 147.

[18] Chen, P.; Kung, K. Y.; Shen, Y. R.; Somorjai, G. A. Surface Science, 2001, 494, 289.

[19] Kinne, M.; Fuhrmann, T.; Whelan, C. M.; Zhu, J. F.; Pantforder, J.; Probst, M.; Held, G.; Denecke, R.; Steinruck, H.-P. *Journal of Chemical Physics*, **2002**, 117, 10852.

[20] Bondino, F.; Comelli, G.; Esch, F.; Locatelli, A.; Baraldi, A.; Lizzit, S.; Paolucci, G.; Rosei, R. *Surface Science*, **2000**, *459*, L467.

[21] Mitsui, T.; Rose, M. K.; Formin, E.; Ogletree, D. F.; Salmeron, M. *Nature*, **2003**, *422*, 705.

[22] Zheng, C. Z.; Yeung, C. K.; Loy, M. M. T.; Xiao, X. *Physical Review B*. **2004**, *70*, 205402.

[23] Ma, J.; Xiao, X.; DiNardo, N. J.; Loy, M. M. T. *Physical Review B*, **1998**, *58*, 4977.

[24]

[25] Su, X.; Cremer, P.; Shen, Y. R.; Somorjai, G. A. *Physical Review Letters*, **1996**, *77*, 3858.

[26] McCrea, K.; Parker, J. S.; Chen, P.; Somorjai, G. A. *Surface Science*, **2001**, *494*, 238.

[27] Harle, H.; Mendel, K.; Metka, U.; Volpp, H.-R.; Willms, L., Wolfrum, *Journal of Chemical Physic Letters*,**1997**, *279*, 275.

[28] Klunker, C.; Balden, M.; Lehwald, S.; Daum, W., *Surface Science,* **1996,** *360,* 104.

[29] Hayden, B.E.; Kretzschmar, K.; Bradshaw, A.M.; Greenler, R.G.; *Surface Science,* **1985***, 149,* 394..

[30] Lu, K. E.; Rye, R. R.; *Journal of Vacuum Science and Technology*, **1975**, *12*, 334.

[31] Norton, P. R.; Richards, P. J. *Surface Science*, **1974**, *41*, 293.

[32] Hwang, K. S.; Yang, M.; Zhu, J.; Grunes, J.; Somorjai, G. A. *Journal of Molecular Catalysis A*. **2003**, *204-205*, 499.

[33] Grunes, J.; Zhu, J.; Yang, M.; Somorjai, G. A. *Catalysis Letters*, **2003**, *86*, 157.

Chapter 7 : High-Pressure Scanning Tunneling Microscopy Studies of Benzene Hydrogenation on Pt(111) and Its Poisoning with Carbon Monoxide

High-pressure scanning tunneling microscopy (HP-STM) has been used to study the high-pressure hydrogenation of benzene on a Pt(111) single crystal catalyst, as well as its poisoning with carbon monoxide.. STM has been able to identify surface intermediates *in-situ* during benzene hydrogenation on a Pt(111) single crystal surface at Torr pressures. In a background of 10 Torr of benzene STM is able to image small ordered regions corresponding to the c(2√3 x 3)*rect* structure in which each molecule is chemisorbed at a bridge site. In addition, individual benzene molecules are also observed between the ordered regions. These individual molecules are assumed to be physisorbed benzene based on previous sum frequency generation (SFG) results showing both chemisorbed and physisorbed molecules. The surface becomes too mobile to image upon addition of hydrogen but is determined to have physisorbed and chemisorbed benzene present by SFG. Poisoning the surface with CO at 353K produces a disordered surface composed mostly of CO. Cooling the sample back to room temperature yields the high-coverage pure CO structure of (√19 x √19) *R*23.4˚ imaged with STM.

7.1 Introduction

High-pressure scanning tunneling microscopy (HP-STM) has been widely used to study high-pressure reactions by means of atomically resolved images of surfaces at catalytically and industrially relevant conditions [1-4]. Traditionally, benzene, however, has been studied at low pressure ($<10^{-6}$ Torr) and low temperatures (<300K), which are far removed from catalytically relevant conditions. Briefly, benzene has been shown to preferentially adsorb to bridge sites at low coverages and to three-fold hollow sites at high coverages by STM [5] and density functional theory (DFT) [6]. Electron energy loss spectroscopy (EELS)[7-9] studies have shown two distinct vibrational signatures for low and high coverages, chemisorbed and physisorbed benzene. The chemisorbed species is thought to be dienyl in nature while the physisorbed benzene is thought to be flat lying by EELS[9,10] and near edge X-ray absorption spectroscopy (NEXAFS). [11]

In this study, high-pressure STM, is used for the first time to investigate and identify the surface species present during benzene hydrogenation (10 Torr of benzene) in the presence of excess hydrogen (100 Torr) and in a range of temperatures from 300 – 353K. This reaction is also studied by poisoning the platinum surface with 5 Torr of CO. High-pressure STM has the ability to monitor adsorbates and metal atoms provided their mobility occurs at speeds comparable or less than the scan rate of approximately 10 μm/sec. The unique ability to detect surface dynamics, structure and bonding information can give much insight into the catalytic process.

Sum frequency generation vibration spectroscopy studies of the same system have shown that both physisorbed and chemisorbed benzene are present on the surface in a background of 10 Torr of benzene. Small ordered regions are observed by STM and

identified as the c(2√3 x 3)*rect* structure in which each molecule is chemisorbed at a bridge site. Individual benzene molecules are also observed between the ordered regions that likely correspond to the physisorbed benzene identified by SFG. Adding hydrogen to the system mobilizes the surface by STM. SFG is able to detect physisorbed and chemisorbed benzene. Heating the platinum surface after poisoning with CO displaces benzene molecules evidenced by SFG. STM is able to verify this after imaging the (√19 x √19) *R*23.4˚ structure after cooling to room temperature, corresponding to the high-coverage pure CO structure.

7.2 Experimental

Scanning tunneling microscopy experiments were performed in a high-pressure, high-temperature STM that has been described in detail elsewhere.[12,13] The system combines a UHV surface analysis/preparation chamber with a variable temperature (298K - 675K) and pressure (10^{-10} - 10^{3} Torr) scanning tunneling microscope from RHK (model VT-UHV 300). The base pressure of the system was 1 x 10^{-10} Torr with a background mostly made up of H_2, CO and H_2O. Using three gate valves, the STM chamber can be isolated from the rest of the system and filled with any gas mixture up to a total pressure of 1 atm.

The sample was a platinum single crystal of (111) orientation from Matek Corporation with a miscut angle of < 0.3˚. Before each experiment the sample was sputtered in 5 x 10^{-6} Torr Ar for 15 minutes at an ion energy of 500 eV and current of 4 μA. After sputtering the sample was heated with an electron beam to 1073 K for 10 min. The sample was then sputtered again and annealed at 1073 K for 4 min before being

transferred to the STM chamber. Sample composition was monitored using AES and its cleanliness / flatness checked with STM prior to gas introduction.

During experiments, the STM chamber was isolated from the rest of the system while combinations of benzene, hydrogen, argon, and carbon monoxide were introduced. The hydrogen, argon, and CO were of ultrahigh purity grade, while the benzene (>99.5%, Aldrich) was further purified by freeze-pump-thaw cycles prior to use. If the experiment involved CO it was introduced after the sample had reached experimental temperature. A 150 W quartz projector bulb positioned just below the sample without making mechanical contact accomplished sample heating. A type K thermocouple spot-welded to the side of the crystal monitored sample temperature. The sample was always allowed to equilibrate at least 5 min prior to imaging. Images were taken with electrochemically etched tungsten tips, following the technique described by Klein *et al*.[14] STM settings during image acquisition were I = 0.05 - 0.2 nA and V = 50 - 100 mV. An MKS Instrument Baratron model 122A was used for 0.1mTorr - 10 Torr and model 722A for experiments exceeding 10 Torr.

7.3 Results and Discussion

In-situ HP- STM of surface species present on Pt(111) at 300 K under 10 Torr of benzene

Imaging the Pt(111) surface with HP-STM in the presence of 10 Torr of benzene reveals a surface covered with immobile adsorbed benzene, as shown in figures 7.1 & 7.2. The surface is largely disordered with patches of short-range order composed of 15-30 adsorbed molecules. Previous studies of Pt(111) electrodes in a benzene solution by Yau *et al.*[15] yields very similar results with small ordered regions separated by

disordered areas. These small patches appear to be the c(2√3 x 3)*rect* structure reported by Yau *et al.*[15] in which each molecule is chemisorbed at a bridge site. Between the patches of order, easily resolved individual benzene molecules are also bound, which are likely bound to the 3-fold hollow site and are responsible for the physisorbed species observed with SFG. In addition, several six member hexagonal rings (see figure 7.3) form where the small ordered regions intersect. The benzene molecules that form the ring most likely are bound to the 3-fold hollow site These hexagonal rings, however, have an apparently hollow center that most likely contains a weakly bound physisorbed species that is difficult to image due to its shorter residence time.

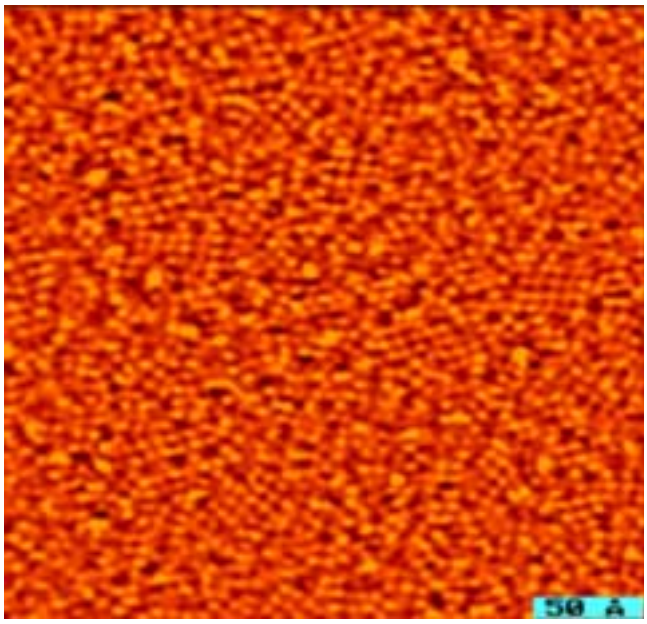

Figure 7.1 300Å × 300Å STM image of Pt(111) in the presence of 10 Torr of benzene at 298K. Strongly adsorbed immobile benzene molecule can be imaged and form small patches or order.

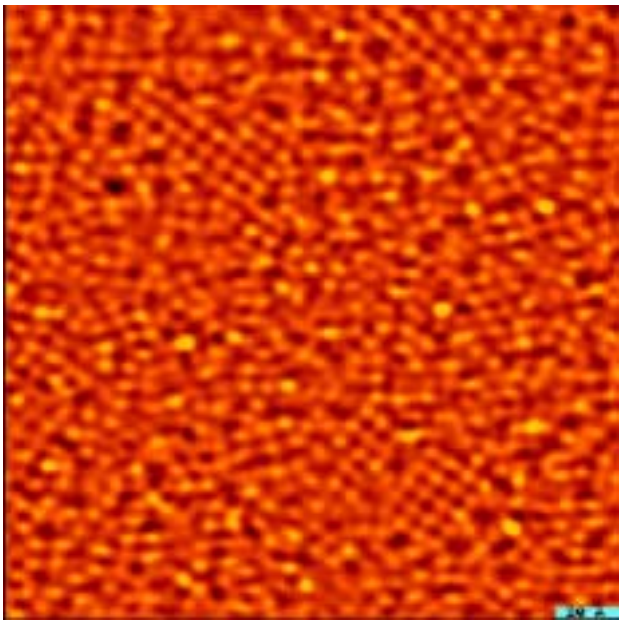

Figure 7.2 - 200Å × 200Å STM image of Pt(111) in the presence of 10 Torr of benzene at 298K.

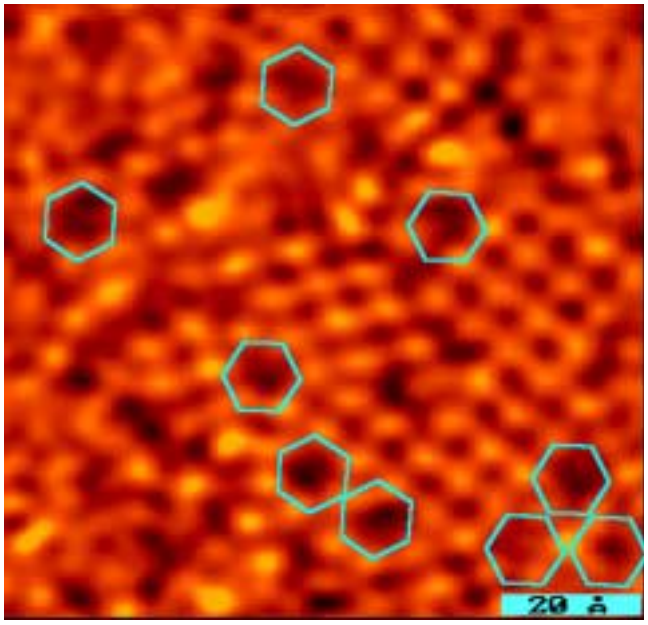

Figure 7.3 - 95Å × 95Å STM image of Pt(111) in the presence of 10 Torr of benzene. Hexagons represent six benzene molecules forming a hexagonal ring with an apparently hollow center, most likely containing a weakly bound physisorbed species

Temperature dependence of the major surface species under 10 Torr of benzene and 100 Torr of H_2 as studied by HP-STM

Upon the addition of 100 Torr of H_2 and 630 Torr of Ar the surface changes dramatically, as evidenced by STM (see figure 7.4). The patches of ordered benzene disappear and only a few isolated benzene molecules are visible on the largely mobile surface. A few of the benzene molecules that can still be imaged are highlighted in figure 7.4. This is not entirely surprising as excess hydrogen is known to weaken the surface bonding of adsorbed organic species and increase their mobility.[2] When the surface is heated to 353 K, all surface ordering of the resolved adsorbed molecules is lost as the adsorbed monolayer becomes far too mobile to be imaged by our STM, as seen in figure 7.5. At these conditions, the surface is also known to be catalytically active, readily producing cyclohexane.

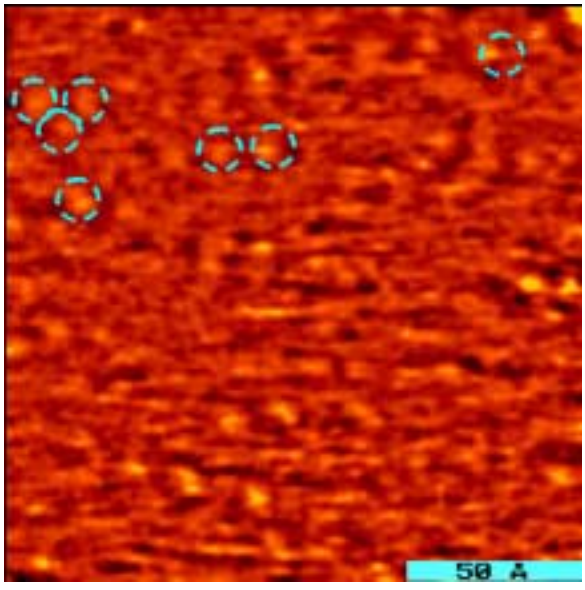

Figure 7.4 - 200Å × 200Å STM image of Pt(111) in the presence of 10 Torr of benzene, 100 Torr of H_2, and 650 Torr Ar at 298 K.

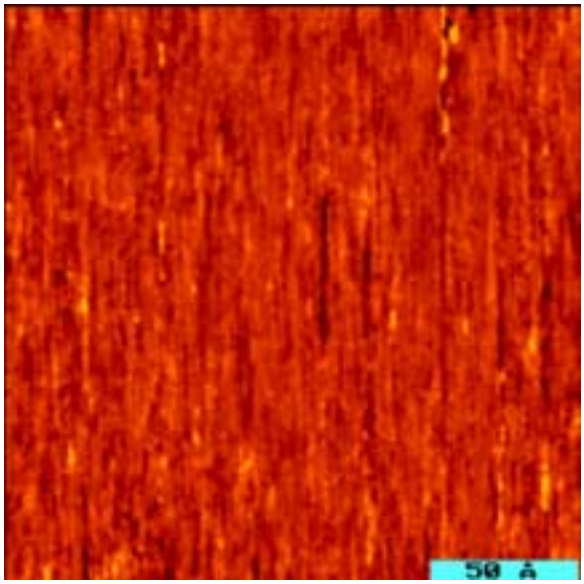

Figure 7.5 - 200Å × 200Å STM image of Pt(111) in the presence of 10 Torr of benzene, 100 Torr of H_2, and 650 Torr Ar heated to 353 K

10 Torr of benzene and 100 Torr of H_2 after poisoning with 5 Torr of CO as studied by HP- STM

Previous studies by Ogletree *et* al.[16] show that adsorbing CO molecules first creates a very large work function for the hydrocarbon to overcome in order to adsorb on the surface. For this reason, 5 Torr of CO was introduced after benzene and H_2 addition. The presence of CO has no effect on the surface structure of the system as observed by STM at 353 K. As can be observed from figure 7.6, no surface order is imaged. Again, this is attributed to the fact that although CO is now present on the surface its high mobility makes imaging with STM difficult. This is also observed previously under lower pressure conditions in the case of poisoning H_2/D_2 exchange as well as cyclohexene hydrogenation/ dehydrogenation[5]. Heating the sample to 350K desorbs

enough CO that some vacancies are created, which allow for relatively high surface diffusion. Sum frequency generation studies indicate that the surface benzene has been displaced by the more strongly bound CO. When the mobile CO dominated surface is cooled to 298K, the increase in CO surface coverage forms an immobile surface structure as can be seen in figure 7.7. This high-coverage pure CO structure was first reported by the Besenbacher group[17] and observed in our laboratory as well [18] The structure corresponds to the (√19 x √19) *R*23.4˚ structure with a total coverage of ~0.7 monolayers. As observed with STM the benzene no longer remains on the surface, as all physisorbed and chemisorbed species are displaced by the stronger bound and more densely packed CO molecules.

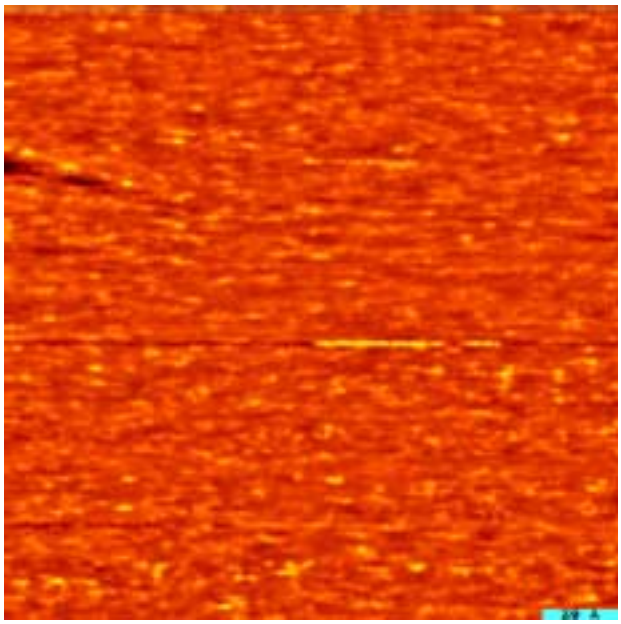

Figure 7.6 - 200Å × 200Å STM image of Pt(111) in the presence of 10 Torr of benzene, 100 Torr of H_2, and 650 Torr Ar heated to 353 K and 5 Torr of CO added. Surface is catalytically deactivated. CO molecules cannot be resolved due to their high mobility.

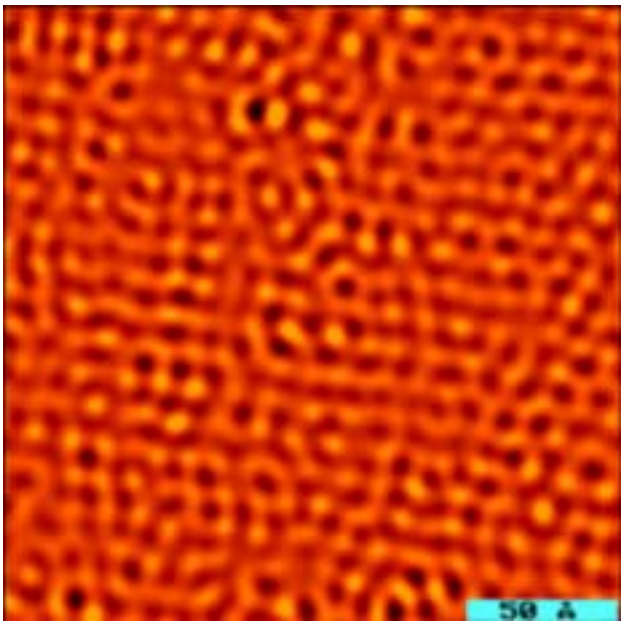

Figure 7.7 - 200Å × 200Å STM image of Pt(111) in the presence of 10 Torr of benzene, 100 Torr of H_2, and 630 Torr Ar heated to 353 K, 5 Torr CO added, and cooled to 298 K. The high-coverage pure CO structure corresponds to the (√19 x √19) R23.4° structure. All benzene adsorbates have been displaced by the strongly bound and closely packed CO molecules.

7.4. Conclusions

The structure of the Pt(111) surface in the presence of benzene, hydrogen and carbon monoxide was studied over a range of temperature from 300-350K with high-pressure STM. Small ordered regions corresponding to the c(2√3 x 3)*rect* structure, in which each molecule is chemisorbed at a bridge site, are imaged in a 10 Torr background of benzene at room temperature. Individual physisorbed benzene molecules are observed between these ordered regions. Several six member hexagonal rings with a seemingly hollow center are imaged as well. The hollow center most likely contains a physisorbed species. Upon the addition of hydrogen, the surface becomes very mobile and only a few

isolated benzene molecules are imaged. Raising the temperature to 353K results in a completely disordered surface with no molecular resolution since the mobility of the adsorbates has now exceeded the capacity of the STM. The addition of 5 Torr of CO has been known to poison the catalytically active system. The surface is composed of exclusively CO molecules, but is still too mobile to image. Cooling the system back to room temperature yields a completely ordered surface composed of the (√19 x √19) *R*23.4˚ high-pressure pure CO structure.

References

[1] Montano, M. O.; Bratlie, K.M.; Salmeron, M.B.; Somorjai, G.A., *in preparation* **2006**.

[2] Montano, M. O.; Salmeron, M.B.; Somorjai, G.A.; *Surface Science. accepted for publication* **2006.**

[3] Yang, M.; Tang, D. C.; Somorjai, G. A.; *Review of Scientific Instruments.* **2003,** *74*, 4554.

[4] Tang, D. C.; Hwang, K. S.; Salmeron, M.; Somorjai, G. A. *Journal of Physical Chemistry B*. **2004**, *108*, 13300.

[5] Weiss, P. S.; Eigler, D.M.; *Physical Review Letters.* **1993,** *71*, 3139.

[6] Sautet, P.; Bocquet, M.-L., *Physical reviews B ,* **1996,** *53*, 4910.

[7] Abon, M.; Bertolini, J.C.; Billy, J.; Massardier, J.; Tardy, B., *Surface Science.* **1985,** *162*, 395.

[8] Lehwald, S.; Ibach, H.; Demuth, J.E., *Surface Science.* **1978,** *78*, 577.

[9] Thomas, F. S.; Chen, N. S.; Ford, L. P. ; Masel R. I., *Surface Science* . **2001,** *486*, 1.

[10] Grassian, V. H.; Muetterties, E.L., *Journal of Physical Chemistry.* **1987,** *91*, 389.

[11] Horsley, J. A.; Stohr, J.; Hitchcock, A.P.; Newbury, D.C.; Johnson, A.L.; Sette, F., *Journal of Chemical Physics.* **1985,** *83*, 6099.

[12] Jenson, J. A.; Rider, K.B.; Chen, Y.; Salmeron, M.B.; Somorjai G.A., *Journal of Vacuum Science and Technology B.* **1999,** *17*, 1080.

[13] McIntyre, B. J.; Samleron, M.; Somorjai, G. A. *Review of Scientific Instruments* **1993**, *64*, 687.

[14] Klein, M.; Schwitzgebel, G. *Review of Scientific Instruments*, **1997**, *68*, 3099

[15] Yau, S.-L.; Kim, Y.-G.; Itaya, K., *Journal of the American Chemical Society.* **1996,** *118*, 7795.

[16] Ogletree, D. F.; Van Hove, M. A.; Somorjai, G. A., *Surface Science.* **1987,** *183*, 1.

[17] Longwitz, S. R.; Schnadt, J.; Vestergaard, E.K.; Vang, R.T.; Laegagaard, E.; Stensgaard, I.; Brune, H.; Besenbacher, F., *Journal of Physical Chemistry B* **2004,** *108*, 14497.

[18] Montano, M.; Tang, D. C.; Somorjai, G. A. *Catalysis Letters,* **2006**, *107*, 131.

Chapter 8: Concluding Remarks and Future Directions

8.1 Summary

In this dissertation a high-pressure high-temperature scanning tunneling microscope and a high-pressure x-ray photoelectron spectrometer were used to study the surface structures of adsorbates on a platinum single crystal of (111) orientation. Systems were monitored under catalytically active and inactive conditions in attempt to establish trends corresponding to each type of surface.

Low pressure (10^{-6} Torr) adsorption structures of cyclic C_6 hydrocarbon monolayers on the platinum (111) crystal surface were studied using STM. It was found, that upon adsorption at a back pressure of 5 x 10^{-6} Torr on Pt(111) both cyclohexane and cyclohexene produce the same structure. This structure is the ($\sqrt{7}$ x $\sqrt{7}$) R19.1˚ structure composed of the partially dehydrogenated π-allyl (C_6H_9) adsorbed to the three fold hollow adsorption site. Previous spectroscopic studies confirm these results. 1,3-cyclohexadiene and benzene form a ($2\sqrt{3}$ x $2\sqrt{3}$) R30.0˚ structure composed of molecular benzene adsorbed to the bridge site. 1,4-cyclohexadiene forms a structure very different from the other two. It is a ($\sqrt{43}$ x $\sqrt{43}$) R7.6º structure most likely composed of molecular 1,4-cyclohexadiene. This structure also contains large vacancies, which should be occupied by weakly bound species. The low residence time of these species makes them difficult to image with our STM. Increasing the backpressure of

cyclohexene from 5 x 10^{-6} Torr incrementally up to 10 Torr, results in no surface structure change until 10 Torr. At this point, a structure similar to that observed for 1,4-cyclohexadiene is observed as well as the original π-allyl structure. The presence of the 1,4-cyclohexadiene at high pressures of cyclohexene has previously been proposed from vibrational spectroscopy experiments.

HPSTM was also employed to study the hydrogenation/ dehydrogenation of cyclohexene on platinum(111) and its poisoning with carbon monoxide from 298-353K. The surface structures were monitored by STM during the reaction and mass spectrometry was used to monitor the catalytic activity of the system. When 20 mTorr of H_2 and 20 mTorr of cyclohexene were introduced at 300K the surface formed the same structure seen at low pressures of pure cyclohexene, corresponding to the (√7 x √7) R19.1˚ structure. Under these conditions, no gaseous cyclohexane or benzene is observed. Heating to 350K disorders the surface but the catalyst remains inactive as the platinum surface is suspected to become covered with benzene and other dehydrogenated carbonaceous fragments. Increasing the pressure of H_2 to 200 mTorr, while remaining at 20 mTorr of cyclohexene at 300K cause the surface to disorder and both cyclohexane and benzene gaseous products can be detected. Continuous catalytic reaction was detected for as long as the system was monitored (1.5 days). Adding 5 mTorr of CO stops all catalysis and orders the surface with an incommensurate CO structure. Repeating this experiment at 350K yields the same result of poisoning the reaction except the surface stays disordered upon addition of CO due to high adsorbate mobility. Lowering the temperature to 325K recovers the ordered CO structure. Using higher pressures of gases (1.5 Torr cyclohexene, 15Torr H_2 and 1 Torr CO) also yields a disordered surface during

catalysis, and an ordered surface upon introducing CO at 300K that poisons the reaction. Again the CO structures disorders when heated to 350K.

Three high pressure surface sensitive techniques were used to study the catalytic hydrogen/deuterium exchange on a platinum (111) single crystal and its poisoning with carbon monoxide, under reaction conditions at pressures in the mTorr to atmospheric range.. These techniques were scanning tunneling microscopy (STM), X-ray photoelectron spectroscopy (HPXPS), and sum frequency generation vibrational spectroscopy (SFG). Mass spectrometry was used to monitor catalytic activity. At 298K and in the presence of 200 mTorr of H_2 and 20 mTorr of deuterium the surface is catalytically active producing HD with an activation energy of ~5.3 kcal/mol. Introduction of 5 mTorr of CO to the system poisoned the catalyst. An ordered surface structure of chemisorbed CO corresponding to the incommensurate structure previously seen, was revealed by STM. At 353K, the addition of 5 mTorr of CO slowed the reaction but sustainable HD production continued with activation energy of 17.4 kcal/mol. The spectroscopic studies showed that the amount of adsorbed CO at 353K is only ~10% less than at room temperature. Changes in the adsorption site of CO as the coverage changes during reaction are detected by SFG and XPS, and a phase change near 370K was detected.. These data suggest a CO dominated, mobile and catalytically active surface. In addition a CO poisoning model of inhibiting adsorption and surface mobility is proposed

STM was used to study the high-pressure(~100 Torr) hydrogenation of benzene on a Pt(111) single crystal catalyst, and its poisoning with carbon monoxide. In a background of 10 Torr of benzene STM imaged small ordered regions of individual molecules, corresponding to the c(2√3 x 3)*rect* structure In this structure, each molecule

is chemisorbed at a bridge site. Individual benzene molecules are also observed between the ordered regions, and some six member rings with hollow centers are imaged as well. These individual molecules are physisorbed benzene and the hollow centers most likely contain weakly bound physisorbed species as well. Addition of H_2 in a 10:1 ratio creates a surface that is too mobile to image but is determined to have physisorbed and chemisorbed benzene present by SFG. A few strongly adsorbed molecules can be resolved. Heating the surface to 353K results in absolutely no surface structure. Poisoning the surface with CO at 353K produces a disordered surface composed mostly of CO. Cooling the sample back to room temperature yields the high-coverage pure CO structure of ($\sqrt{19}$ x $\sqrt{19}$) *R*23.4˚ imaged with STM.

8.2 Future Directions

In the research presented in this dissertation, I have shown the capabilities of scanning tunneling microscopy to probe surfaces under conditions far removed from the UHV/ cryogenic conditions generally used for surface science. STM has proven especially powerful in the area of heterogeneous catalysis, a vitally important but poorly understood area. The major problem with most STM studies is the difficulty in extracting chemical data from images. The use of the newly developed high-pressure x-ray photoelectron spectroscopy provides an excellent complement to STM by providing chemical data under identical conditions. Sum frequency generation vibrational spectroscopy (SFG) can also provide chemical information and local chemical environment at even higher pressures. The focus of the research in our laboratory over

the next 3-5 years should aim to exploit the fact that these three techniques work so well together. At Berkeley, we are in an enviable and unique position of having all three of these high pressure surface sensitive techniques at our disposal. The systems that shall be studied are as follows:

(1) The constant temperature CO poisoning of H_2/D_2 exchange on Pt(111) as a function of CO coverage studied by HPXPS. By studying the reactivity vs. coverage at constant temperature, we can investigate the number of vacancies necessary for H D combination or H_2 adsorption.

(2) HPXPS study of Pt(111) catalyzed ethylene hydrogenation and it poisoning with CO. This study should confirm the existence of various intermediates proposed by other methods, and discover whether the poisoning mechanism of CO is inhibiting mobility, or simply displacing reactant molecules.

(3) Benzene hydrogenation on Pt(100). The goal of this study is to use SFG and STM together to investigate benzene hydrogenation on another platinum crystal face to find differences relating to the different crystal structure.

These studies look to continue the work that has been performed with our instrument over the past few years, and in our group over the last four decades, and help us in our goal of a complete understanding of surfaces.